

Summer 2007

Layer -by -layer self -assembly of micro-capsules for the magnetic activation of semi-permeable nano-shells

Malcolm D. Prouty
Louisiana Tech University

Follow this and additional works at: <https://digitalcommons.latech.edu/dissertations>



Part of the [Pharmacology Commons](#)

Recommended Citation

Prouty, Malcolm D., "" (2007). *Dissertation*. 532.
<https://digitalcommons.latech.edu/dissertations/532>

This Dissertation is brought to you for free and open access by the Graduate School at Louisiana Tech Digital Commons. It has been accepted for inclusion in Doctoral Dissertations by an authorized administrator of Louisiana Tech Digital Commons. For more information, please contact digitalcommons@latech.edu.

LAYER-BY-LAYER SELF-ASSEMBLY OF MICRO-
CAPSULES FOR THE MAGNETIC ACTIVATION
OF SEMI-PERMEABLE NANO-SHELLS

by

Malcolm D. Prouty, B.S.

A Dissertation Presented in Partial Fulfillment
of the Requirements for the Degree
Doctor of Philosophy

COLLEGE OF ENGINEERING AND SCIENCE
LOUISIANA TECH UNIVERSITY

August, 2007

UMI Number: 3270928

INFORMATION TO USERS

The quality of this reproduction is dependent upon the quality of the copy submitted. Broken or indistinct print, colored or poor quality illustrations and photographs, print bleed-through, substandard margins, and improper alignment can adversely affect reproduction.

In the unlikely event that the author did not send a complete manuscript and there are missing pages, these will be noted. Also, if unauthorized copyright material had to be removed, a note will indicate the deletion.

UMI[®]

UMI Microform 3270928

Copyright 2007 by ProQuest Information and Learning Company.

All rights reserved. This microform edition is protected against unauthorized copying under Title 17, United States Code.

ProQuest Information and Learning Company
300 North Zeeb Road
P.O. Box 1346
Ann Arbor, MI 48106-1346

LOUISIANA TECH UNIVERSITY

THE GRADUATE SCHOOL

28 June 2007

Date

We hereby recommend that the dissertation prepared under our supervision
by Malcolm D. Prouty

entitled Layer-by-Layer Self-Assembly of Micro-Capsules for the Magnetic Activation of
Semi-Permeable Nano-Shells

be accepted in partial fulfillment of the requirements for the Degree of
Doctor of Philosophy in Engineering

Yusuf Levou

Supervisor of Dissertation Research

Engineering

Head of Department

Department

Recommendation concurred in:

S Selman

P D DeCath

Hafni

Labbetha Q. Dobb

Advisory Committee

Approved:

Pat Ramachandran

Director of Graduate Studies

Approved:

Terry M. Conally

Dean of the Graduate School

Stan Nagyn

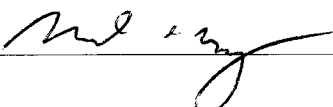
Dean of the College

GS Form 13
(5/03)

APPROVAL FOR SCHOLARLY DISSEMINATION

The author grants to the Prescott Memorial Library of Louisiana Tech University the right to reproduce, by appropriate methods, upon request, any or all portions of this Dissertation. It is understood that "proper request" consists of the agreement, on the part of the requesting party, that said reproduction is for his personal use and that subsequent reproduction will not occur without written approval of the author of this Dissertation. Further, any portions of the Dissertation used in books, papers, and other works must be appropriately referenced to this Dissertation.

Finally, the author of this Dissertation reserves the right to publish freely, in the literature, at any time, any or all portions of this Dissertation.

Author 
Date 28 June 2007

ABSTRACT

Layer-by-layer (LbL) self-assembly has demonstrated broad perspectives for encapsulating, and the controllable delivery, of drugs. The nano-scale polymer layers have the capability of material protection. Magnetic nanoparticles have great potential to be applied with LbL technology to achieve both "focusing" of the encapsulated drugs to a specific location followed by "switching" them on to release the encapsulated drugs. In this work, Phor21- β CG(ala), dextran, and dexamethasone were used as model drugs. Encapsulation of these drugs with layer-by-layer self-assembly formed bio/nano robotic capsules for controlled delivery and drug release.

Silica nanoparticles coated with polyelectrolyte layers of sodium carboxymethyl cellulose (CMC) or gelatin B, along with an oppositely charged peptide drug (Phor21- β CG(ala)), were prepared using LbL self-assembly and confirmed using QCM and zeta potential measurements. The peptide drug was assembled as a component of the multilayer walls. The release kinetics of the embedded peptide were determined. Up to 18 % of the embedded Phor21- β CG(ala) was released from the CMC multilayers over a period of 28 hours. The release was based on physiological conditions, and an external control mechanism using magnetic nanoparticles needed to be developed.

Magnetic permeability control experiments were setup by applying LbL self-assembly on MnCO_3 micro-cores to fabricate polyelectrolyte microcapsules embedded with superparamagnetic gold coated cobalt (Co@Au) nanoparticles. An alternating

magnetic field was applied to the microcapsules to check for changes in permeability. Permeability experiments were achieved by adding fluorescein isothiocyanate (FITC) labeled dextran to the microcapsule solution. Before an alternating magnetic field was applied, the capsules remained impermeable to the FITC-dextran; however, after an alternating magnetic field was applied for 30 minutes, approximately 99 % of the capsules were filled with FITC-dextran, showing that the Co@Au embedded microcapsules were indeed “switched on” using an alternating magnetic field.

LbL assembly was then applied to encapsulate micronized dexamethasone with biocompatible polyelectrolytes such as protamine sulfate C, chondroitin sulfate sodium salt, and gelatin B, along with a layer of superparamagnetic nanoparticles. The biocompatible polymers were used to retain and protect the vulnerable drug. *In vitro* drug release kinetics were investigated according to different environmental factors such as temperature and pH. An external oscillating magnetic field was applied to “switch on” and accelerate the drug release. The results were compared to those without applying a magnetic field.

TABLE OF CONTENTS

ABSTRACT.....	iv
TABLE OF CONTENTS	vi
LIST OF TABLES	ix
LIST OF FIGURES.....	x
ACKNOWLEDGMENTS	xiv
CHAPTER 1: INTRODUCTION	1
Research Goals.....	1
Dissertation Overview	2
CHAPTER 2: LITERATURE REVIEW.....	4
Metallic Nanoshells	5
Applications in Nanomedicine.....	6
Nanoshells Formed by Polyion Electrostatic Layer-by-Layer Self-Assembly	10
Preparation of LbL Nanoshells	11
Proving the Nanoshells	17
Influence of the Core on Nanoshell Properties	22
Barrier Properties of LbL Assembled Nanoshells.....	24
Controlled Release of Active Pharmaceutical Ingredients Encapsulated by LbL Assembled Nanoshells.....	27
Nanoshell Permeability for Low Molecular Weight Compounds.....	28
Nanoshell Permeability for High Molecular Weight Compounds.....	33
Magnetic Nanoshells	34

CHAPTER 3: PROPERTIES OF MAGNETIC PARTICLES	36
Magnetism in Bulk Materials.....	36
Magnetic Anisotropy	36
Magnetic Domains.....	38
Magnetism in Nano-Scale Materials	41
Definition of Nano-Scale Materials.....	41
Superparamagnetism	42
CHAPTER 4: RELEASE OF PHOR21- β CG(ALA) POLYPEPTIDE INCORPORATED IN A POLYELECTROLYTE SHELL.....	45
Introduction.....	45
Materials and Methods	47
Preparation of Silica-Peptide Nanoshells	47
Characterization of Silica-Peptide Nanoshells.....	48
Release Kinetics <i>In Vitro</i>	49
Results.....	50
Discussion	55
Conclusion	58
CHAPTER 5: CONTROLLABLE PERMEABILITY USING MAGNETIC NANOPARTICLES	60
Introduction.....	60
Experimental	61
Materials	61
Co@Au Nanoparticle Fabrication and Characterization	62
Capsule Preparation.....	63
Capsule Permeability Test	64
Capsule Characterization	65

Results and Discussion	66
Co@Au Nanoparticle Characterization	66
Layer-by-Layer Assembly on QCM Electrodes and Microcores.....	69
Magnetic Field Modification of Capsule Permeability	75
Temperature and Frequency Effects.....	79
Optimization of the Capsule Wall Composition	81
Theoretical Considerations	82
Conclusion	86
CHAPTER 6: MAGNETICALLY ACTIVATED MICROCAPSULES FOR THE CONTROLLED RELEASE OF ENCAPSULATED DEXAMETHASONE.....	88
Introduction.....	88
Experimental	88
Materials	88
Capsule Preparation.....	89
Drug Release	89
Results and Discussion	90
Conclusion	92
CHAPTER 7: CONCLUSION.....	93
Future Work.....	94
REFERENCES.....	95
VITA.....	106
Peer Reviewed Journals.....	107
Conference Proceedings	107
Invited Talks	108
Conference Talks.....	108
Conference Posters	108

LIST OF TABLES

Table 3.1: Magnetic anisotropy constants, K_1 and K_2 , for selected materials in $\text{J}\cdot\text{m}^{-3}$ [82]. K_{u1} and K_{u2} , for cobalt, are listed under K_1 and K_2 , respectively.	37
---	----

LIST OF FIGURES

- Figure 2.1: Release of bovine serum albumin (BSA) from nonirradiated and irradiated hydrogels with and without nanoshells. Irradiation was done at 1,064 nm with 164 mJ/pulse, a 7 nanosecond pulse length, and a 10 Hz repetition rate [3].....8
- Figure 2.2: Scheme of electrostatic layer-by-layer self-assembly on 2-D substrates with (top) polycations and polyanions, and (bottom) polycations and negatively charged nanoparticles..... 13
- Figure 2.3: Scheme of electrostatic layer-by-layer self-assembly on 3-D microtemplates, or cores, followed by core dissolution..... 14
- Figure 2.4: Frequency shift and film thickness of each assembled layer for (PSS/PAH)₂(TA/PAH)₃ adsorption on QCM electrodes. The first two precursor layers are PSS/PAH, and the next three layers are TA/PAH. The tannic acid and poly(allylamine hydrochloride) has an average thickness of 1.57 ± 0.11 nm and 1.69 ± 0.35 nm, respectively [46]..... 18
- Figure 2.5: The increase in UV/Vis absorbance with an increase in the number of PAH/TA layers deposited on a quartz slide. The absorbance of PAH (black, dotted line) and TA (blue, dashed line) increases with the deposition of material on the quartz slide. The inset shows the linear increase in layer mass of tannic acid [46]. .20
- Figure 2.6: Changes in the zeta potential of coated dexamethasone (Dexa) particles as a function of the number of adsorption steps for capsule compositions of (Dexa/PDDA)₁(PSS/PDDA)₄ (solid line and solid squares), (Dexa/PDDA)₁(Gelatin A/PDDA)₄ (broken line and open squares), and (Dexa/PDDA)₁(PSS/Gelatin A)₄(PSS/PDDA)₁ (solid line and open triangles) [52].....21
- Figure 2.7: (left) Confocal image of polyelectrolyte microcapsules with a wall composition of (PSS/PAH)₅ loaded with FITC-labeled glucose-oxidase, and (right) atomic force microscopy tapping mode image of the same broken dry capsule on mica. Release of the encapsulated material is visible [35].27
- Figure 2.8: (a) Illustration of the furosemide microcrystal encapsulation and release study, and (b) dissolution profiles of (PSS/PDDA)₂(PSS/gelatin)₄ coated furosemide microparticles compared to uncoated particles and a commercially available tablet in physiologically relevant media [18]. Here, 1 corresponds to 100 % release on the fraction of drug released axis.30

- Figure 2.9: Illustration of the monodispersion of micronized dexamethasone drug particles by electrostatic layer-by-layer encapsulation, followed by subsequent controlled release of the drug through the insoluble porous shell [52].32
- Figure 2.10: A 400 nm diameter glucose-oxidase core coated with (PSS/PEI)₂(Magnetite/PEI)₂ shells. The 12 nm diameter magnetite nanoparticles are visible on the surface.35
- Figure 3.1: Anisotropy energy surface for cobalt. Cobalt naturally aligns to the z-axis, or easy-axis, because that is where the lowest anisotropy energy is located.38
- Figure 3.2: Schematic of a ferromagnetic material containing a 180° domain wall. Domain #1 (blue arrows, left) and domain #2 (red arrows, right) have magnetization vectors 180° to each other. The domain wall (middle arrows) is composed of N atomic distances, and is where the transition from one domain to another takes place.39
- Figure 3.3: Graph showing the magnetization orientation profile and the domain wall thickness for cobalt. The magnetization orientation profile is represented by the red line, and the domain wall thickness, $\delta_{dw} = 15.5$ nm, is shown in blue.41
- Figure 3.4: (a) 1-dimensional, (b) 2-dimensional, and (c) 3-dimensional nano-scale materials represented by stacked thin-films, rods, and particles, respectively. The small dimensions are 100 nm each. Here, the large dimensions are 1 μ m each; however, any dimension over 100 nm is considered a large dimension for nano-scale objects.42
- Figure 3.5: Critical radius for single-domain behavior versus saturation magnetization for spherical particles of cobalt. The blue line shows r_c for 0 – 500 nm, the red line zooms in to show r_c for 0 – 100 nm, and the green line zooms in further to show r_c for 0 – 10 nm.43
- Figure 4.1: Scheme of Phor21- β CG(ala) adsorption on 450 nm silica nanoparticles, and the release of the drug (large, blue spheres = silica cores; small, red dots = Phor21- β CG(ala) peptide; and wavy, green lines = polyelectrolytes).50
- Figure 4.2: Zeta potential of the silica nanoparticles demonstrating the surface changes during adsorption of Phor21- β CG(ala) alternating with (a) sodium carboxymethyl cellulose and (b) gelatin B. The error bars represent one standard deviation from the mean.51
- Figure 4.3: (a) QCM and (b) UV/Vis data showing the peptide adsorption on QCM resonators and 450 nm silica particles, respectively. For the UV/Vis data, the peptide assembly was alternated with CMC. The error bars represent one standard deviation from the mean.53

- Figure 4.4: Release kinetics of Phor21- β CG(ala) from glass slides coated with 20 layers of peptide in 0.9 % NaCl USP injection media..... 54
- Figure 4.5: Release kinetics of Phor21- β CG(ala) from peptide-silica nanoparticles with four (open diamonds) and eight (closed boxes) peptide layer coatings with CMC as the alternate layer. The error bars represent one standard deviation from the mean. 55
- Figure 5.1: Scheme of the assembly and permeability test for microcapsules embedded with Co@Au nanoparticles. 61
- Figure 5.2: UV/Vis spectrum of Co@Au nanoparticles showing the Au absorbance peak at 585 nm..... 67
- Figure 5.3: Transmission electron microscopy (TEM) image of Co@Au nanoparticles. The particles are \sim 3 nm in diameter. 68
- Figure 5.4: Temperature dependences of the magnetic moment measured in zero field cooled (ZFC) and field cooled (FC) modes for Co@Au nanoparticles (open squares) and pure cobalt nanoparticles (closed squares). The blocking temperatures for Co@Au and pure Co nanoparticles are approximately 300 K and 125 K, respectively..... 69
- Figure 5.5: Thickness changes by the alternating adsorption of Co@Au nanoparticles with PSS monitored using QCM. 70
- Figure 5.6: Zeta potential changes by alternating adsorption of Co@Au with PSS on MnCO₃ cores. 72
- Figure 5.7: Confocal image of RBITC-labeled (shown in red fluorescence) microcapsules with one layer of embedded Co@Au nanoparticles. The capsule structure is (PSS/PAH)₄(PSS/Co@Au)₁(PSS/PAH)₆. The bottom-right inset shows the fluorescence intensity of the RBITC in the cross-section of one capsule..... 73
- Figure 5.8: (a) SEM image of hollow capsules with (PSS/PAH)₁₁, and (b) SEM image of magnetic capsules with one layer of embedded Co@Au nanoparticles: (PSS/PAH)₄(PSS/Co@Au)₁(PSS/PAH)₆. Insets show zoomed image of one capsule. 75
- Figure 5.9: Confocal laser scanning microscopy images of magnetic capsules, (PSS/PAH)₄(PSS/Co@Au)₁(PSS/PAH)₆, mixed with FITC-dextran (a) without applying an alternating magnetic field, and (b) after applying an alternating magnetic field for 30 minutes, with corresponding optical density profiles..... 78
- Figure 5.10: (a) Co@Au nanoparticles suspended in DI water. (b) After application of a permanent magnetic field, the magnetic nanoparticles migrate towards the magnet leaving a clear solution of DI water behind. 79

- Figure 5.11: (a) Temperature increase tendency of capsule suspensions when applying a magnetic field, and (b) confocal image of magnetic capsules, $(\text{PSS}/\text{PAH})_4(\text{PSS}/\text{Co@Au})_1(\text{PSS}/\text{PAH})_6$, in a 1:1 mixture with FITC-dextran after heating to 50 °C for 30 minutes..... 80
- Figure 5.12: Influence of polyelectrolyte bi-layer numbers on the permeability of capsules with and without an embedded layer of Co@Au nanoparticles at pH 7.5..82
- Figure 5.13: Magnetic hysteresis curve for Co@Au nanoparticles. Inset shows zoomed curve. The small hysteresis indicates slight ferromagnetic properties in the material. 84
- Figure 6.1: Charge reversal of layers as they are assembled on dexamethasone cores with the following composition: $(\text{PS}/\text{CS})_1(\text{PS}/\text{GB})_1(\text{Co@Au}/\text{GB})_1(\text{PS}/\text{GB})_1$ 91
- Figure 6.2: Release of dexamethasone with (blue triangles) and without (red squares) an applied alternating magnetic field (200 Hz, 0.1 T). The dexamethasone release was monitored using UV/Vis at 242 nm. The dexamethasone was encapsulated in $(\text{PS}/\text{CS})_1(\text{PS}/\text{GB})_1(\text{Co@Au}/\text{GB})_1(\text{PS}/\text{GB})_1$ microcapsules. 92

ACKNOWLEDGMENTS

I would like to extend my gratitude to my advisor and mentor, Dr. Yuri Lvov, who has supported me throughout my doctoral research. Also, I would like to thank Dr. Tianhong Cui for introducing me to graduate research, for whom without I would have not began the pursuit of my doctoral degree. My current advisory committee, Dr. Sandra Selmic, Dr. Haifeng (Frank) Ji, Dr. Tabbetha Dobbins, and Dr. Mark DeCoster, along with my previous advisory committee members, Dr. Michael McShane and Dr. Yi Su, also deserve commendation.

I would like to thank Dr. Carola Leuchner and Dr. Challa Kumar for supplying materials and insight for my research work. Special thanks needs to be given to two of the post-doctoral research associates in our group, Dr. Zonghuan Lu and Dr. Tatsiana Shutava, for their invaluable experience and help in guiding my research.

I cannot forget my fellow lab mates, those who have already graduated and those who are still pursuing their degrees, for their advice and assistance in the laboratory. Additionally, the IfM faculty and staff have always been there when I needed their assistance.

I would also like to acknowledge Dr. Vladimir Golub for his helpful discussions and insight into building the magnetic theory sections of my dissertation. Joseph Cannon and Gerard Heineken deserve credit for helping me through the rough areas of writing my dissertation, as well as with assistance in creating some of the figures.

This work would not be possible without financial support provided by research grants from organizations such as the National Science Foundation, the National Institute of Health, the National Aeronautics and Space Administration, the Louisiana Board of Regents, and others.

Finally, I would like to thank my wife, Lê Bích Đào, as well as the rest of our family and friends, for their unyielding support and patience while I have been studying for my doctoral degree.

CHAPTER 1

INTRODUCTION

In this research, magnetic nanoparticles incorporated in polymeric shells for the enhanced delivery of encapsulated drug molecules was explored. The polymeric shells, embedded with a layer of magnetic nanoparticles, were formed via layer-by-layer self-assembly around a core formed from the releasing agent. After formation of the core-shell capsules, a low frequency, alternating magnetic field was applied to the capsules to allow the encapsulated drug to be released through the polymeric walls, delivering the agent to the specified target. These capsules can be considered as bio/nano robots activated by external magnetic fields for the controlled release of macromolecules.

Research Goals

Five goals were established as a guide for this research work. The goals were used as a basis on which the work was developed. Some of the goals are as follows:

- Use layer-by-layer self-assembly to develop a semi-permeable polyelectrolyte shell around a core;
- Include a layer of magnetic nanoparticles in the polyelectrolyte shells;
- Use an external permanent magnet for “focusing” the core-shell capsules;

- Use an external alternating magnet for increasing the permeability of the polyelectrolyte shells; and
- Encapsulate a drug in the polyelectrolyte shells embedded with magnetic nanoparticles for enhanced controlled release of the drug.

Dissertation Overview

Chapter 2 gives a brief overview of the background needed for this dissertation. It covers the different methods used to encapsulate and release macromolecules. Furthermore, various characterization methods for the encapsulation and release of the macromolecules are explained.

Chapter 3 describes the magnetic characteristics of cobalt, and shows how these characteristics change as these materials are reduced in size to the nano-scale.

Chapter 4 discusses the nanoshell formation of the encapsulation of an anticancer polypeptide using the layer-by-layer self-assembly technique. Here, the polypeptide is used as the releasing agent. The polypeptide has a net positive charge due to its amino acid groups, hence the polypeptide is able to be incorporated in the shells as one of the layers itself, allowing for release of the polypeptide in different pH conditions.

Chapter 5 describes the results obtained from incorporating magnetic nanoparticles in polyelectrolyte layers to form a semi-permeable shell using layer-by-layer self-assembly. A high molecular weight dextran can selectively diffuse through the shell with application of an alternating magnetic field. It is shown that these shells can be “focused” to a specific target using a permanent magnetic field, and then “switched on” to allow diffusion using a low frequency, alternating magnetic field.

Chapter 6 builds upon these results by encapsulating micronized dexamethasone within these semi-permeable shells. The dexamethasone is able to diffuse through these polyelectrolyte layers naturally due to its low molecular weight. However, by switching on the enhanced permeability feature of these shells by applying an alternating magnetic field, the dexamethasone is able to release at a higher rate.

Chapter 7 concludes the dissertation by giving an overview of the encapsulation and release techniques used. Future work that can be added to these encapsulation experiments is also given.

CHAPTER 2

LITERATURE REVIEW

Nanomedicine, and especially the field of nanopharmaceuticals (drugs and drug delivery systems), describe the preparation of nanoscale assemblies, which can be relatively simple nanoemulsions, nanoparticles, polymer conjugates of proteins or drugs, or complex multicomponent systems containing drugs, proteins, or genes, as well as arrays of targeting ligands and/or signal systems, to enable *in vitro* or *in vivo* detection. Therefore, nanopharmaceutics is defined as the science and technology of nanometer scale complex drug delivery systems, consisting of at least two components, one of which is the active ingredient. In this field, the concept of nanoscale is seen to range from 1 to 100 nm. Currently, just one nanoparticle product, Abraxane[®], an albumin nanoparticle containing paclitaxel, is FDA approved, but many more are being developed, and are in phase I, II, or III of the drug development process. This means that this class of drug delivery systems is rapidly growing and is moving from the development of individual building blocks to multifunctional, often biomimetic and bioresponsive systems.

These more complex nanosized drug delivery systems are either self-assembling or involve covalent conjugation of multicomponent systems; for example drugs, proteins, and polymers. The bioresponsive and/or biomimetic materials used to create such drug delivery systems typically include synthetic or semi-synthetic polymers, and/or natural materials such as lipids, polymers, and proteins. One nanosystem that is being proposed

as a drug carrier is nanoshells or nanocapsules because these novel “nanoparticles” can address the three principal goals of drug delivery research today: more specific drug delivery and targeting; greater safety and biocompatibility; and faster development of new, safe medicines. Current research in nanoshell drug delivery could lead to, amongst others, vectors that will overcome the biological barriers for effective gene delivery, cancer targeting, brain delivery, and the combination of the potential of antibody targeting with nanoparticle technology. This would improve drug targeting to the whole body or cellular and sub-cellular localization of drugs, proteins, and genes.

The nanoshells most widely studied as potential nanopharmaceuticals are metallic nanoparticles composed of a dielectric core coated with an ultrathin metallic layer and nanoshells formed by electrostatic layer-by-layer (LbL) self-assembly [1].

Metallic Nanoshells

In the past few years, silica–gold nanoshells have emerged as powerful building blocks for devices in which electromagnetic waves are able to control the nanometer length scale [2]. Due to this unique property, Halas and West, in a series of clever experiments, demonstrated how silica–gold nanoshells are uniquely suitable for use in whole-blood immunoassays, optically triggered drug delivery, and targeted photothermal destruction of cancer cells [3]. Mie provided the theory explaining this phenomenon [4]. This theory predicts that metallic nanoclusters strongly absorb visible light at a well-defined plasmon-resonance frequency that depends on the particle size and shape, the presence of other particles, and the dielectric environment [5]. Due to this phenomenon, silica–gold nanoshells offer enormous flexibility to tune the resonance frequency by

varying the relative dimensions of the silica core and gold shell [6, 7]. In contrast to solid-core metallic nanoparticles, the resonance of a silica–gold nanoshell particle can easily be positioned in the near-infrared region between 800 – 1,300 nm, where absorption by biomatter is low. Together, with the high degree of biocompatibility of these nanoshells, low bioabsorption opens the door to a wide variety of biological applications.

Applications in Nanomedicine

In one study, Halas and West showed how near-infrared resonant nanoshells could be used to enable fast whole-blood immunoassays [8]. For conventional blood immunoassays, optical tests were performed at visible wavelengths. Because a purification step needed to be performed to separate out a variety of unwanted biomaterials that absorb visible light, the whole procedure could take several hours or days. In the proposed immunoassay procedure, nanoshells were conjugated with antibodies that acted as recognition sites for a specific analyte. The analyte caused the formation of dimers, which modified the plasmon-related absorption feature in a known way. The presence of analyte was then determined by a fast absorption measurement in the water window, circumventing the time-intensive purification step.

Gold nanoshells can also be incorporated into temperature-sensitive hydrogels to synthesize a new type of composite material that collapses on laser irradiation [3]. Upon irradiation, plasmon excitations are quickly damped, and the electron kinetic energy is converted into heat through electron–phonon interactions. This fast damping is usually undesirable, but here the efficient light-to-heat conversion in metallic nanoshells is used

to shrink the volume of the hydrogel from a remote location. The absorption cross-section of a nanoshell is about a million times larger than that of a typical molecular chromophore, and hydrogel collapse thus occurs at relatively low pump-power densities. By incorporating nanoshells with different resonance frequencies, one can selectively collapse specific hydrogel volumes. Such remotely addressable hydrogels may find application in drug delivery and microfluidic valves or pumps.

For example, composites of thermally sensitive hydrogels and optically active nanoparticles have been developed for the purpose of photothermally modulated drug delivery [3]. Copolymers of N-isopropylacrylamide (NIPAAm) and acrylamide (AAm) exhibit a lower critical solution temperature (LCST) that is slightly above body temperature. When the temperature of the copolymer exceeds the LCST, the hydrogel collapses, causing a burst release of any soluble material held within the hydrogel matrix. When gold–gold sulfide nanoshells, a new class of nanoparticles designed to strongly absorb near-infrared light, were incorporated into the poly(NIPAAm-co-AAm) hydrogels, temperature changes in the hydrogel could be induced with light. Light at wavelengths between 800 and 1,200 nm, which is transmitted through tissue with relatively little attenuation, was absorbed by the nanoparticles, and converted to heat. Using this system, significantly enhanced drug release from composite hydrogels was achieved in response to irradiation by light at 1,064 nm as shown in Figure 2.1 (see page 8). This system controlled the release of methylene blue and proteins of varying molecular weight.

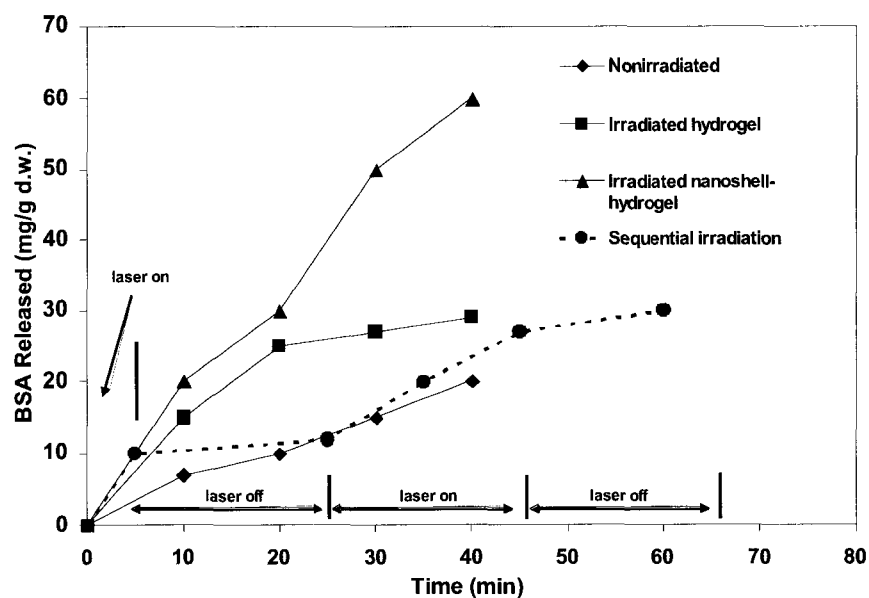


Figure 2.1: Release of bovine serum albumin (BSA) from nonirradiated and irradiated hydrogels with and without nanoshells. Irradiation was done at 1,064 nm with 164 mJ/pulse, a 7 nanosecond pulse length, and a 10 Hz repetition rate [3].

The nanoshell-composite hydrogels can also release multiple bursts of protein in response to repeated near-IR irradiation [3]. If the entire loaded drug is not released during the initial irradiation sequence, additional bursts of release of the drug can be elicited by subsequent irradiation. Once the laser irradiation is stopped, the driving force for the convective transport of material out of the hydrogel matrix is removed. During this time, the drug release is driven by diffusion, and the amount released is much less than that generated by irradiation. The hydrogel will begin to swell as soon as the laser is turned off, returning to its equilibrium state. A second irradiation sequence delivered at this time will cause the hydrogel to collapse again, resulting in another burst of release of the drug molecule. In Figure 2.1, such a release pattern for bovine serum albumin (BSA) is shown. This type of release profile may be useful in insulin therapy as well as in other applications where controlled pulsatile release of a drug is necessary.

Additionally, it has been speculated that metallic nanoshells could play a role in future cancer treatments. These particles are small enough to find their way through the human circulatory system via injection. Bioactive molecules can be attached to the nanoshell surface to cause selective binding or accumulation of these particles within a tumor. Using a near-infrared laser, carcinoma tissue can then be destroyed by local thermal heating around the nanoshells. For example, by tuning the nanoshells to strongly absorb light in the near-infrared, where optical transmission through tissue is optimal, a distribution of nanoshells at depths near the tissue's surface can be used to deliver a therapeutic dose of heat by using moderately low exposures of extracorporeally applied near-infrared (NIR) light [9]. In this study, human breast carcinoma cells incubated with nanoshells *in vitro* were found to have undergone photothermally induced morbidity on exposure to NIR light (820 nm, 35 W·cm⁻²), as determined by using a fluorescent viability stain. Cells without nanoshells displayed no loss in viability after the same periods and conditions of NIR illumination. Likewise, *in vivo* studies under magnetic resonance guidance revealed that exposure to low doses of NIR light (820 nm, 4 W·cm⁻²) in solid tumors treated with metal nanoshells reached average maximum temperatures capable of inducing irreversible tissue damage ($\Delta T \sim 38$ °C) within 5 minutes. Controls treated without nanoshells demonstrated significantly lower average temperatures on exposure to NIR light ($\Delta T < 10$ °C). These findings demonstrated good correlation with histological findings. Tissues heated above the thermal damage threshold displayed coagulation, cell shrinkage, and loss of nuclear staining, which are indicators of irreversible thermal damage. Control tissues appeared undamaged.

Due to all these positive developments, the design and fabrication of new types of plasmonic metallic nanostructures have seen a flurry of activity. In particular, the unique properties of nanoshells seem to promise a golden future for metallic nanostructures in drug delivery, and it will be fascinating to see what other applications arise in the near future [8-10].

Nanoshells Formed by Polyion Electrostatic Layer-by-Layer Self-Assembly

The layer-by-layer (LbL) nanoencapsulation method involves the formation of an outer nanothick shell around a core that is stable, permeable, compatible, and allows the release of the core material through the shell. In the last decade, electrostatic layer-by-layer self-assembly has been developed as a practical and versatile nanoencapsulation method to form nanoshells. The core templates may be “passive” (such as 50 – 300 nm latex or silica), which later will be dissolved, or “active” and functional (such as drug micro- and nano-crystals). Tailoring of the different components of individual particles becomes important in order to develop these functionalized colloids; i.e. to combine several properties in one core-shell structure. Because of these advantages, electrostatic layer-by-layer assembly has the capacity to employ a great variety of substances as shell constituents as well as core materials. Of recently, only general aspects of the method have been elaborated to demonstrate its potential, and it still has to be further developed and better understood [1, 11-15].

Preparation of LbL Nanoshells

The sequential adsorption of oppositely charged colloids was reported in a seminal paper in 1966 by Iler [16]. The technique of LbL self-assembly for thin films by means of alternate adsorption of oppositely charged linear polyions was then further developed in the early 1990s [17-20]. The basis of the method involves resaturation of polyion adsorption, resulting in the reversal of the terminal surface charges of the film after deposition of each layer.

Layer-by-layer self-assembly can construct an ultrathin film via alternate adsorption of oppositely charged polyions, nanoparticles, and biomolecules. The obtained films have thicknesses in the nanometer range and tunable properties to their environment, such as permeability, solubility, and morphology [12, 21-24]. The development of polyelectrolyte microcapsules is based on LbL assembly on nano- or micro-scale cores, for instance cells, and inorganic or organic particles, including drugs, which have recently gained intensive attention [17, 25-30].

Cores, with diameters ranging from nanometers to microns, are coated with alternating layers of linear polycations, polyanions, and other materials. After dissolving the cores, hollow microcapsules were gained with ordered walls of desired composition, and thicknesses in the range of 5 – 100 nm. The capsules have tunable permeability for molecules of different sizes on the basis of open-and-close mechanisms by adjusting the environmental stimuli [31-37]. These capsules offer broad perspectives in encapsulation, transport, and controllable delivery of drugs, minerals, and proteins. Changing the pH value of solutions induces the formation of tiny pores in the nanometer range, which allows macromolecules to pass through the capsule walls [33, 36]; adjusting solution

ionic strength or adding organic solvent will also influence permeability [34, 35, 37]. These permeability controls are achieved by changing the charge densities of linear polyelectrolytes, which results in relaxing the capsule walls. However, the austere conditions of these methods limit the utilization of them in the biomedical field for controlled drug delivery applications because they are often not consistent with physiological conditions that occur within the human body.

As a standard approach for film preparation on a solid planar support, the following steps are employed [17, 19, 38]:

- Prepare aqueous solutions of polyions, nanoparticles, or proteins at a concentration of 0.1 – 5 mg/mL, and adjust the pH in such a way that the components are oppositely charged.
- Prepare a planar substrate carrying a surface charge for LbL deposition to take place; for example silicon, glass, or quartz.
- Carry out alternate immersions of the substrate in the aqueous solutions for 10 minutes with 1 minute intermediate rinsing in deionized (DI) water. During rinsing, be sure the DI water has a pH that keeps the respective assembled materials properly ionized. Optionally dry the substrate using a stream of nitrogen after each rinse. Drying may hinder the assembly process, and it is not necessary for the procedure.
- Repeat the previous step until all of the desired layers have been assembled.

Figure 2.2 (see page 13) shows the scheme of assembly on a two-dimensional, planar substrate for assembly with polyelectrolytes and nanoparticles.

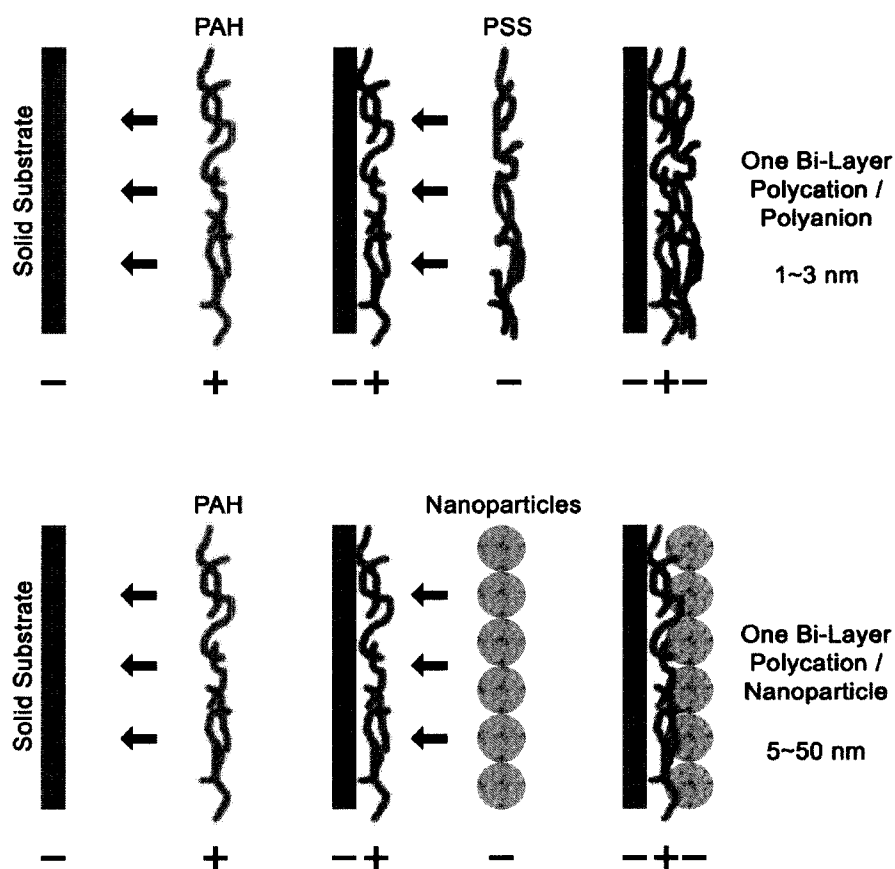


Figure 2.2: Scheme of electrostatic layer-by-layer self-assembly on 2-D substrates with (top) polycations and polyanions, and (bottom) polycations and negatively charged nanoparticles.

The steps for layer-by-layer self-assembly on a 3-D microtemplate are similar to the above procedure with minor modifications [17, 19, 38]:

- Prepare aqueous solutions of polyions, nanoparticles, or proteins at a concentration of 0.1 – 5 mg/mL, and adjust the pH in such a way that the components are oppositely charged.
- Prepare a solution of microtemplates carrying a surface charge for LbL deposition to take place; for example glass beads, MnCO_3 cores, or micronized drug crystals.

- Alternately add the materials used for assembly to the microtemplates for 10 minutes with 1 minute intermediate rinsing by centrifugation in deionized (DI) water. During rinsing, be sure the DI water has a pH that keeps the respective assembled materials properly ionized.
- Repeat the previous step until all of the desired layers have been assembled.

Figure 2.3 gives the scheme of assembly on a three-dimensional microtemplate, followed by core dissolution. The core is dissolved with solvents depending upon the type of core used in the assembly

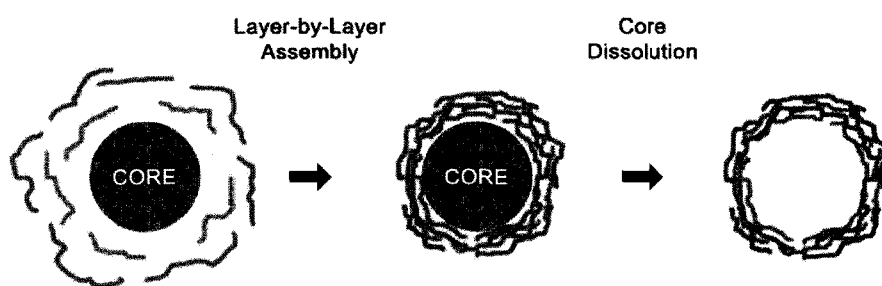


Figure 2.3: Scheme of electrostatic layer-by-layer self-assembly on 3-D microtemplates, or cores, followed by core dissolution.

These methods provide the possibility of designing ultrathin multilayer films with a precision better than one nanometer of defined molecular composition. To date, these methods have been used with more than 50 different charged macromolecules. The polyions predominately used in the assembly are:

- Polycations: chitosan (CH), gelatin A (GA), poly(allylamine hydrochloride) (PAH), poly(dimethyldiallylammonium chloride) (PDDA), polyethylenimine (PEI), poly-L-lysine (PLL), and protamine sulfate C (PS).

- Polyanions: sodium carboxymethyl cellulose (CMC), chondroitin sulfate sodium salt (CS), deoxyribonucleic acid (DNA), dextran sulfate sodium salt (DS), gelatin B (GB), heparin sodium salt (HEP), poly(acrylic acid) (PAA), poly(sodium 4-styrenesulfonate) (PSS), poly(vinyl sulfate) (PVS), sodium alginate (SA), and tannic acid (TA).

These charged materials can be combined with enzymes, antibodies, viruses, and inorganic nanoparticles to produce multifunctional shells in both 2-D and 3-D nanoassembly processes. The architecture of these shells can be designed with nanometer precision to meet different requirements such as thickness, biocompatibility, controlled permeability, targeting, and optical or magnetic properties.

The only crucial factor for successful deposition is the surface charge reversal upon deposition of layers, which can be achieved by choice of proper deposition conditions. Since then, various polyelectrolyte species could be adsorbed onto the surface of solid or liquid materials by means of electrostatic adsorption, forming layered structures with unique properties. It has been established that films can contain more than 1,000 polyelectrolyte multilayers [39]. The universal character of the method does not impose any restriction on the type of polyelectrolyte. The multilayers can also produce diverse shapes when various materials beside polyelectrolytes, such as organic or inorganic nanoparticles and crystals, biomolecules, lipids, or viruses, are used in the coating process. Such coatings produce complicated laminated structures. The use of polymers as the coating component is often advantageous in comparison with employment of their low-molecular weight analogues. Mechanical strength, elasticity, electrical and optical characteristics, and other properties make them unique building

blocks for the creation of composite materials. In addition, the incorporation of proteins and nucleic acids in multilayer films may lead to applications in biosensors and biotechnology [34, 40, 41].

The latter may even provide a base for development of ultrathin multi-step chemical catalysts or photosynthesis systems mimicking plants. Applications can also be found in fabrication of optical devices [42] and gas separation membranes [43]. The efficient use of this unique multilayer coating is interlinked with investigation of their properties. Although the methods of studying multilayer properties are straightforward, they are very often not applicable, or are too time consuming, because of the low amount of material studied. Additionally, the possible influence of the surface used as a support for layer growth further limits these studies. To eliminate the first factor, one should increase drastically the total surface area of the multilayers, which can be done by using colloidal particles as templates [44]. Dissolution of the colloidal cores could avoid the second objection. The derived hollow capsules allow the study of polyelectrolyte multilayers at the liquid–liquid interface, which seems to be very difficult while working on a solid support [18, 45].

After the first publications on nanoshell formation in the 1990s [11-13], the structure of nanoshells has been well characterized, and the procedures to increase the functionality of the nanoshells have been elaborated through efforts of several research groups [13, 17, 41]. For example, pore-openings in these polyion multilayers was first discovered by Mendelsohn *et al.* [31], and then later applied for enzyme loading into nanoshells by Lvov and Caruso [13]. This growth, in the extent of our knowledge regarding LbL nanoshell fabrication, structure, and properties, has led to noteworthy

achievements that have many advantages. However, many practical clinical applications in nanomedicine remain to be developed.

Proving the Nanoshells

For the time-dependent monitoring of LbL assembly *in situ*, a quartz crystal microbalance (QCM) is most often used because of its proven suitability [17, 46, 47]. First of all, the kinetics of the adsorption process can be delineated by the QCM technique, which is indispensable for establishing proper assembly conditions (e.g. saturation adsorption time). Multilayer assembly is generally characterized by means of the quartz crystal microbalance technique in two ways: 1) after drying a sample in a nitrogen stream, the resonance frequency shift is measured and the calculation of the adsorbed mass is done by the Sauerbrey equation; or 2) by monitoring of the resonance frequency during the adsorption process onto one side of the resonator, which is in permanent contact with the polyion solutions. The Sauerbrey equation is given as

$$\Delta f = -\frac{\Delta m f^2}{\rho v}, \quad (2.1)$$

where Δf is the change in frequency, Δm is the change in mass per surface area, f is the frequency of the resonator (9 MHz), ρ is the density of the quartz ($2,650 \text{ kg}\cdot\text{m}^{-3}$), and v is the propagation of sound in quartz ($3,340 \text{ m}\cdot\text{s}^{-1}$). In solution, QCM frequency shifts of about 800 Hz are seen for every adsorption cycle, which is more than that detected for a dried film of PSS/PAH. This difference is ascribed to the strong hydration of the most recently adsorbed layer. The bound water is included in the film, and is removed after drying. This means that most polyion films swell by 40 – 60 % before drying, and that

only 5 – 10 % of the water remains in polyion films after drying. Figure 2.4 shows the thickness of (PSS/PAH)₂(TA/PAH)₃ films adsorbed on QCM resonators.

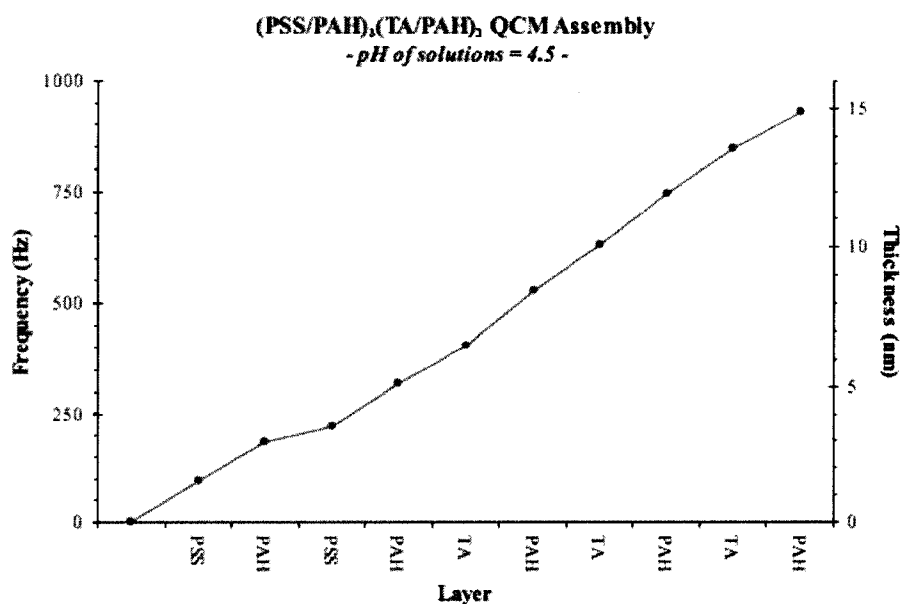


Figure 2.4: Frequency shift and film thickness of each assembled layer for (PSS/PAH)₂(TA/PAH)₃ adsorption on QCM electrodes. The first two precursor layers are PSS/PAH, and the next three layers are TA/PAH. The tannic acid and poly(allylamine hydrochloride) has an average thickness of 1.57 ± 0.11 nm and 1.69 ± 0.35 nm, respectively [45].

To reach a surface charge reversion during linear polyion adsorption, one needs a concentration greater than 5 – 10 M [46]. However, the dependence of polyion layer thickness on concentration is not great because in the concentration range of 0.1 – 5 mg/mL, the PSS/PAH pair yield a similar bi-layer thickness. A further decrease in polyion concentration (using 0.01 mg/mL) decreases the layer thickness of the adsorbed polyion. On the other hand, an increase in the component concentrations to 20 – 30 mg/mL may result in the non-linear (exponential) enlargement of the growth rate with adsorption steps, especially if an intermediate sample rinsing is not long enough [48]. In

addition, at the beginning of the alternate assembly process, one often sees non-linear film growth [46, 49]. Tsukruk *et al.* [50] explained this as an island-type adsorption of the first polyion layer on a weakly charged solid support. In the following 2 – 3 adsorption cycles, these islands spread and cover the entire surface, and further multilayer growth occurs linearly. If a substrate is well charged, then a linear growth with repeatable steps begins earlier.

In addition to measuring weight changes with a QCM resonator, following changes in the UV/Vis spectra is another simple method to control LbL assembly on glass or quartz slides. After every other layer, one can measure the sample UV/Vis spectra and use Beer's law (absorbance is proportional to the material mass) to judge the amount of adsorbed polymer, and whether or not the assembly process is linear with the number of adsorbed layers. In Figure 2.5 (see page 20), the UV/Vis spectra for 5 bi-layers of PAH/TA deposited on a quartz slide is shown. There is a linear increase of absorbance with an increase in the number of layers (see inset); therefore, the mass of the film increased linearly as well. The absorbance maximum at 283 nm corresponds to the neutral form of tannic acid.

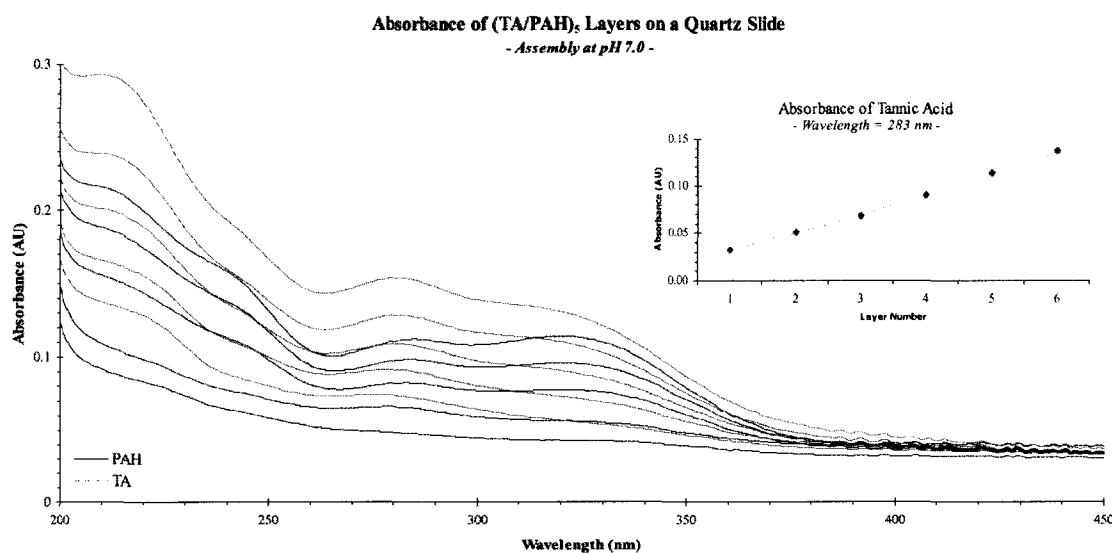


Figure 2.5: The increase in UV/Vis absorbance with an increase in the number of PAH/TA layers deposited on a quartz slide. The absorbance of PAH (black, dotted line) and TA (blue, dashed line) increases with the deposition of material on the quartz slide. The inset shows the linear increase in layer mass of tannic acid [45].

Another method to monitor the assembly process is to ensure the reversal of charge after each polyion coating as shown in Figure 2.6 (see page 21) [51]. For this, the zeta-potential, or surface potential, of the suspended nanoshells are measured after each layer has been applied. Because the adsorption is carried out at a relatively high concentration of polyelectrolytes, a number of ionic groups remain exposed at the interface with the solution, and thus the surface charge is effectively reversed. The reversed surface charge prevents further polyion adsorption. The microtemplates are then washed by centrifugation to remove excess free polyions. The surface is then immersed in a solution of anionic polyelectrolytes. Again, a layer is adsorbed, but now the original surface charge (negative) is restored, and the surface is ready for further assembly. These two steps are repeated alternately until a layer of the desired thickness is obtained. More

than two components can be used in the assembly as long as one condition, a proper alternation of positive and negative charge, is observed [1, 17, 51].

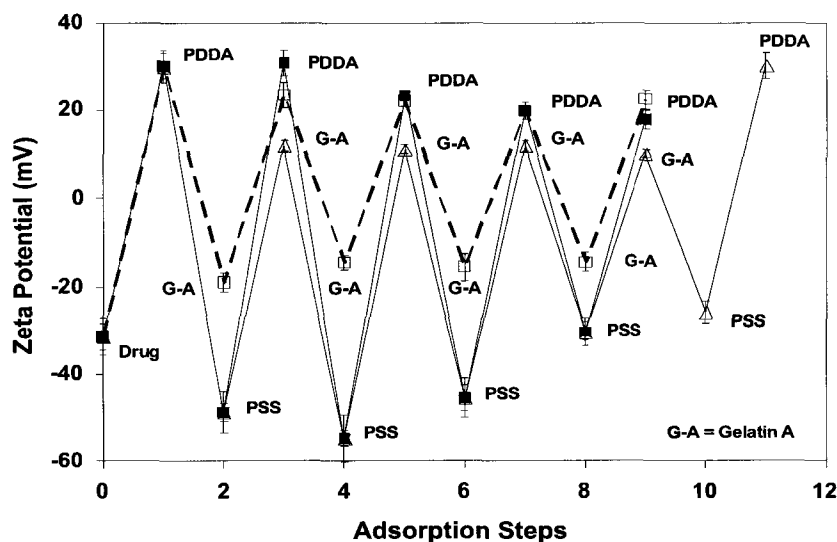


Figure 2.6: Changes in the zeta potential of coated dexamethasone (Dexa) particles as a function of the number of adsorption steps for capsule compositions of $(\text{Dexa/PDDA})_1(\text{PSS/PDDA})_4$ (solid line and solid squares), $(\text{Dexa/PDDA})_1(\text{Gelatin A/PDDA})_4$ (broken line and open squares), and $(\text{Dexa/PDDA})_1(\text{PSS/Gelatin A})_4$ (solid line and open triangles) [51].

More detailed structural information can be obtained from X-ray and neutron reflectivity data. X-ray or neutron reflectivity measurements of polyion films show patterns with profound intensity oscillations, or Kiessig fringes, due to the interference of radiation beams reflected from the interfaces [52]. From the periodicity of these oscillations, one can calculate the film thickness (with the help of the Bragg-like equation and taking into account refraction phenomena, which are essential at small-angles). Growth steps of 1.1 – 2.0 nm for a bi-layer of polyelectrolytes are typical for alternate linear polyion assembly, and a thickness of one layer often equals to half of this value [53]. These values correspond to a polyion cross-section, and show that in one cycle of

excessive adsorption, approximately a one-monolayer coverage of the substrate takes place. The nanoparticle/polyion bi-layer thickness is determined by the diameter of the particles. Model fitting of X-ray data gives a surface roughness of the polyion film on the order of 1 nm, while atomic force microscopy and scanning electron microscopy data reveal a surface roughness of 1 – 2 nm [52]. Polyion films are insoluble in water and in many organic solvents, and are stable to 250 – 280 °C [54].

The polycation/polyanion bi-layer thickness depends on the charge density of the polyions. It was shown that more than 10 % of polyion side groups have to be ionized for a stable reproducible multilayer assembly via alternate electrostatic adsorption [55]. High ionization of polyions results in a smaller step of film growth (1 – 2 nm), and lower ionization gives a larger growth step (3 – 6 nm). It can be reached either by adding salt to a polyion solution (as discussed above for strong polyelectrolytes, such as PDDA and PSS), or by varying the pH for weak polyelectrolytes [21].

Influence of the Core on Nanoshell Properties

So far it has been shown that the procedure of LbL nanoshell formation is a multi-step process. Though capsule properties depend strongly on the choice of polyelectrolytes employed, adsorption conditions, and the number of layers, determining the success of an experiment is based on the proper choice of a core for assembly to take place [39]. This is especially important when fabricating intact capsules consisting only of the material used during the coating. The process of core dissolution should result in 100 % elimination of the core without affecting the multilayers. In fact, the molecular weight of core components is typically a hundred times more than that of the polymers forming the

shell, and the task of complete core removal seems to be complicated from a chemical point of view. At present, cores that have been exploited as templates for hollow capsules can be classified into three groups differing by dissolution properties and chemical interactions with components of the shell [39].

The first class of cores are organic cores made of water-insoluble oligomers including the widely studied melamine formaldehyde (MF) cores dissolvable at low pH and in some organic solvents, and polystyrene (PS) cores soluble in tetrahydrofuran (THF) and bio-friendly polylactic acid/polylactic-co-glycolic acid (PLA/PLGA).

The second class of cores are cores that dissolve into small molecules and ions. These can be either ionic or molecular crystals soluble in acidic or basic conditions, or in an organic solvent. At present, different carbonate particles (CaCO_3 , CdCO_3 , and MnCO_3) [32], and SiO_2 particles [56], have been used for multilayer templating. The main advantage of exploitation of such inorganic particles is the absence of osmotic stress upon dissolution, and complete elimination of the cores.

The third class of cores are those subjected to strong oxidation. A biological cell is a typical example of this kind of core. For example, the assembly of polyelectrolyte multilayers can be performed using fixed erythrocyte cells as templates [57, 58]. The removal of the cell cores can be achieved by oxidation with sodium hypochlorite solution. The main effect of changing the core type is that the employment of a different core material will result in different permeability properties of the shell.

Barrier Properties of LbL Assembled Nanoshells

The barrier properties of nanoshells formed by LbL self-assembly depend on film thickness, ionic strength, charge of the permeating molecule, temperature annealing, resealing by additional layers, and chemical modification. If the permeability of the polyelectrolyte multilayer is provided by diffusion through the entangled polymer network, it should scale with the inverse of the layer thickness. However, most studies show that the permeability decreases with increasing layer numbers much faster than expected from a straightforward thickness increase. Only from approximately eight layers onward does the permeability multiplied by the shell thickness become constant, indicating that the permeability is now controlled by the thickness increase, and the diffusion-limiting region is the properties of the polyelectrolyte layer [59]. Normally, the deeper layers are denser resulting in a five-fold reduction of the estimated diffusion coefficient, while the loose structure of the interfacial layers leads to a very slow increase in the dissolution time. This means that only presence of the internal dense layers can slow down the dissolution time. For thinner walls, the drastic dependence on shell thickness may be explained either by the existence of pores that are successively closed by further layer deposition, or by a thickness dependent diffusion coefficient. Diffusion dependent on layer depth was indeed observed when the diffusion of polar labels in planar polyelectrolyte films was studied [59].

Another parameter that can influence the multilayer structure is the ionic strength [39]. It has been shown that the multilayer structure is affected if the salt concentration is changed once the film is built up. Polyelectrolyte multilayer vesicles can be subjected to temperature treatment, which significantly influences their properties. For example, at

temperatures up to 95 °C, the polyelectrolyte capsules keep their integrity, but undergo irreversible structural changes [60]. The resulting structure is characterized by decreasing the capsule diameter while simultaneously increasing the shell thickness as revealed by scanning force microscopy. From a thermodynamic point of view, this effect can be explained by approaching the equilibrium state of the polyelectrolyte complexes. In another example, hollow capsules were fabricated by LbL deposition of oppositely charged diblock co-polymers each containing a poly(N-isopropylacrylamide) (PNIPAM) block and a charged negative or positive block (20 mol %) [61]. PNIPAM is known to undergo a phase transition at a temperature of 32 °C (lower critical solution temperature), after which it is not soluble. This transition is rather sharp and completely reversible upon cooling. The obtained capsules exhibit changes in morphology and permeability at elevated temperatures. However, this process is only partially reversible in the multilayers. Relaxation requires more than a month, which limits their thermosensitivity to one heating cycle.

Chemical modification can be another way to induce the excessive charge into the polyelectrolyte multilayers and change other characteristics of the film. One method proposed is using poly(acrylic acid), partially modified by Fischer esterification with different alcohols, as a multilayer constituent [62]. Depending on the nature of the derivatizing alcohol, the hydrophobicity of the film could be tuned. The hydrophobicity of ester groups was shown to result in advancing water contact angles to more than 100 degrees. Cross-linking of these hydrophobic films via heat-induced amidation stabilized coatings over a wide pH range, but did not significantly influence their permeability. It has been proposed that cross-linking of the reactive groups in the multilayers is

sometimes the only possibility of making films composed of weak polyelectrolytes stable at a wide range of pH and ionic strengths. One example is PAA/PAH multilayers, which readily decompose upon shift of pH or ionic strength, which can be crosslinked in order to gain stability [63]. In contrast, nanoshells composed of PSS/PAH multilayers have semi-permeable properties [38]. They are permeable for small molecules, such as dyes and ions, while under most conditions the high molecular weight compounds are excluded. One of the explanations for this is the much smaller size of the pores in the multilayer film in comparison to the hydrodynamic radius of the permeating molecules.

Filled capsules can also serve as microreactors [34]. This is advantageous because encapsulating enzymes and proteins in macromolecules shields them from inhibitors. This means the activity of enzymes encapsulated is higher as compared with typical values of chemically immobilized enzymes. In addition, the native conformation of proteins, such as hemoglobin, does not change with encapsulation due to contact with nanoshells because there is no change registered in a position of the Soret band, which is very sensitive to changes in the heme conformation. All of these studies showed that the possibility exists to control the capsule permeability as shown in Figure 2.7 (see page 27). This can be desirable for many applications, including drug delivery. This means that the exploration of the permeability properties of capsules and multilayers must be further developed because it promises many possibilities as drug carriers, biosensing, microreactors and catalysts, construction materials, and many others [59].

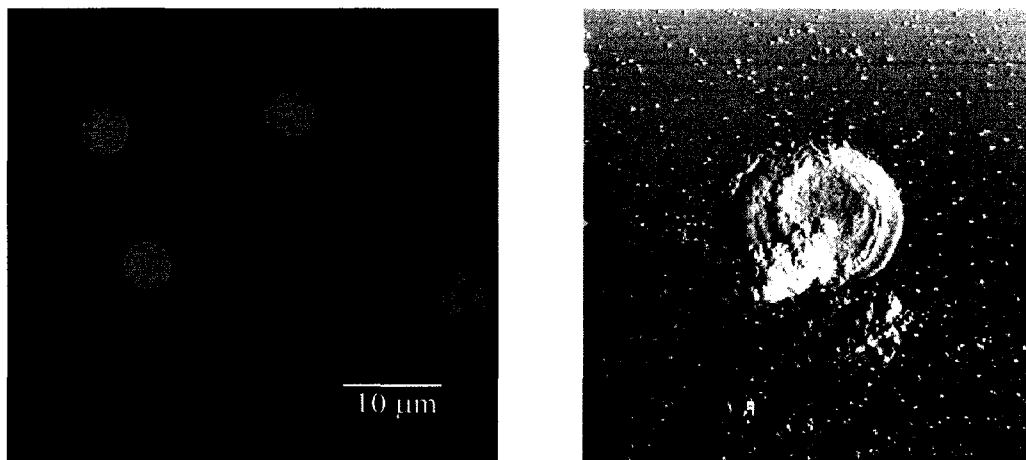


Figure 2.7: (left) Confocal image of polyelectrolyte microcapsules with a wall composition of (PSS/PAH)₅ loaded with FITC-labeled glucose-oxidase, and (right) atomic force microscopy tipping mode image of the same broken dry capsule on mica. Release of the encapsulated material is visible [34].

Controlled Release of Active Pharmaceutical Ingredients Encapsulated by LbL Assembled Nanoshells

A major challenge in the development of carrier systems of submicron dimensions lies in the field of advanced drug formulations, especially when it comprises the elaboration of delivering systems capable to provide sustained release of bioactive materials [39]. Mainly, these bioactive compounds are small molecules with different solubility and diffusion coefficients. If we consider only physical entrapment without any covalent binding in order to develop a delivery system, one has to encapsulate the active molecules within the shell proving certain release characteristics. The potential use of polyelectrolyte capsules with drug entrapped in the nanoshell for controlled drug delivery currently requires more study and is not well established. In contrast, micro-encapsulation of drug microparticles is a well established technique for prolonging release. When microcapsules are coated with appropriate antibodies, they can also be targeted to specific regions in the body. This can lead to lowered overall dosage

requirements, increased drug concentrations in the needed regions, and reduced side effects. Polymer-based and liposome-based systems have been used for drug encapsulation, mostly as unordered drug/polymer conjugates [64-67].

The LbL self-assembly technique based on alternate adsorption of oppositely charged components was developed to add nanometer-thick films to surfaces [11, 12, 31, 68, 69], offering the opportunity to design controlled release systems by encapsulating micron-scale cores with a very thin outer shell. The core must be insoluble under some conditions, such as low pH, and soluble under the conditions at which controlled release is to take place. The release rate generally depends on the thickness of the encapsulating shell and the material used in the coating. Thicker shells lead to longer release times.

Nanoshell Permeability for Low Molecular Weight Compounds

In the first report on controlled release, fluorescent dye microcrystals were used as a model system for controlled release studies [19]. Poly(sodium 4-styrenesulfonate) (PSS) and poly(allylamine hydrochloride) (PAH) were used to form a polyelectrolyte shell on the fluorescein core. Increasing the number of layers decreased the shell permeability and resulted in prolonged dye-core dissolution. Encapsulation of ibuprofen also resulted in prolonged release at different pH values [70]. The ibuprofen dissolution time from capsules with walls built from 15 bi-layers of chitosan/dextran was 40 seconds at pH 7.4, compared to 10 seconds with no coating. Therefore, prolongation of the release was minimal.

To determine whether encapsulation by LbL assembly can substantially increase drug release times, the technique was used to assemble polypeptides and polyions on

microcrystals of 5-(aminosulfonyl)-4-chloro-2-[(2-furanylmethyl)amino]benzoic acid, commonly known as furosemide [17]. Furosemide is a diuretic and anti-hypertension drug that is practically insoluble in water. Although the therapeutic effect is fast and intense after oral administration of furosemide, the oral bioavailability of the drug from an immediate release dosage form is poor and highly variable [71]. These problems can potentially be overcome by developing a modified release dosage form. Ai *et al.* encapsulated furosemide microcrystals with polyions and gelatin to control the release of the drug in aqueous solutions (Figure 2.8, see page 30) [17]. In step 1, precursor layers of (PSS/PDDA)₂ were assembled onto positively charged furosemide microcrystals. In step 2, (PSS/Gelatin)₂₋₆ layers were added via LbL self-assembly. In step 3, drug release in aqueous solution was monitored at different pH values. Charged linear polyions and gelatin were alternatively deposited on 5 μm drug microcrystals through LbL self-assembly. Sequential layers of poly(dimethyldiallylammonium chloride) (PDDA) and poly(sodium 4-styrenesulfonate) (PSS) were followed by adsorption of two to six gelatin/PSS bi-layers with corresponding capsule wall thicknesses ranging from 45 to 115 nm. Furosemide release was then determined from the LbL encapsulated crystals under two physiological pH conditions, pH 1.4 (stomach) and pH 7.4 (blood). At both pH values, the release rate of furosemide from the encapsulated particles was reduced by 50 – 300 times (for capsules coated with 2 – 6 bi-layers) compared to uncoated furosemide. The results provide a method of achieving prolonged drug release through self-assembly of polymeric nanoshells on drug microcrystals.

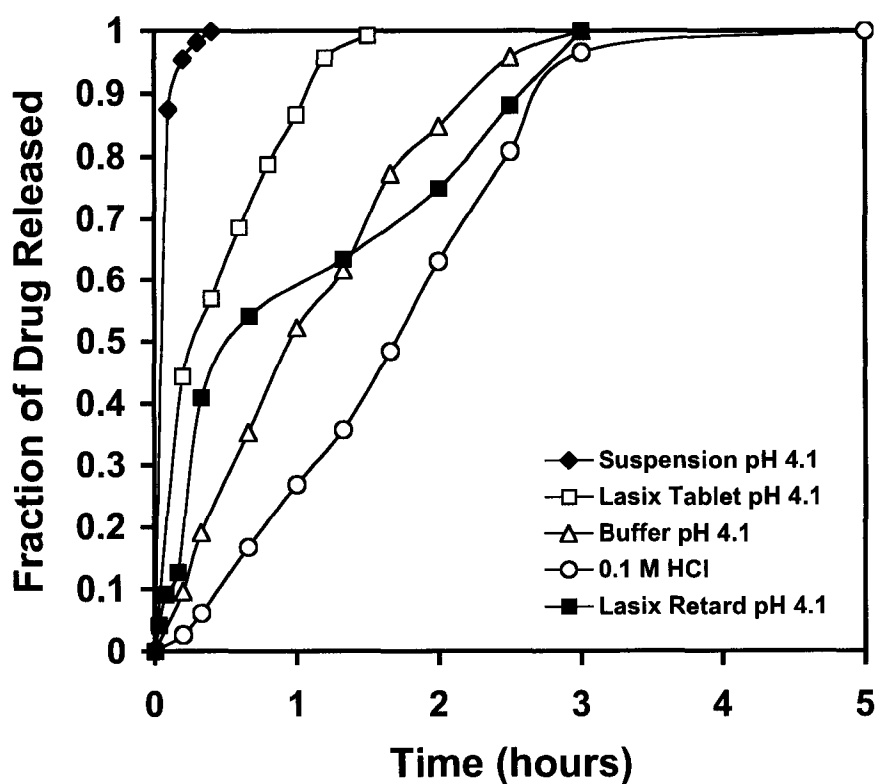
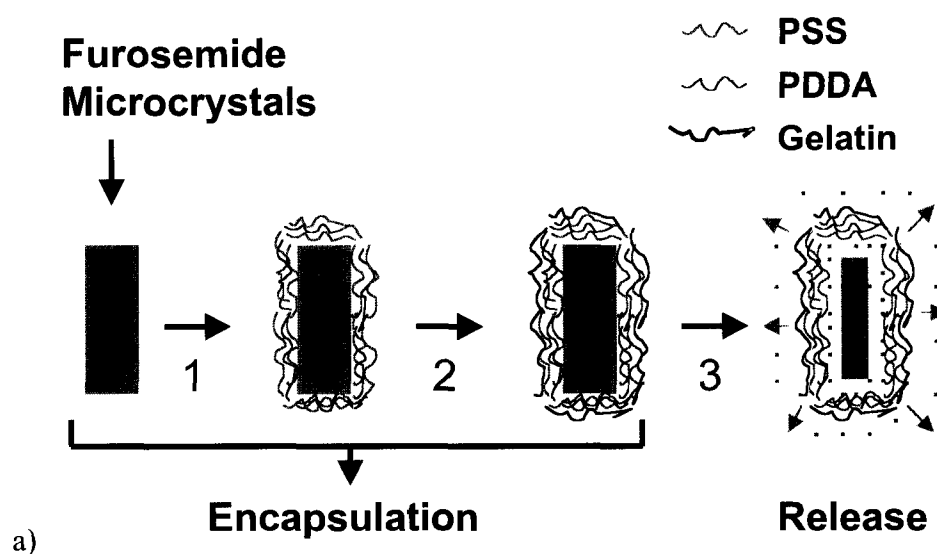


Figure 2.8: (a) Illustration of the furosemide microcrystal encapsulation and release study, and (b) dissolution profiles of $(\text{PSS}/\text{PDDA})_2(\text{PSS}/\text{gelatin})_4$ coated furosemide microparticles compared to uncoated particles and a commercially available tablet in physiologically relevant media [17]. Here, 1 corresponds to 100 % release on the fraction of drug released axis.

In a study that further expanded the application of core-shell structures fabricated by electrostatic layer-by-layer self-assembly for drug delivery, Pargaonkar *et al.* reported the controlled release of dexamethasone from microcrystals encapsulated with a polyelectrolyte shell [51]. The LbL self-assembly process was used to produce dexamethasone particles layered with (PDDA/PSS)₄PDDA, (PDDA/Gelatin A)₄PDDA, (Dexa/PDDA)₁(Gelatin B/PDDA)₄, or (Dexa/PDDA)₁(PSS/Gelatin A)₄(PSS/PDDA)₁. The nanothin shells were characterized by quartz crystal microbalance measurements, microelectrophoresis, microcalorimetry, confocal laser scanning microscopy, and scanning electron microscopy. The *in vitro* release of dexamethasone from the microcapsules suspended in water or carboxymethyl cellulose gels, measured using vertical Franz-type diffusion cells, showed that the assembly of multiple polyelectrolyte layers around these monodispersed cores produced a polyelectrolyte multilayer shell around the drug microcrystals, which allowed for controlled release depending on the composition and the number of layers.

Sonication of dexamethasone during the layering process helped to reduce the particle size of the drug, thereby increasing the dissolution rate of this practically water insoluble drug while also increasing the suspension stability [51]. For negatively charged micronized dexamethasone particles, the effective adsorption of a first layer of PDDA during sonication, as evidenced by microelectrophoresis measurement of the reversal in charge, caused enhanced dispersability of the dexamethasone particles because of the colloidal stabilization produced by the positively charged PDDA coating combined with a significant reduction in particles size to below 2 μm . Stabilizing of the practically monodispersed particles also reduced the Ostwald maturation, or the phenomenon where

small particles gradually increase in size, of the colloidal particles of the scarcely soluble dexamethasone, thereby preserving the reduction in particle size, and the integrity and shape of the original crystals. A schematic of this process is shown in Figure 2.9.

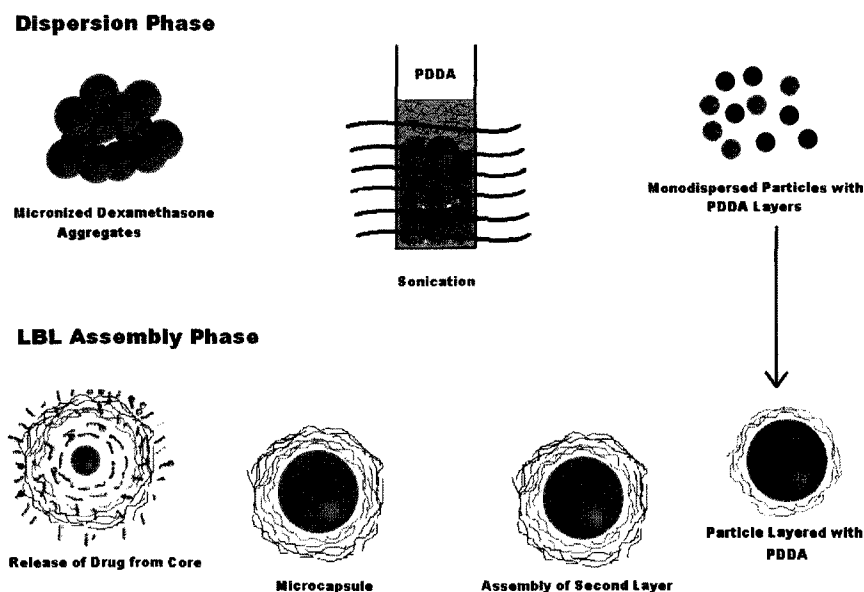


Figure 2.9: Illustration of the monodispersion of micronized dexamethasone drug particles by electrostatic layer-by-layer encapsulation, followed by subsequent controlled release of the drug through the insoluble porous shell [51].

Ye *et al.* showed that indomethacin microcrystals can be directly encapsulated with polysaccharides, sodium alginate, and chitosan multilayers through the LbL self-assembly method [72]. The retention of the drug microcrystal was found to gradually decrease due to its partial dissolution in the deposition solution. It was very significant that increasing deposition temperature from 20 – 60 °C reduced the release rate efficiently, owing to the increase in multilayer thickness and formation of a more ordered multilayer film. This finding provides a new and simple method to control the permeability of the LbL assembled multilayer films.

Nanoshell Permeability for High Molecular Weight Compounds

Deoxyribonucleic acid (DNA) and polynucleotides can be readily assembled in alternation with polycations [73]. Alternate adsorption of 0.1 mg/mL DNA at pH 5.2 with polycations gave multilayers with a DNA/PEI bi-layer thickness of 4.4 nm and DNA/PAH bi-layer thickness of 3.6 nm. Fourier transform infrared (FTIR) spectra confirmed the native doublestranded DNA conformation in DNA/PEI and DNA/PAH multilayers. Coating DNA/polyion films on medical implants may have applications in local gene therapy. In other studies, proteins including lysozyme, horseradish peroxidase, albumin, bacteriorhodopsin, immunoglobulins, glucoamylase, glucose-oxidase (GOx), catalase, glucose isomerase, and diaphorase were used at a concentration of 0.1 – 2.0 mg/mL for LbL assembly [1]. Because the surface structure of the solid support can affect the stability of the proteins, precursor films of alternate PEI/PSS are normally used as standard surfaces. Proteins immobilized in multilayers with strong polyions, such as PSS, PEI, and PDDA, are insoluble in buffers in a pH range between 3 and 10. Protein multilayers with weak polyions are partially soluble in solutions with a pH close to the isoelectric point of one of the components, but such multilayers can be stabilized with crosslinking agents. Assembled proteins are in most cases not denatured [74, 75].

Nano-organized encapsulation of protein microcores, such as insulin nanoparticles in the presence of a high concentration of neutral polymers, was also elaborated with LbL assembly. Uncoated insulin PROMAXX[®] microparticles formed by controlled phase separation from hydrophilic compounds undergo to a fast dissolution if the poly(ethyl glycol) (PEG) concentration is decreased [76]. Insulin release from PROMAXX[®] was extended with LbL encapsulation. After the complex of insulin in the

core, and the first layer of oppositely charged polymer, is formed, the microparticle is stabilized, and adding new polyelectrolyte layers can be continued. Balancing strong interactions of the first polyelectrolyte layer with protein microcores, and easing this interaction by depositing the second oppositely charged polyelectrolyte (polyanion/polycation for positive cores at pH 5.8, and polycation/polyanion for negative cores at pH 7.0), gave the ability to control complexation of the encapsulated proteins, and to reach a sustained insulin release. Fine tuning of the release profile was reached by using additional polyelectrolyte layers.

Therefore, the general idea of the controllable complex formation is as follows: adsorption of the first polyelectrolyte layer results in strong complex formation and very slow release. An addition of the second, oppositely charged polyelectrolyte layer, results in a relaxed complex and quicker release. The third oppositely charged layer again gives slower release, and so on. Simply growing the thickness of the capsule walls within 5 – 10 bi-layers (30 – 60 nm) did not slow insulin release from the microparticles. With this, the concept formulated by Möhwald *et al.* [18, 19, 34], defining LbL multilayers as a tight diffusion barrier with adjustable thickness in the range of 5 – 12 bi-layers, was converted to a new approach where the main role in the controlled release from protein micro-aggregates is given to adjustable interpolyelectrolyte complex formation controlled by alternate polycation/polyanion coatings of 2 – 3 monolayers.

Magnetic Nanoshells

By using LbL assembly, it is also possible to include magnetic nanoparticles, such as magnetite, into the shell, thereby making the entire capsule magnetic. This is shown in

Figure 2.10. In this example, a 400 nm diameter capsule was composed of a glucose-oxidase core covered with a shell composed of two bi-layers of 12 nm diameter magnetite alternated with cationic PEI. Deposition of magnetite nanoparticles provided a magnetic momentum that allowed the nano/bio reactors to be self-stirred, and even be separated by the application of an external magnetic field [77].

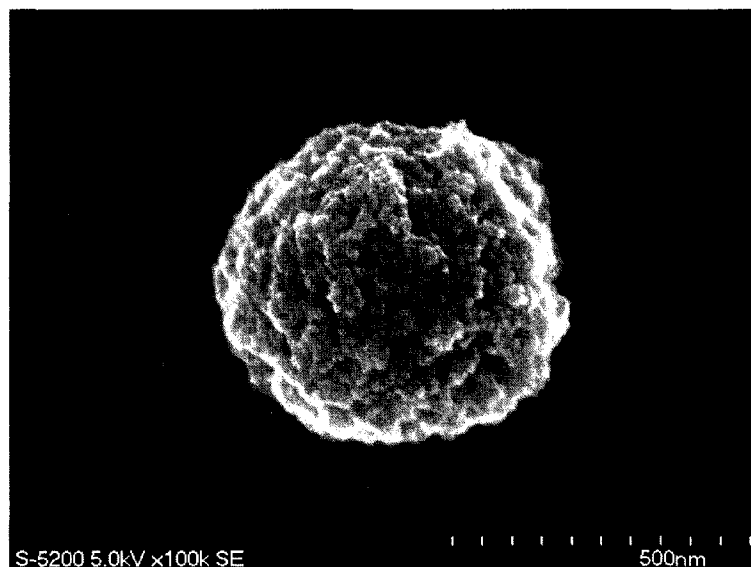


Figure 2.10: A 400 nm diameter glucose-oxidase core coated with $(\text{PSS/PEI})_2(\text{Magnetite/PEI})_2$ shells. The 12 nm diameter magnetite nanoparticles are visible on the surface.

The magnetic fluid hyperthermia (MFH) method applies a high frequency alternating magnetic field to heat superparamagnetic nanoparticles localized in a tumor to destroy diseased cells without damaging healthy tissue [78-80]. In this technique, magnetic nanoparticles are injected in a local tumor site. A high frequency magnetic field agitates the particles rapidly to generate local heating at the tumor site. This localized heating destroys the tumor cells.

CHAPTER 3
PROPERTIES OF MAGNETIC
PARTICLES

Bulk magnetic materials exhibit well-known magnetic properties; however, as these materials are shrunk to the nano-scale their properties change due to the decreased number of domains per particle.

Magnetism in Bulk Materials

Magnetic Anisotropy

Many magnetic materials have a preference for the direction in which the magnetization lies. This preference is known as magnetic anisotropy, and is dependent on the sample shape, crystal symmetry, stress, and directed atomic pair ordering [81, 82]. The uniaxial crystal anisotropy energy density for a magnetic material, μ_a , can be expressed as

$$\mu_a = \frac{U_0}{V_0} = \sum_n K_{un} \sin^{2n} \theta, \quad (3.1)$$

where K_u is the uniaxial anisotropy energy density. The uniaxial crystal anisotropy energy density can be simplified to three terms giving

$$\mu_a = K_{u0} + K_{u1} \sin^2 \theta + K_{u2} \sin^4 \theta. \quad (3.2)$$

$K_{u0} = 0$ for anisotropic properties because it is independent of the orientation of the magnetic movement. For cobalt, at room temperature, K_{u1} and K_{u2} were experimentally found to be $4.1 \times 10^5 \text{ J}\cdot\text{m}^{-3}$ and $1.5 \times 10^5 \text{ J}\cdot\text{m}^{-3}$, respectively [81]. Table 3.1 gives a list of magnetic anisotropy constants for selected materials [81].

Table 3.1: Magnetic anisotropy constants, K_1 and K_2 , for selected materials in $\text{J}\cdot\text{m}^{-3}$ [81]. K_{u1} and K_{u2} , for cobalt, are listed under K_1 and K_2 , respectively.

	$(T = 4.2 \text{ K})$		$(T = 300 \text{ K})$	
	K_1	K_2	K_1	K_2
Fe	5.2×10^4	-1.8×10^4	4.8×10^4	-1.0×10^4
Co ^u	7.0×10^5	1.8×10^5	4.1×10^5	1.5×10^5
Ni	-12.0×10^4	3.0×10^4	-4.5×10^3	-2.3×10^3
Fe ₃ O ₄	-2.0×10^4	–	-0.9×10^4	–

^u K_{u1} and K_{u2} are listed under K_1 and K_2 , respectively.

Plugging in these values for cobalt, the uniaxial crystal anisotropy energy density becomes

$$\mu_a = 4.1 \times 10^5 \sin^2 \theta + 1.5 \times 10^5 \sin^4 \theta, \quad (3.3)$$

where μ_a is in terms of $\text{J}\cdot\text{m}^{-3}$. A graph of the uniaxial crystal anisotropy energy density is given in Figure 3.1 (see page 38). When a magnetic field is applied, the magnetization seeks the lowest energy orientation along the $\pm z$ -axis, or easy axis.

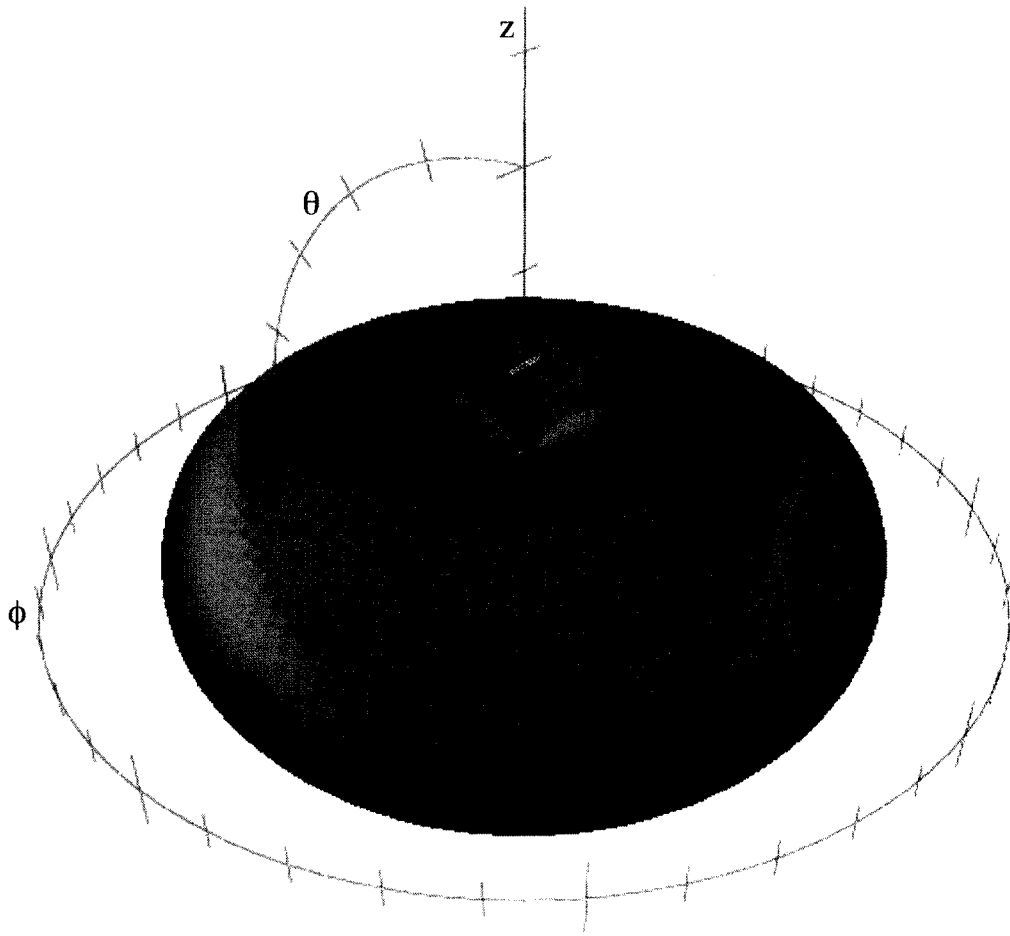


Figure 3.1: Anisotropy energy surface for cobalt. Cobalt naturally aligns to the z -axis, or easy-axis, because that is where the lowest anisotropy energy is located.

Magnetic Domains

Magnetic materials are composed of several magnetic domains throughout the material, each of which has a separate magnetization. The combined magnetization of these domains gives the material a net magnetization, which is observable on the macro-scale. Soft magnetic materials consist of many randomly orientated domains, which give the material a net magnetization of nearly zero when no external magnetic field is present [81].

Domains are formed to reduce the magnetostatic energy of a finite, uniformly magnetized sample. For uniaxial anisotropy materials, such as cobalt, the magnetization vectors in adjacent domains are antiparallel to each other, or 180° to each other. The energy is reduced by a gradual reversal in direction over N atomic distances within the domain wall, where at one domain boundary $\theta(z)$ approaches 0, at the center of the domain wall $\theta(z)$ is $\pi/2$, and at the opposite domain boundary $\theta(z)$ approaches π as shown in Figure 3.2.

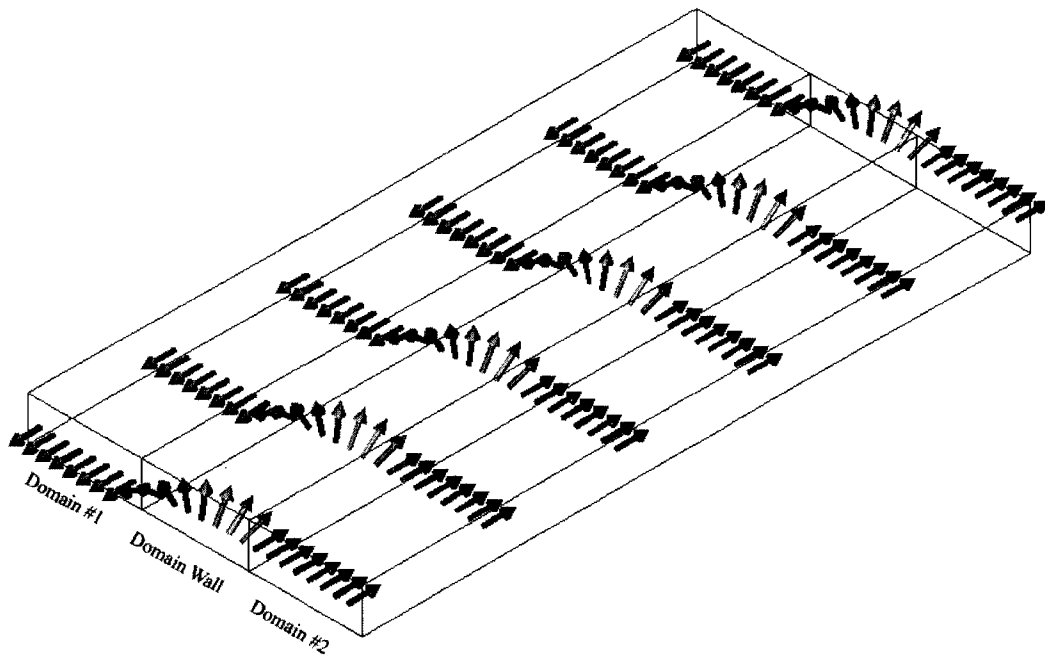


Figure 3.2: Schematic of a ferromagnetic material containing a 180° domain wall. Domain #1 (blue arrows, left) and domain #2 (red arrows, right) have magnetization vectors 180° to each other. The domain wall (middle arrows) is composed of N atomic distances, and is where the transition from one domain to another takes place.

The analytical form for the magnetization orientation profile, $\theta(z)$, is given by

$$\theta(z) = -\arctan \left[\sinh \left(\frac{\pi z}{\delta} \right) \right] + \frac{\pi}{2}, \quad (3.4)$$

where z is the distance in nm and δ is

$$\delta = \pi \left(\frac{A}{K_u} \right)^{1/2}, \quad (3.5)$$

where A is the exchange stiffness constant and K_u is the uniaxial anisotropy energy density. The domain wall thickness, δ_{dw} , can also be calculated using

$$\delta_{dw} = \pi \left(\frac{A}{K_u} \right)^{1/2}. \quad (3.6)$$

This is equal to δ given in Equation 3.5. A graph of the magnetization orientation profile, along with the domain wall thickness, is given in Figure 3.3 (see page 41) for cobalt. The exchange stiffness constant and uniaxial anisotropy energy density are $1 \times 10^{-11} \text{ J}\cdot\text{m}^{-1}$ and $4.1 \times 10^5 \text{ J}\cdot\text{m}^{-3}$, respectively, for cobalt [81]. The domain wall thickness for cobalt is calculated to be approximately 15.5 nm. As the size of magnetic particles is reduced to the nano-scale, the number of domains in the material decreases to one, and no domain wall exists.

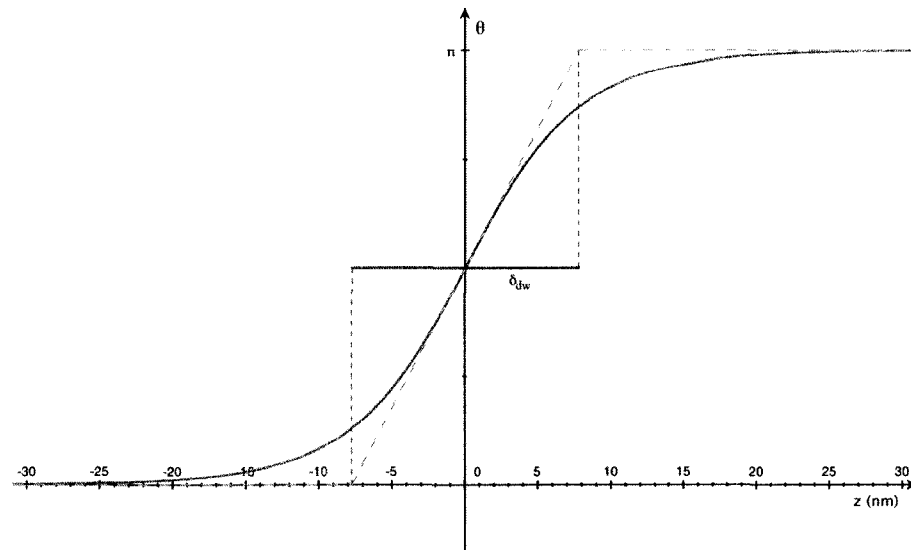


Figure 3.3: Graph showing the magnetization orientation profile and the domain wall thickness for cobalt. The magnetization orientation profile is represented by the red line, and the domain wall thickness, $\delta_{dw} = 15.5$ nm, is shown in blue.

Magnetism in Nano-Scale Materials

Definition of Nano-Scale Materials

Nano-scale materials can be defined as materials with one or more dimensions in the nano-regime, or less than 100 nm in each dimension. These materials have unique properties not achievable in their bulk form [81]. A 1-dimensional nano-scale material would have one of its dimensions less than 100 nm, for example a thin-film (Figure 3.4a, see page 42); a 2-dimensional nano-scale materials would have two of its dimensions less than 100 nm, for example a rod (Figure 3.4b, see page 42); and a 3-dimensional nano-scale material would have all three of its dimensions less than 100 nm, for example a nanoparticle (Figure 3.4c, see page 42).

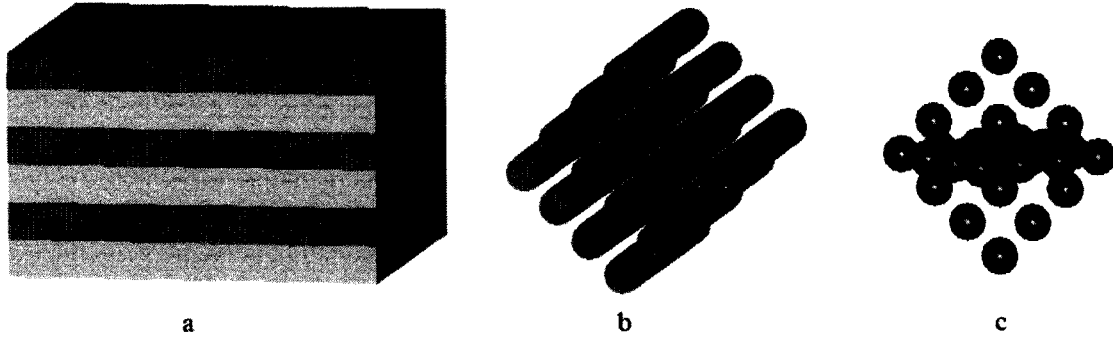


Figure 3.4: (a) 1-dimensional, (b) 2-dimensional, and (c) 3-dimensional nano-scale materials represented by stacked thin-films, rods, and particles, respectively. The small dimensions are 100 nm each. Here, the large dimensions are 1 μm each; however, any dimension over 100 nm is considered a large dimension for nano-scale objects.

Superparamagnetism

The superparamagnetic particle size limit, r_0 , can be defined as

$$r_0 = \left(\frac{9k_b T}{K_u} \right)^{1/3}, \quad (3.7)$$

where k_b is the Boltzmann constant ($1.38 \times 10^{-23} \text{ J}\cdot\text{K}^{-1}$), T is the temperature in degrees Kelvin (room temperature is $\sim 300 \text{ K}$), and K_u is the uniaxial anisotropy energy density ($4.1 \times 10^5 \text{ J}\cdot\text{m}^{-3}$ for cobalt). For cobalt, this limit is approximately 4.4 nm in diameter.

Similarly, the single-domain limit, r_c , can be calculated as

$$r_c \approx 9 \frac{\sqrt{AK_u}}{\mu_0 M_s^2}, \quad (3.8)$$

where A is the exchange stiffness constant ($1 \times 10^{-11} \text{ J}\cdot\text{m}^{-1}$), μ_0 is the free space permeability constant ($4\pi \times 10^{-7} \text{ H}\cdot\text{m}^{-1}$), and M_s is the magnetic saturation in $\text{A}\cdot\text{m}^{-1}$.

Using Equation 3.8, $\mu_0 M_s$ can be plotted as a function of r_c to obtain the critical radius of cobalt as shown in Figure 3.5 (see page 43).

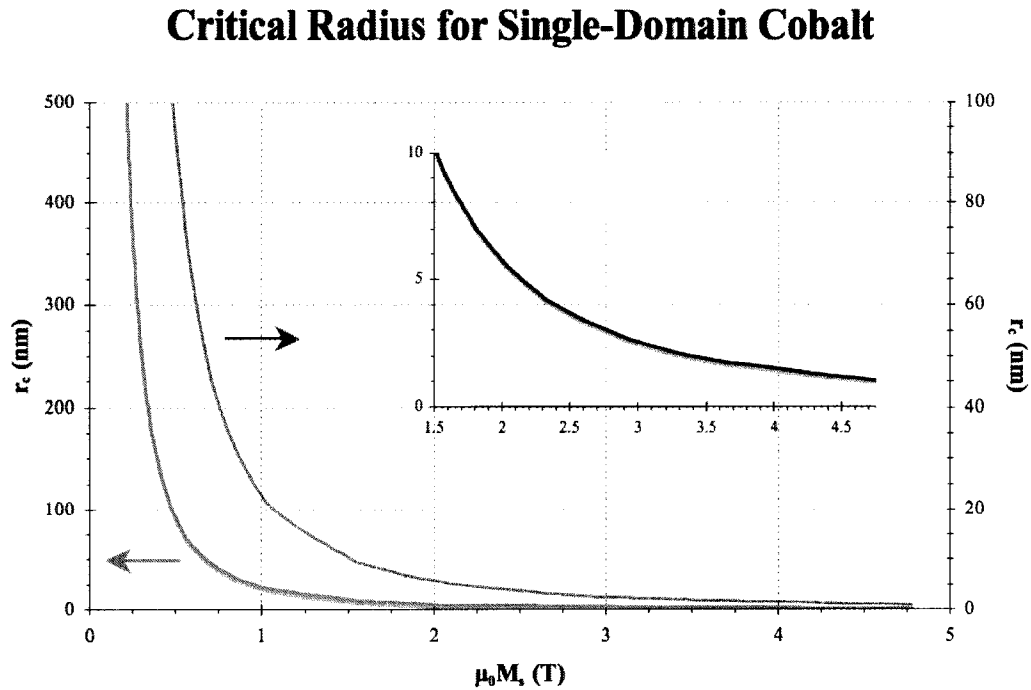


Figure 3.5: Critical radius for single-domain behavior versus saturation magnetization for spherical particles of cobalt. The blue line shows r_c for 0 – 500 nm, the red line zooms in to show r_c for 0 – 100 nm, and the green line zooms in further to show r_c for 0 – 10 nm.

The size of a magnetic particle cannot be reduced indefinitely because the particle's useful magnetic properties will diminish [81]. Below the superparamagnetic particle size limit, thermal energy may be large enough to overcome the magnetization of the particle. For these small particles, magnetization is spontaneous, and demagnetization occurs as quickly as an external field is turned off [81]. The magnetization is uniform over the entire particle at any instant. These superparamagnetic particles have a larger response to an external magnetic field than paramagnetic material because the local moment has a magnitude of $N'\mu_m$ instead of μ_m , and the susceptibility of a superparamagnet is increased $(N')^2$ -fold [81].

Hysteresis curves of superparamagnetic particles resemble those of ferromagnetic materials with two unique differences [81]:

- the approach to saturation follows a Langevin behavior; and
- there is no coercivity.

Superparamagnetic demagnetization occurs without coercivity because it is not the result of an applied magnetic field, but of thermal energy. The demagnetization effect of superparamagnetic materials indicates that these materials have no memory, and have the ability to disperse without the application of external magnetic fields; whereas ferromagnetic materials tend to retain memory, even after the external magnetic field is removed, leaving the particles magnetically attracted to each other.

Superparamagnetic particles will be used in this work to enhance the release of macromolecules through polyelectrolyte shells fabricated via layer-by-layer self-assembly. These particles will allow the capsules to be “focused” to a specified location using a permanent magnet through magnetic attraction, and “switched on” using low frequency, alternating magnetic fields by agitating the particles in the polymer matrix. The release conditions are novel in that the release does not depend on physiological conditions within the body, but on external magnetic fields, which can be applied when needed, transforming polyelectrolyte microcapsules into nano/bio robots for enhanced drug release.

CHAPTER 4

RELEASE OF PHOR21- β CG(ALA) POLYPEPTIDE INCORPORATED IN A POLYELECTROLYTE SHELL

Introduction

The use of layer-by-layer (LbL) nanoassembled multilayers as drug carrier systems has been studied widely by a number of research groups. Typically, drugs were loaded in polyelectrolyte nanocapsules, where adjustable, self-assembled, multilayer walls served as diffusion barriers giving 1 ~ 4 hours release time [17, 70, 72]. The procedure was useful for drugs that do not aggregate and lose their potency at higher concentrations. Less attention was given to the inclusion of drug molecules as an intrinsic component of the multilayers by alternating the assembly of the drug molecules with oppositely charged polyelectrolytes. Such an approach could avoid the preparation of highly concentrated drug suspensions. Being tightly bound within the polyelectrolyte multilayers, such drug molecules could be released much slower in a sustained fashion, thus retaining their biological activity. Different kinds of dye molecules (indole blue, chromotrope 2R, methylene blue, rhodamine 6G), as well as plasmid DNA induced in the polyelectrolyte multilayers, have been investigated for their release according to varying

environmental conditions [83-87]. Numerous studies have been concentrated on the stability of self-assembled polyelectrolyte layers on either planar or spherical surfaces; and further studies have been directed to the possibility of assembling drugs directly in the polyelectrolyte layers for delivery. The polyelectrolyte layers can prevent peptide degradation through proteolysis, and can serve as a storage device.

Most of the current LbL drug delivery studies have been conducted on planar or spherical surfaces with polyelectrolyte materials as the controlling release membrane. Nanoparticles have recently shown great promise in biomedical and biotechnological applications. The nanometer size ranges of the particles offer distinct advantages for drug delivery; nanoparticles can penetrate deep into tissues through fine capillaries. Common materials used in nanoparticle fabrication include iron oxide, gold, silica, and polymers. For silica, its surface can be modified to contain avidin, sulfide, amine, or carboxylate groups, which facilitate not only in bioconjugation, but introduce surface charges for LbL nanoassembly. Up to now, silica nanoparticles have been widely applied in the biomedical field, such as in biomarkers for cell imaging, biosensor applications, DNA detection and protection, etc. [88, 89]. Here, silica nanoparticles were used as model drug carriers to study the release of Phor21- β CG(ala) drug molecules introduced in the nanoshells.

Phor21- β CG(ala) is an anticancer polypeptide used to treat breast tumors [90]. In this study, a newly developed membrane disrupting peptide, Phor21, was used, which is more potent in destroying cancer cells than Hecate or Phor14. Phor21 is a membrane disrupting lytic peptide, similar to those identified as defense agents in insects, invertebrates, vertebrates, and humans [90]. Phor21- β CG(ala) contains 36 amino acid

residues, with an amino acid sequence of KFAKFAKKFAKFAKKFAKFAK-SYAVASAQAALAARR. The conjugated gonadotropin ligand, β CG(ala), with an amino acid sequence of SYAVASAQAALAARR, facilitates and increases the cell selectivity of the lytic peptide. In the β CG(ala) fragment, the cysteins were replaced by alanines, which increased the synthetic yield of this fragment. The calculated isoelectric point of the peptide is 11.4.

In this work, multilayer nanoshells of the cationic peptide Phor21- β CG(ala), assembled in alternation with biocompatible, biodegradable polyanions like gelatin B and sodium carboxymethyl cellulose on silica core nanoparticles, were studied. Furthermore, multilayer decomposition and peptide release with characteristic times of 20 – 30 hours were analyzed.

Materials and Methods

Sodium carboxymethyl cellulose (CMC, MW 90,000 dal) and gelatin from bovine skin, type B (Gelatin B, MW 20,000 – 25,000 dal) were purchased from Sigma Aldrich and used without further treatment. Anticancer lytic polypeptide Phor21- β CG(ala) (MW 4,010 dal) was obtained in the lyophilized form from the National Cancer Institute (Bethesda, MD). Silica nanoparticles (diameter 450 nm \pm 30 nm) were purchase from Polysciences Inc. in a 5.7 % aqueous dispersion. The release media used in this work was 0.9 % sodium chloride injection USP solution (B. Braun Medical Inc., pH 5.6).

Preparation of Silica-Peptide Nanoshells

Deposition of polyelectrolyte multilayers on silica nanoparticles was accomplished using a procedure elucidated elsewhere [13, 91]. In this case, CMC and

gelatin B were negatively charged, while Phor21- β CG(ala) was positively charged in deionized (DI) water. Typically, CMC or gelatin B (0.5 mL of 2 mg/mL in 0.2 M NaCl) and Phor21- β CG(ala) solutions (0.5 mL of 1 mg/mL in 0.2 M NaCl) were alternately added into 1.5 mL silica particle suspensions (20 mg silica total mass). Adsorption of the polyelectrolyte layer was completed within 30 minutes at 4 °C. Subsequently, three intermediate washings with DI water were made at 4 °C using centrifugation at 2,000 RPM for 10 minutes before the addition of the next layer to remove any remaining polyelectrolytes or peptide from the supernatant solution.

Characterization of Silica-Peptide Nanoshells

The assembly of layers on silica nanocores was confirmed by monitoring quartz crystal microbalance resonance frequency changes (QCM, USI-Systems, Japan), and determining the changes of the electrophoretic potential (ζ -potential) after deposition of every layer using a zeta potential analyzer (Brookhaven Instruments Corporation). After the desired number of layers was obtained, the assembled cores were lyophilized or stored at -20 °C before use.

The amount of peptide adsorbed on the nanoparticles was monitored using UV/Vis absorbance (Agilent model 8543). A 500 μ L solution of 1.0 mg/mL peptide was added into 1.5 mL of 20 mg silica nanoparticle suspensions. After 30 minute adsorption of peptide on silica cores, the cores and solution were centrifuged at 2,000 RPM for 8 minutes and the obtained supernatant was centrifuged again at 5,000 RPM for 10 minutes. The absorbance of the supernatant was checked using UV/Vis at 281 nm. The amount of Phor21- β CG(ala) adsorbed on the cores was calculated by subtracting the

original concentration of peptide with the amount of peptide remaining in the supernatant.

Release Kinetics *In Vitro*

In the peptide release experiments, first the peptide release was evaluated using negatively charged planar glass slides: 20 layers of peptide were alternatingly coated on slides with CMC. The initial and final peptide concentrations were detected by UV/Vis; the amount of peptide adsorbed on the slides was then calculated using the difference of the peptide concentrations. Then, the release kinetics were determined in 0.9 % NaCl USP injection media at 37 °C. The peptide coated glass slides were immersed in the release media while stirring at 800 RPM. The UV absorbance of the release media was measured after certain time intervals by removing the slides. The percentage of peptide released was calculated.

In the second stage, for the peptide released from silica nanoparticles, a similar procedure was carried out to examine the amount of peptide adsorption as mentioned above. A 20 mg batch of silica nanoparticles (15 mg/mL) was coated with a certain number of peptide layers and added into a 2.0 mL release buffer in a centrifuge tube (in a 37 °C water bath) with continuous stirring at 800 RPM. At certain time intervals, a 0.5 mL particle suspension was centrifuged at 5,000 RPM for 10 minutes. The supernatant was checked using UV/Vis with a UV absorbance at 281 nm, and the supernatant was transferred back into the original suspension.

Results

First, the assembly of Phor21- β CG(ala) with CMC and gelatin B on 450 nm SiO₂ nanoparticles was elaborated, and the surface charge using a ζ -potential analyzer was analyzed. Figure 4.1 describes the basic nanoparticle assembly with Phor21- β CG(ala)/(CMC or gelatin B) coatings.

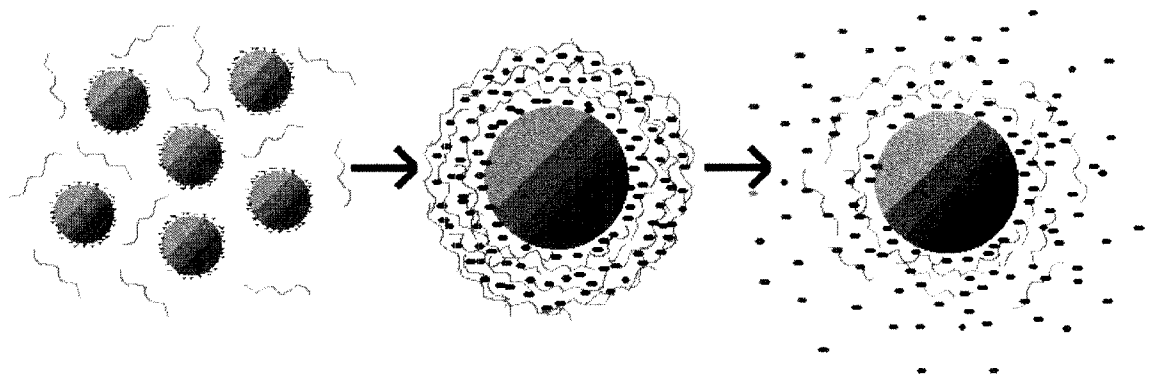


Figure 4.1: Scheme of Phor21- β CG(ala) adsorption on 450 nm silica nanoparticles, and the release of the drug (large, blue spheres = silica cores; small, red dots = Phor21- β CG(ala) peptide; and wavy, green lines = polyelectrolytes).

Figure 4.2 (see page 51) shows the alternation of ζ -potential of the particles with the adsorption of each polyelectrolyte layer. After the washing steps, the silica nanoparticles had a ζ -potential of -70 ± 10 mV. The Phor21- β CG(ala)/CMC adsorption followed the general scheme of alternate adsorption of oppositely charged linear polyelectrolytes [12, 13]. After adsorption of the cationic peptide, the surface potential became positive ($+20 \pm 3$ mV); after consequent deposition of anionic CMC, it became negative (-48 ± 4 mV); and so on until the shell reached a certain number of polyelectrolyte layers. The core surface charges totally reversed during the adsorption process. However, this is not the case when alternating adsorption was conducted using Phor21- β CG(ala) with gelatin B. In this case, with the exception of the first peptide layer, the surface charges did not

totally reverse when the peptide was adsorbed on the cores. The surface charges of the peptide layers remained negative (ca. -10 mV) during the assembly and adsorption process.

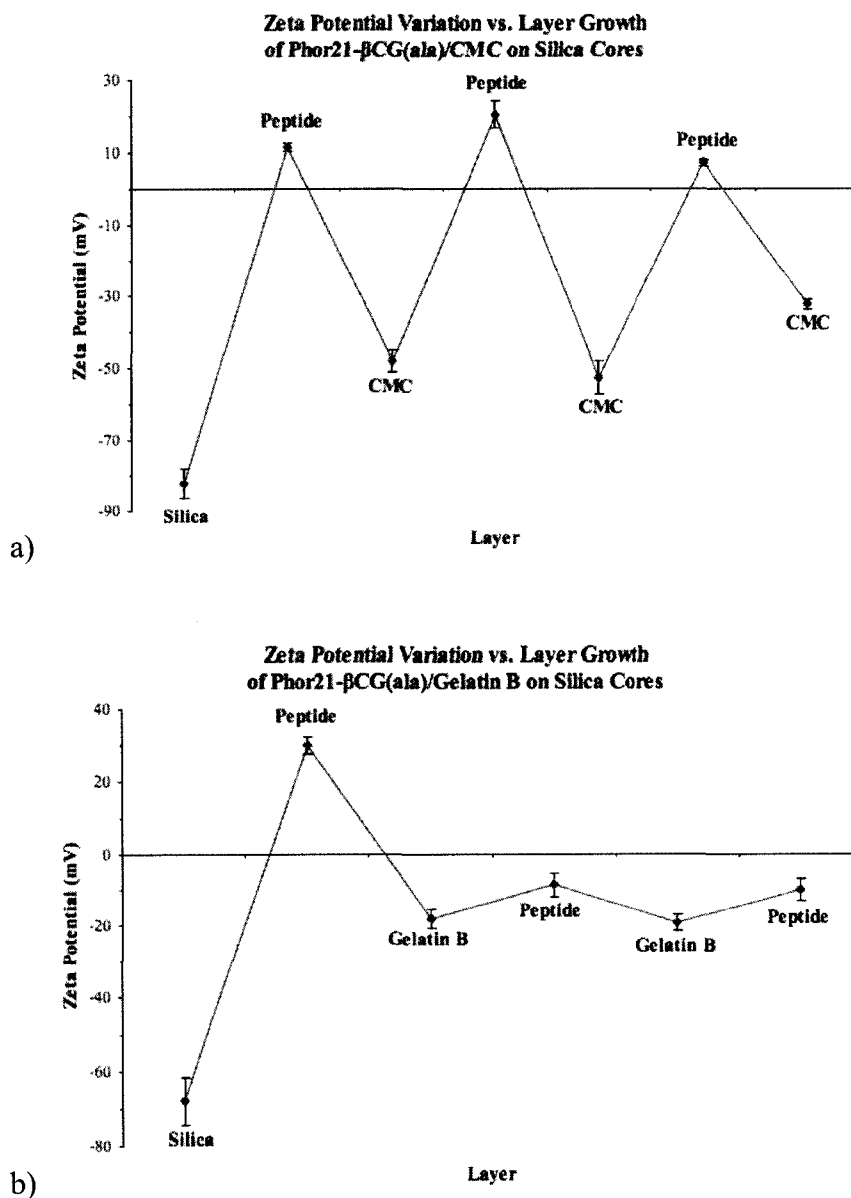


Figure 4.2: Zeta potential of the silica nanoparticles demonstrating the surface changes during adsorption of Phor21- β CG(ala) alternating with (a) sodium carboxymethyl cellulose and (b) gelatin B. The error bars represent one standard deviation from the mean.

The assembly results of the peptide and polyelectrolytes on QCM resonators are shown in Figure 4.3a (see page 53), which monitored the process by the weight addition on every deposition cycle. The plot shows a stable growth of Phor21- β CG(ala) layers alternated with polyanions on QCM resonators. The QCM frequency shift plot in Figure 4.3a (see page 53) shows that the formation of the multilayers corresponding to the planned wall composition of the silica nanoshells, and the layer growths, was rather linear on QCM resonators. The average thickness of peptide layers alternating with CMC was estimated as ca. 0.81 ± 0.18 nm using the Sauerbrey equation [13, 92]. The mass of one peptide layer on 20 mg silica nanoshells thus could be estimated as ca. 0.10 ± 0.02 mg using the QCM data, reaching adsorption efficacy of 20 %. The average thickness of peptide layers was ca. 0.72 ± 0.37 nm. The calculated mass of one peptide layer on 20 mg silica nanoparticles was ca. 0.09 ± 0.02 mg from the QCM data. These values were consistent with the results obtained from peptide/CMC adsorption.

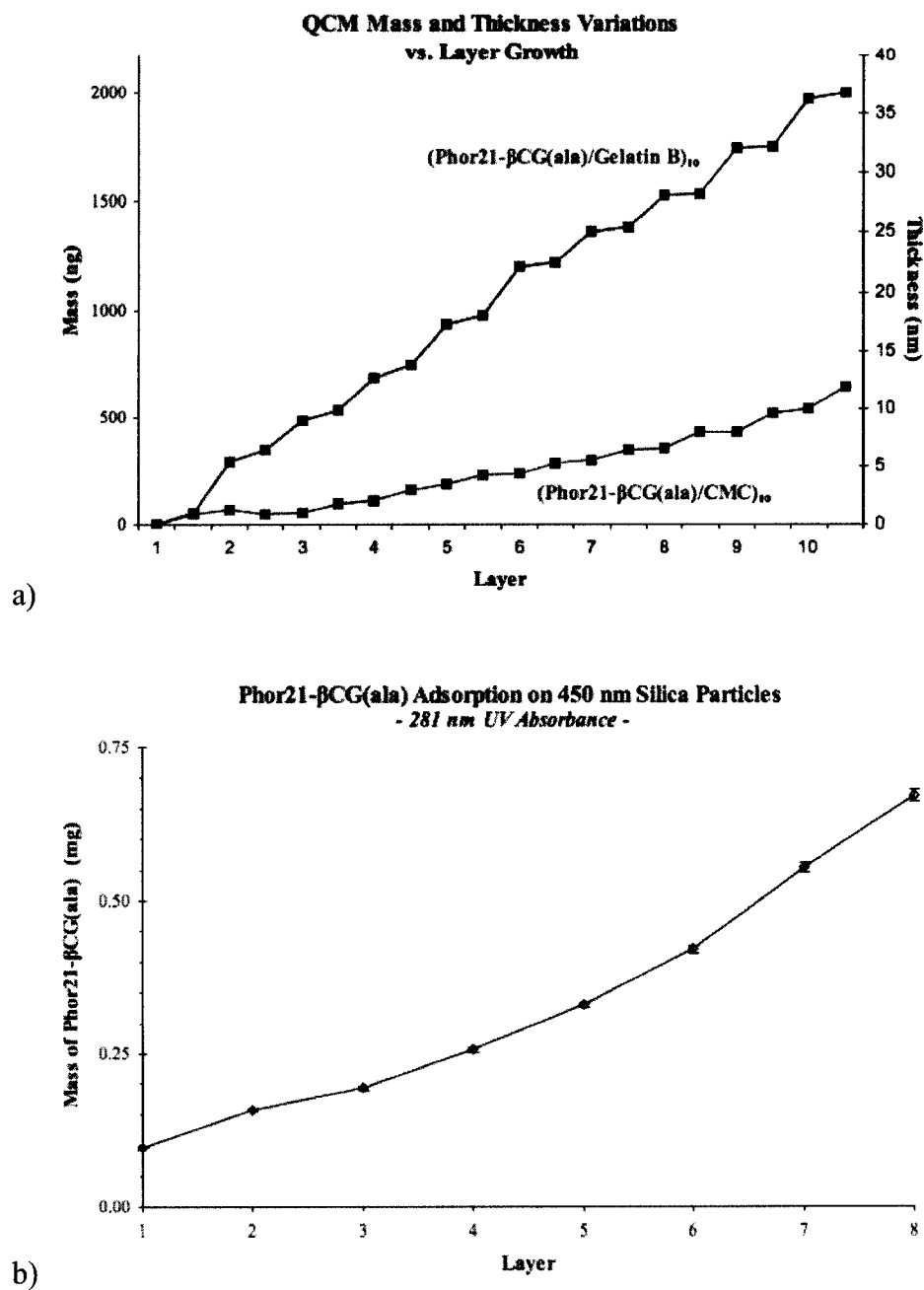


Figure 4.3: (a) QCM and (b) UV/Vis data showing the peptide adsorption on QCM resonators and 450 nm silica particles, respectively. For the UV/Vis data, the peptide assembly was alternated with CMC. The error bars represent one standard deviation from the mean.

Figure 4.3b shows the amount of peptide absorbed on silica nanoparticles. By subtracting the original peptide concentration with the peptide concentration in the

supernatant, the amount of peptide adsorbed on the 20 mg silica nanoparticles alternated with CMC was calculated as ca. 0.26 ± 0.01 mg for four peptide layer coatings and ca. 0.67 ± 0.01 mg for eight peptide layer coatings. The calculated amount of peptide adsorbed from QCM data showed ca. 0.40 ± 0.09 mg for four peptide layer coatings and ca. 0.81 ± 0.18 mg for eight peptide layer coatings.

The kinetics of the decomposition of Phor21- β CG(ala)/CMC multilayers was first elaborated using peptide coated glass slides. The results in Figure 4.4 show that the release of the peptide in 0.9 % NaCl USP injection solution was ca. 16 % after 17 hours.

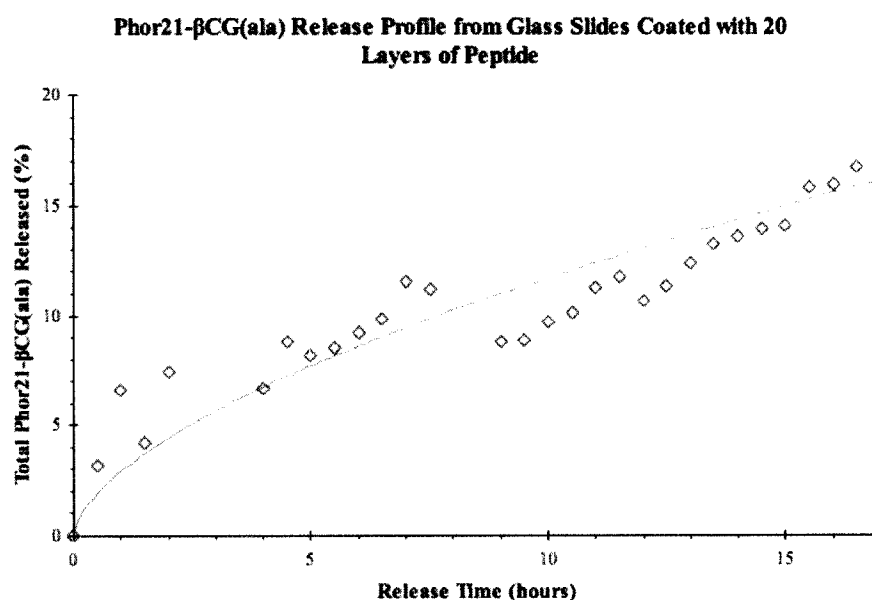


Figure 4.4: Release kinetics of Phor21- β CG(ala) from glass slides coated with 20 layers of peptide in 0.9 % NaCl USP injection media.

The release kinetics from peptide-silica nanoshells are shown in Figure 4.5 (see page 55). The 0.9 % sodium chloride injection USP solution was used as the *in vitro* release media, which kept the peptide active. The release media is biocompatible, non pyrogenic, and can be used in future *in vivo* studies. The results showed that for 4 layer

and 8 layer peptide coatings in alteration with CMC, the release is ca. 18 % for 28 hours. The peptide release rates from the slides and nanoparticles followed an exponential tendency [93].

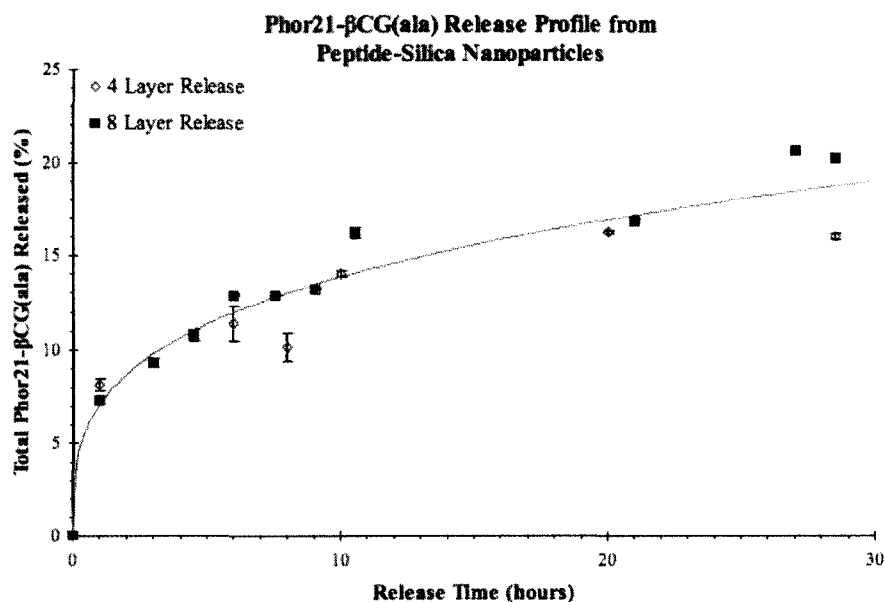


Figure 4.5: Release kinetics of Phor21- β CG(ala) from peptide-silica nanoparticles with four (open diamonds) and eight (closed boxes) peptide layer coatings with CMC as the alternate layer. The error bars represent one standard deviation from the mean.

Discussion

The layer-by-layer assembly procedure resulted in nanoparticles that contained increased amounts of membrane disrupting peptide, Phor21- β CG(ala), which showed sustained release over an extended time period.

The assembly of Phor21- β CG(ala) with CMC and gelatin B on 450 nm SiO₂ nanoparticles was expected to follow the general scheme of alternate adsorption of oppositely charged linear polyelectrolytes [12, 13]. The 450 \pm 30 nm diameter silica cores were used for the drug shell assembly, but their diameter may be taken as small as

100 nm without changing the technique (smaller diameter cores only need larger centrifugation speeds at the sample separation stage). While this pattern was true for silica nanoshells containing CMC, this was not the case when alternating adsorption was conducted using Phor21- β CG(ala) with gelatin B. In this case, the surface charges did not totally reverse when the peptide was adsorbed on the cores, except for the first peptide layer. The surface charges of the peptide layers remained negative (ca. -10 mV) during the assembly and adsorption process. This may suggest weak electrostatic interactions between the molecules of the peptide and gelatin B [94, 95]. Combined with the QCM results, it is still a useful indicator of multilayer film growth on particles, even though they alternated between higher and lower negative values [95].

The assembly results of the peptide and polyelectrolytes on QCM resonators confirmed the formation of the multilayers corresponding to the planned wall composition of the silica nanoshells. The layer growths were linear on QCM resonators.

As to the peptide adsorption with gelatin B, one can see from Figure 4.3a (see page 53) that the frequency decrease is sharper for peptide/gelatin B bi-layers than for peptide/CMC bi-layers. The average thickness of peptide layers was similar regardless of the polyelectrolyte used. The average thickness of peptide layers was 0.72 ± 0.37 nm (CMC) and 0.81 ± 0.18 nm (gelatin B) with estimated peptide amounts of 0.09 – 0.10 mg Phor21- β CG(ala) per 20 mg of silica shells per peptide layer. The substantial frequency decrease was therefore due to the adsorption of gelatin B rather than the peptide adsorption.

Because the QCM experiments showed the peptide adsorption on planar substrates with materials different from spherical silica nanoparticles, it can only

indirectly estimate the amount of peptide adsorbed in LbL multilayers, the amount of peptide/CMC adsorption on silica nanoshells was further examined using the UV/Vis method. By comparing the results obtained from UV/Vis and QCM, one can see that the results obtained from QCM data was about 20 – 50 % higher than the results obtained from UV/Vis data, and the UV/Vis results showed the exponential mass growth of the peptide adsorption, which is different from the linear growth of the QCM results. The reduced peptide adsorption could be due to the centrifugation and strong vortexing applied to wash and resuspend the particles, and might explain the mass differences between the QCM and UV/Vis results. The calculated amount of peptide adsorbed from QCM data showed 0.40 ± 0.09 mg for four peptide layer coatings and 0.81 ± 0.18 mg for eight peptide layer coatings.

Usually, LbL assembled multilayers constructed from strong polyelectrolytes with molecular weight larger than 10,000 are resistant to harsh environments [95]. The stability of layers composed of smaller molecules and weak polyelectrolytes could be affected significantly by surrounding conditions such as pH, ionic strength, enzymes, etc., and can be decomposed slowly. Hiller *et al.* reported that protamine assembled in multilayers on colloidal particles could be exchanged and released up to 90 % [96]. Schüller *et al.* reported that hollow capsules based on deoxyribonucleic acid and spermidine were decomposed after exposure to different concentrations of sodium chloride solutions [97], and Khopade *et al.* reported that the multilayers composed of dextran sulfate sodium salt and drug aminoglycoside tobramycin sulfate can be decomposed in physiological buffer followed by mannitol and water [95].

This data showed insignificant differences in the release kinetics of peptides from four layer compared to eight layer nanoshells. Both indicated a slow release of Phor21- β CG(ala) from LbL multilayers. This indicates the peptide release rate is not increased with an increase in the number of layers. An extrapolation of the release curves predicted that ca. 50 % release will be reached after 7 days or even longer.

Conclusion

The positively charged anticancer peptide, Phor21- β CG(ala), was assembled in organized multilayer shells with sodium carboxymethyl cellulose (CMC) and gelatin B on 450 nm diameter silica nanocores using the LbL technique. ζ -potential experiments confirmed the assembly of nanoshells with drug molecules electrostatically bound into the multilayers. The amount of peptide included in the shell was estimated using both the QCM and UV/Vis methods. The *in vitro* release kinetic results showed that Phor21- β CG(ala) released from silica-peptide nanoshells was ca. 18 % in 28 hours.

Consequently, the encapsulation and sustained systemic release of these peptides could further improve treatment efficacy by avoiding toxicity of systemic exposure at high dosage and preserve the potency of this highly sensitive drug through controlled and sustained release. Layer-by-layer silica-peptide nanoshells may be used for sustained release of a membrane disrupting peptide drug to destroy primary tumors and metastases in an effective and controlled fashion.

Although release of peptide incorporated as part of a polyelectrolyte multilayer shell is novel, the technique is still dependent on physiological conditions such as pH. A

different release technique, not dependent on physiological conditions, needs to be developed. The use of magnetics may be the answer.

CHAPTER 5

CONTROLLABLE PERMEABILITY USING MAGNETIC NANOPARTICLES

Introduction

Another promising way to achieve permeability control is to embed magnetic nanoparticles into capsule walls. The capsules might be modulated by an external oscillating magnetic field to control the permeability when needed, thus control the release of the substances in the capsules. Numerous studies have been conducted on applying magnetic particles to treat human diseases, such as cancer [78-80, 98-102]. A new concept for targeted as well as controlled release of anticancer drugs, using magnetic nanoparticles within a polymeric shell, has been recently proposed [103, 104]. The magnetic fluid hyperthermia (MFH) method applies a high frequency alternating magnetic field to heat superparamagnetic nanoparticles localized in a tumor to destroy diseased cells without damaging healthy tissue [78-80]. Magnetic particles, with diameters ranging from nanometers to millimeters, were also studied to be embedded inside alginate or liposome matrixes combined with drugs and tested for their controllable drug release behavior using a low frequency external magnetic field [98, 99, 102]. Magnetic particles of interest include magnetite, strontium ferrite, manganese ferrite, and others [79, 101]. However, up to now, there is no study about embedding magnetic nanoparticles into walls of hollow capsules, thereby modulating the permeability and

release behavior of the capsules. In this work, superparamagnetic cobalt nanoparticles coated with gold shells (Co@Au nanoparticles) were embedded into polyelectrolyte capsules fabricated with layer-by-layer assembly of poly(sodium 4-styrene sulfonate) and poly(allylamine hydrochloride) (Figure 5.1). Application of low frequency alternating magnetic fields to such magnetic capsules resulted in an increase of their wall permeability; therefore, external magnetic fields may “switch on” unloading of these microcapsules.

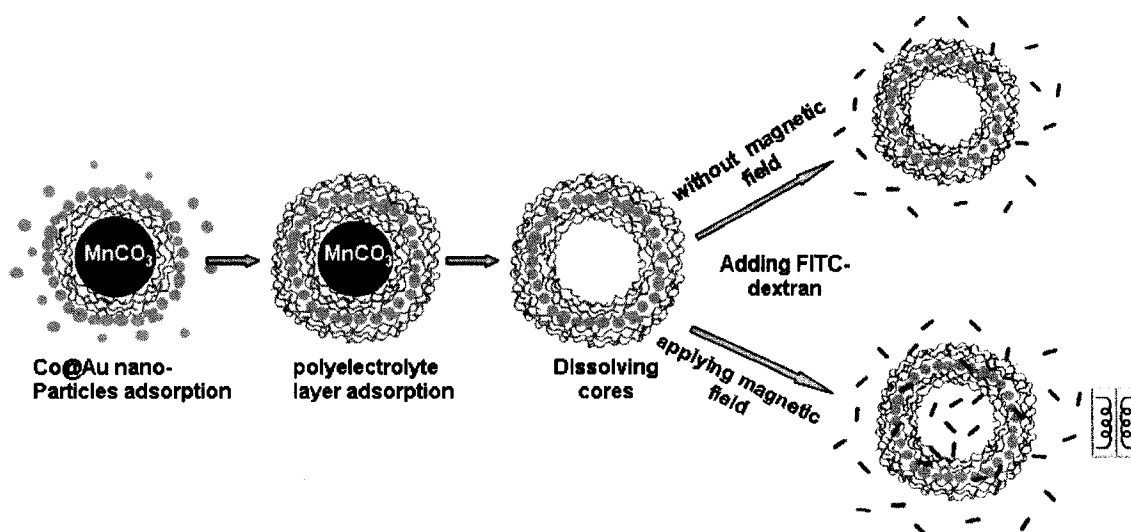


Figure 5.1: Scheme of the assembly and permeability test for microcapsules embedded with Co@Au nanoparticles.

Experimental

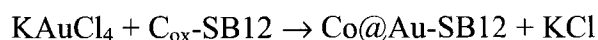
Materials

Poly(sodium 4-styrene sulfonate) (PSS, MW 70,000 dal), poly(allylamine hydrochloride) (PAH, MW 70,000 dal), and poly(diallyldimethylammonium chloride) (PDPA, MW 1,000,000 dal) were used for LbL assembly. Fluorescein isothiocyanate (FITC) and rhodamine B isothiocyanate (RBITC) were used to label dextran and PAH,

respectively, following the procedure described in [26], which helps with capsule visualization under confocal laser scanning microscopy (CLSM). FITC-dextran (MW 2,000,000 dal) was used for capsule permeability tests. Cobalt chloride (anhydrous, beads, 99.99 %, packaged under argon in ampules), potassium tetrachloroaurate III (99.999 %), tetrahydrofuran (THF, 99.9 %, inhibitor free, packaged under nitrogen), lithium hydrotriethyl borate (superhydride) as 1 M solution in THF, dodecyldimethyl 3-sulfopropyl ammonium hydroxide (SB12), and ethanol (reagent grade, anhydrous, water < 0.003 %) were used for the synthesis of Co@Au nanoparticles. All the chemicals were purchased from Sigma Aldrich and used without further treatments.

Co@Au Nanoparticle Fabrication and Characterization

The Co@Au nanoparticles were fabricated using a chemical reduction method [105]. The Co particles were fabricated using dodecyldimethyl 3-sulfopropyl ammonium hydroxide (SB12) as the surfactant to prevent agglomeration, and lithium hydrotriethyl borate (LiBET₃H, superhydride) as the reducing agent. In order to prevent Co nanoparticles from oxidization, a novel gold shell was formed around the Co particles by a displacement method in THF (tetrahydrofuran) media based on the following reaction [105-109]:



In a typical procedure, the precursor cobalt nanoparticles were added to 50 mL KAuCl₄ (0.024 M) in THF solution under ultrasonication and inert atmospheric conditions. The initially brown colored solution changed to blue indicating that the gold ions oxidized the cobalt surface atoms on the cobalt nanoparticles. The reaction was

continued for an additional 1 hour and the core-shell nanoparticles were washed thoroughly with THF and dried under vacuum. The resulted nanoparticles were characterized using transmission electron microscopy (TEM, JEOL 2010) with an accelerated voltage of 200 kV, and a zeta potential analyzer (Zeta Plus, Brookhaven Instruments Corp.).

Co@Au nanoparticles were tested using a superconducting quantum interface device magnetometer (SQUID, Quantum Design Inc., model MPMS 5S) to analyze the magnetic properties of the nanoparticles. The samples for magnetic measurements were prepared in powder form in gelatin capsules. The temperature dependent magnetization process was investigated using the zero field cooled (ZFC) and field cooled (FC) methods [105]. ZFC was done by cooling the sample first to 4 K without a field; then magnetization changes were recorded with the temperature increasing from 4 K to 300 K with an applied field of 100 Oe. FC was recorded immediately after ZFC by decreasing the temperature from 300 K to 4 K with a constant field of 100 Oe. Field dependent magnetization was tested for two temperatures: 10 K and 300 K. In order to test the oxidative stability of the cobalt cores, both the zero field cooled and field cooled methods, with an applied field of 30 kOe at 10 K, were recorded.

Capsule Preparation

Hollow polyelectrolyte microcapsules were prepared using manganese carbonate cores [110] with an average core diameter of about 5.5 μm . First, 200 μL negatively charged PSS solution and positively charged PAH solution, with concentrations of 2 mg/mL, were absorbed alternately on cores in 10 mL, 1 mg/mL MnCO_3 core aqueous suspensions. For each polyelectrolyte layer, washing with DI water three times was

carried out to remove excess polyelectrolytes after a 15 minute adsorption period. Layer forming continued until four bi-layers of PSS and PAH were absorbed on the cores. Then, after another layer of PSS was adsorbed, 500 μL of a 1.2 mg/mL Co@Au nanoparticle solution was added into the MnCO_3 core suspension. After a 30 minute adsorption period, the cores with adsorbed Co@Au nanoparticles were washed three times using DI water, the MnCO_3 cores with adsorbed Co@Au nanoparticles were separated from the free (unadsorbed) nanoparticles in the solution by the precipitation method. The free nanoparticles precipitate much slower than the cores with nanoparticles adsorbed. An additional 2 – 6 PSS/PAH bi-layers were assembled to wrap up the nanoparticles sequentially after the desired number of Co@Au layers were coated on the MnCO_3 cores. The assembly of layers can be confirmed by zeta potential changes of the core surface and quartz crystal microbalance resonance frequency changes (QCM, USI-Systems, Japan).

The manganese carbonate cores were dissolved using 0.1 M EDTA disodium salt solution at a pH of about 4.5 for 3 – 4 hours [110]. After dissolving, the capsules obtained were centrifuged and washed using DI water three to four times and stored in DI water.

Capsule Permeability Test

Hollow capsules were washed using pH 7.5, 0.02 M Tris buffer three times, and then kept in the same buffer overnight to ensure the capsules were in a closed state [32, 33, 36]. Confocal laser scanning microscopy (CLSM) was used to check the permeability of capsules to macromolecules before and after applying alternating magnetic fields. FITC-dextran, with a molecular weight of 2,000,000 dal, was used as a fluorescence indicator for diffusion tests. An alternating electromagnetic field, with frequencies

ranging from 20 Hz to 2,000 Hz, and a magnetic field of 0.1 T, was applied to oscillate and disturb the Co@Au nanoparticles embedded inside the capsule walls. The magnetic capsules were kept inside the alternating magnetic field for 5 – 30 minutes before checking the permeability change of their walls. The ratio of fluorescence intensities inside and outside of the capsules was selected as a measurement for the capsule permeability change. It is considered, in this dissertation, that the capsules are impermeable if the fluorescence intensity inside the capsules is 0.5 ($I/I_o = 0.5$, where I is the internal fluorescence intensity inside the capsules, and I_o is the external intensity outside the capsules) less than that outside of the capsules after adding fluorescence dye for 15 minutes.

Capsule Characterization

Two kinds of capsules were checked using scanning electron microscopy (SEM, AMRAY 1830): capsules with and without embedded Co@Au nanoparticles. Samples were prepared by drying capsules on 1×1 cm silicon wafers. After drying, platinum sputtering was used to apply an ultrathin metal layer (~ 0.5 nm) to enhance the image quality taken in the experiments.

Confocal laser scanning microscopy (CLSM) and atomic force microscopy (AFM) were used to investigate the size, morphology, and structure of hollow microcapsules embedded with Co@Au nanoparticles, and capsule permeability changes before and after applying an alternating magnetic field. For microcapsule checking with atomic force microscopy, the Q-Scope™ 250 Quesant instrument with intermittent-contact mode was used. The samples were prepared by adding about 10 μ L nanoparticle suspensions on a 1.5×1.5 cm mica slide and dried for 24 hours before checking. In order

to allow CLSM to check the capsules and their loading, the capsules were fabricated using RBITC-labeled PAH, and fluorescent FITC-dextran (MW 2,000,000 dal) was used as macromolecules for the permeability tests. Before applying an alternating magnetic field, 20 μL capsule suspensions were mixed with 20 μL FITC-dextran solution (0.5 mg/mL, pH 7.5), and checked by CLSM for fluorescence intensity changes inside the capsules every 5 minutes up to 1 hour. Subsequently, 50 μL capsule suspensions were mixed with 50 μL FITC-dextran solution. The mixture was put in an alternating magnetic field and the fluorescence intensity was checked every 5 minutes. The solution pH values were kept at 7.5 all the time during the experiments. The CLSM used in this work is a confocal laser scanning microscopy (Leica-SP2, Germany) with a 63 \times oil immersion objective.

Results and Discussion

Co@Au Nanoparticle Characterization

Figure 5.2 (see page 67) shows the UV/Vis spectrum of Co@Au core-shell nanoparticles in ethanol solution. The presence of an absorption peak at 585 nm due to the gold plasmon resonance is indicative of the formation of a Au shell around the cobalt nanoparticles. It was reported that the Co nanoparticles have no plasmon resonance peak in the UV region [111-113]. A large red shift of the plasmon absorption, when compared with pure gold nanoparticles (~ 530 nm) [112], could be attributed to the presence of a cobalt core and also indicate that almost no free gold nanoparticles were formed in the displacement reaction, which is consistent with the literature report on gold coated silver nanoparticles [112]. Such a shift was previously noticed in the case of gold coated γ -

Fe₂O₃ core-shell nanoparticles, gold coated silver nanoparticles, and for a silver shell around a silica core [112, 114, 115].

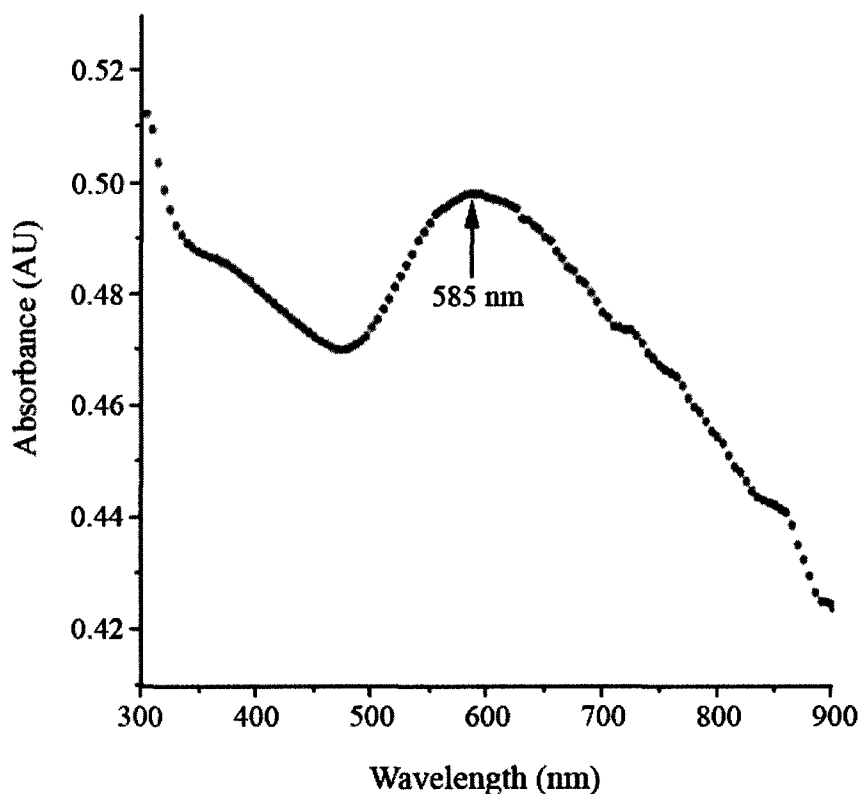


Figure 5.2: UV/Vis spectrum of Co@Au nanoparticles showing the Au absorbance peak at 585 nm.

Figure 5.3 (see page 68) shows a TEM bright-field micrograph of the Co@Au core-shell nanoparticles. The nanoparticles were found to be nearly monodispersed with a diameter of 2.7 ± 0.5 nm (the diameter was calculated using Scion software from Scion Corporation for counting more than 150 nanoparticles). The image contrast, which is directly related to differences in the atomic number or projected specimen mass thickness, has been used as a distinguishing criterion for the core-shell structure [116-118]. The formation of a more spherical shell, rather than other shapes, is due to its lower

surface energy compared with other shapes. The gold shell thickness was also estimated based on the weight percentage of gold in the core-shell nanoparticles (Au wt % = 38.1, determined from atomic absorption analysis) and the particle size from TEM, assuming bulk density and standard spherical shape with symmetric structure.

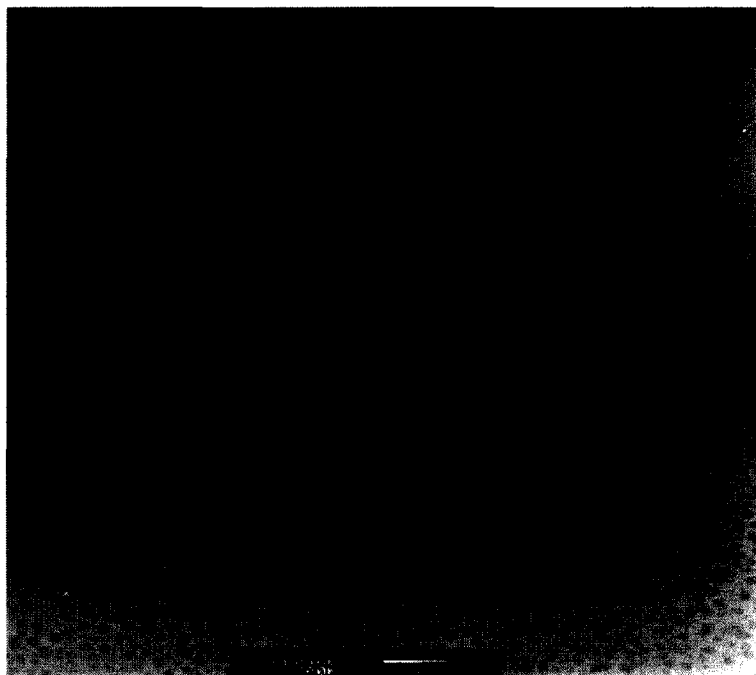


Figure 5.3: Transmission electron microscopy (TEM) image of Co@Au nanoparticles. The particles are ~ 3 nm in diameter.

The blocking temperature (T_B), determined at the maximum of the zero field cooled (ZFC) curve, characterizes the transition temperature between the superparamagnetic state and the ferromagnetic state. At temperatures below the blocking temperature, materials show ferromagnetic properties; whereas, at temperatures above the blocking temperature, materials show paramagnetic properties, otherwise known as superparamagnetism. The blocking temperature for Co@Au nanoparticles is approximately at room temperature (Figure 5.4, see page 69), unlike the blocking

temperature for the precursor pure cobalt nanoparticles (125 K, superparamagnetic) indicating that the core-shell nanoparticles are transitioning between ferromagnetic and superparamagnetic states [105]. The coercivity of a hysteresis loop is the strength of a magnetic field needed to reduce the magnetization of a ferromagnetic material to zero after it has reached saturation [119]. A slight hysteresis observed at room temperature is a confirmation of the ferromagnetic nature of the Co@Au nanoparticles. The reason for this ferromagnetic nature of the Co@Au nanoparticles will be discussed later.

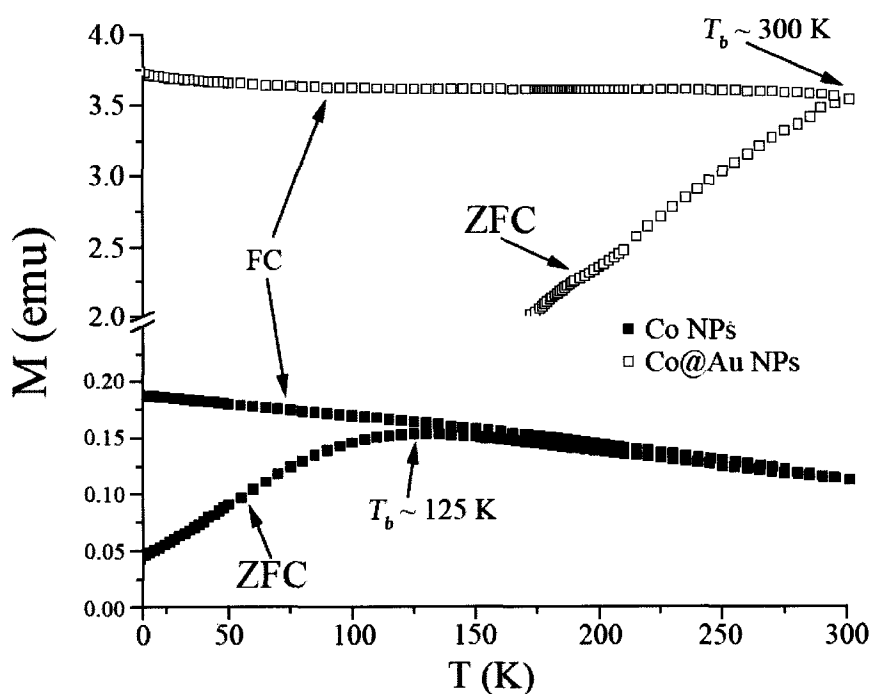


Figure 5.4: Temperature dependences of the magnetic moment measured in zero field cooled (ZFC) and field cooled (FC) modes for Co@Au nanoparticles (open squares) and pure cobalt nanoparticles (closed squares). The blocking temperatures for Co@Au and pure Co nanoparticles are approximately 300 K and 125 K, respectively.

Layer-by-Layer Assembly on QCM Electrodes and Microcores

Co@Au nanoparticles (DI water, pH \sim 7.0) were first checked using zeta potential analysis, the obtained surface potential is $+15 \pm 5$ mV for different nanoparticle batches.

That indicates the surface charges of the nanoparticles are positive, so negatively charged PSS was selected to assemble alternately with the Co@Au nanoparticles.

First, the assembly conditions on QCM resonators monitoring the process by the weight addition on every deposition cycle was elaborated. The results are shown in Figure 5.5. The plot shows a stable growth of nanoparticle layers on the QCM resonator. From the QCM frequency shift plot, one can see formation of the multilayers corresponding to the planned composition of microcapsule walls: Four step precursor layers followed by three bi-layers of nanoparticles and PSS.

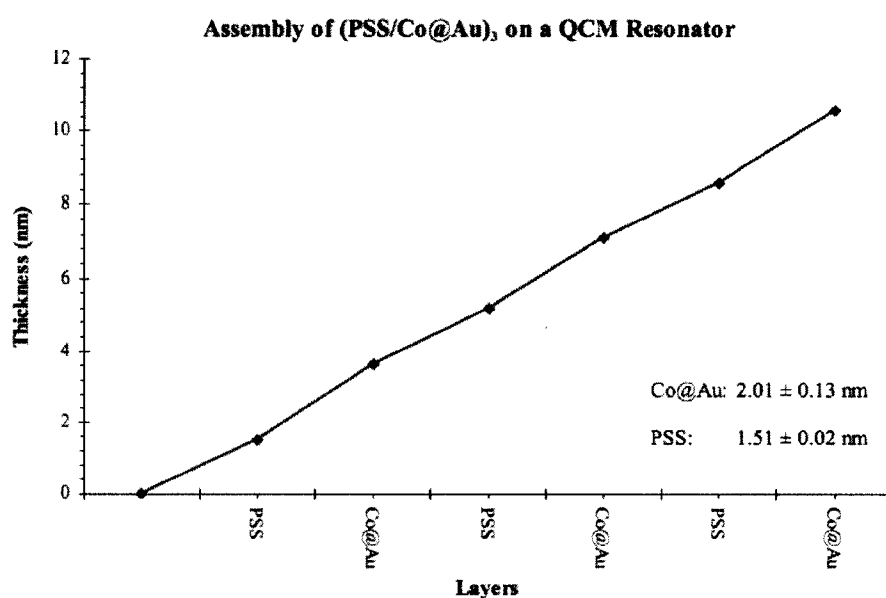


Figure 5.5: Thickness changes by the alternating adsorption of Co@Au nanoparticles with PSS monitored using QCM.

Considering the Co density of $8.7 \text{ g}\cdot\text{cm}^{-3}$ and a particle packing coefficient of ca. 74 %, the estimated monolayer thickness for Co@Au nanoparticles is ca. 4 – 6 nm. Here, each nanoparticle in the monolayer (the nanoparticles were considered to form a monolayer on the surface of the resonator with a hexagonal close-packed (hcp) structure)

was considered as a sphere, which occupies 74 % of a cubic structure as shown in the following formulation:

$$\frac{6\left(\frac{4}{3}\pi r^3\right)}{\frac{3\sqrt{3}}{2}a^2c} = \frac{6\left(\frac{4\pi a^3}{3\cdot 2^3}\right)}{\frac{3\sqrt{3}}{2}a^2c} = \frac{\pi a}{\frac{3\sqrt{3}}{2}c} = \frac{2\pi r}{6\sqrt{2}r} \approx 0.74, \quad (5.1)$$

where a ($a = 2r$) is the side length of the hexagon, c ($c = 3.27r$) is the height of the hexagon, and r is the radius of the sphere. This is just an estimated value. This thickness was obtained from the corresponding frequency shift using the Sauerbrey equation supported with experimental scaling [13]. This value is consistent with the particle diameter obtained from transmission electron microscopy (Figure 5.3, see page 68).

After elaboration of the assembly on planar QCM resonators, a similar nanocomposite shell was assembled on manganese carbonate micro-cores: 4 bi-layers of PSS/PAH + 1 – 2 layers of nanoparticles + 2 – 10 bi-layers of PSS/PAH to cover the nanoparticles. The layers were prepared in aqueous solution with suspended MnCO_3 cores as mentioned in the Experiment Section. The final capsule wall composition was $(\text{PSS/PAH})_4(\text{PSS/Co@Au})_{1-2}(\text{PSS/PAH})_{2-10}$. These capsules were used to evaluate their permeability changes under an external alternating magnetic field in the next sections. The influence of the capsule structure differences on the capsule permeability was also investigated. Figure 5.6 (see page 72) shows the zeta potential changes for Co@Au layers alternated with PSS on MnCO_3 micro-cores. First, there was regular alternation of surface potential with $+45 \pm 5$ mV for PAH and -30 ± 5 mV for PSS. After assembling one layer of Co@Au nanoparticles, the surface charge became positive, $+14$ mV, and the next PSS layer reversed it to negative, -40 mV. Then, again $+8$ mV for Co@Au and -42 mV for

PSS. This is consistent to the general rule of LbL assembly based on alternation of the surface charge after every deposition step [12, 21-24].

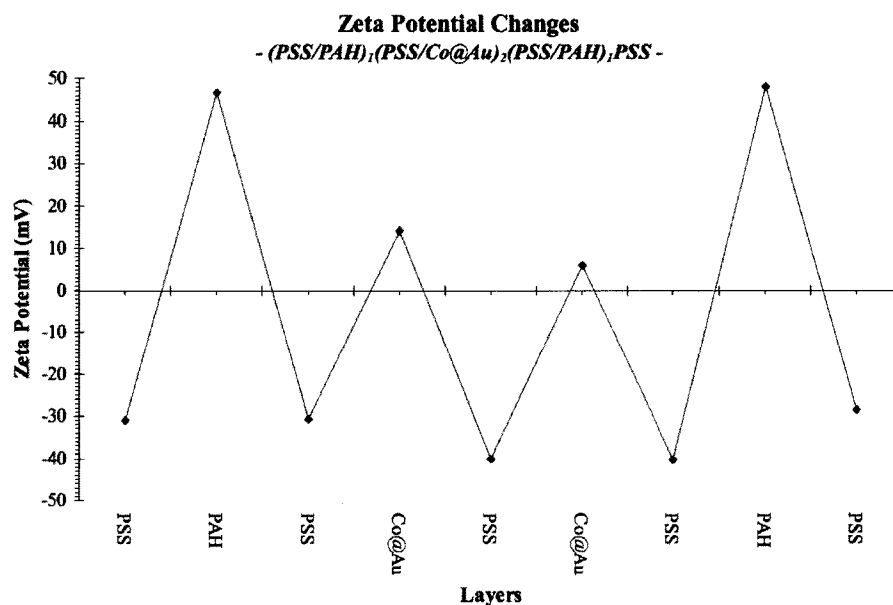


Figure 5.6: Zeta potential changes by alternating adsorption of Co@Au with PSS on MnCO₃ cores.

After formation of the shells, the template cores were dissolved, and hollow microcapsules were obtained, which were studied using confocal and atomic force microscopy. Figure 5.7 (see page 73) shows the image of the fluorescently labeled magnetic capsules under CLSM; the average capsule diameter is about 5.5 μm . The capsules were labeled with RBITC (rhodamine B isothiocyanate) dye. The fluorescence emitting wavelength of the dye is ~ 580 nm under CLSM. This allows us to clearly see the capsule walls outlined in a red color. The capsule wall surface is rather rough with some aggregates, which indicates the adsorption of a larger than one monolayer amount of Co@Au nanoparticles.

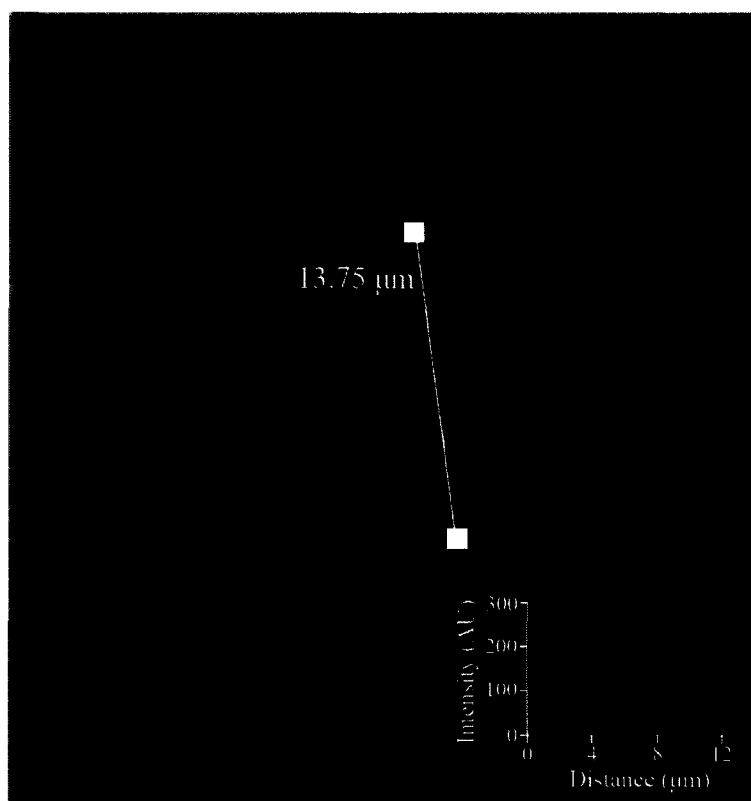


Figure 5.7: Confocal image of RBITC-labeled (shown in red fluorescence) microcapsules with one layer of embedded Co@Au nanoparticles. The capsule structure is $(\text{PSS}/\text{PAH})_4(\text{PSS}/\text{Co@Au})_1(\text{PSS}/\text{PAH})_6$. The bottom-right inset shows the fluorescence intensity of the RBITC in the cross-section of one capsule.

AFM analysis gave information of the capsule wall thickness with and without magnetic nanoparticles: capsules with wall composition of $(\text{PSS}/\text{PAH})_4(\text{PSS}/\text{Co@Au})_1(\text{PSS}/\text{PAH})_6$ and similar capsules without Co@Au were dried and checked with AFM. The resulted average wall thickness of the dried magnetic capsules was ca. 500 nm, referring to the thickness of the entire composition of two overlapped capsule walls, including the polyelectrolyte bi-layers. This can be compared to the usual microcapsule thickness of 200 nm (overlapped capsule walls composed of 10 polyelectrolyte bi-layers without embedded nanoparticles). Therefore, an average thickness of one Co@Au layer on cores may be estimated as ca. 150 nm. The aggregation

of magnetic nanoparticles was considered to be the main contribution of such a large thickness. It is reasonable that aggregation of nanoparticles was seen in this case. Even with charges on their surfaces, particles in the nano-scale have a tendency to aggregate due to their large surface area, high interfacial energy, and hydrophobic effects.

SEM images in Figure 5.8 (see page 75) visually show the difference between hollow capsules with and without embedded Co@Au nanoparticles. One can see a structured surface of magnetic microcapsules as compared with smoother and thinner non-magnetic capsules (10 bi-layers of PSS/PAH form the walls). The dried capsules without Co@Au nanoparticles are rather thin, with smooth surfaces. Some wrinkles indicate the folding of capsule walls during drying. Figure 5.8b (see page 75) shows the morphology of dried capsules embedded with one layer of Co@Au nanoparticles. The average capsule diameter is about 6 μm with a thickness of ca. 0.5 μm ; this is consistent with the AFM results. The bulges on the capsules also indicate the aggregation of Co@Au nanoparticles during LbL assembly. This is different from LbL assembly of nanoparticles on a planar surface like QCM resonators where an overall growth step for Co@Au nanoparticles was 5 ± 1 nm. It is assumed that drying of the sample on QCM resonators produce better layer organization due to capillary force ordering. These aggregates increased the amount of Co@Au adsorbed on the capsule walls and resulted in a rougher topology of the magnetic microcapsules.

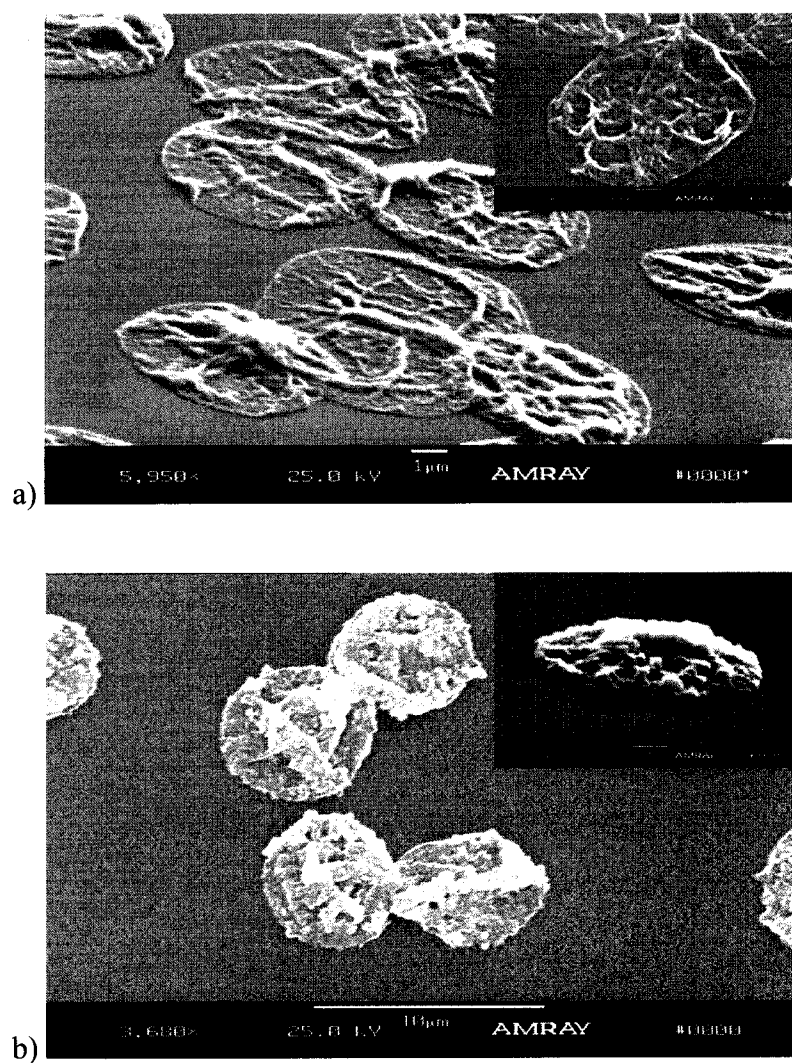


Figure 5.8: (a) SEM image of hollow capsules with $(\text{PSS}/\text{PAH})_{11}$, and (b) SEM image of magnetic capsules with one layer of embedded $\text{Co}@\text{Au}$ nanoparticles: $(\text{PSS}/\text{PAH})_4(\text{PSS}/\text{Co}@\text{Au})_1(\text{PSS}/\text{PAH})_6$. Insets show zoomed image of one capsule.

Magnetic Field Modification of Capsule Permeability

It is assumed in this work that an alternating electromagnetic field influences the $\text{Co}@\text{Au}$ nanoparticles embedded in the capsule walls. Because the $\text{Co}@\text{Au}$ particles are superparamagnetic, the oscillating magnetic field will twist and shake the nanoparticles with frequency corresponding to the frequency of the applied field. This particle agitation will disturb the structure of the surrounding polyelectrolyte layers, which will result in

layer structure distortion (some theoretical estimations of corresponding processes are given in the next section). This may result in loosening of the capsule walls and will allow macromolecules to diffuse through the capsule walls. Thus, the permeability of the magnetic microcapsules may be “switched on” after applying an alternating magnetic field with relatively low frequencies. It is believed that the “switching” rate may be increased by finding the resonant frequency of the capsule structure, and applying an alternating magnetic field at this resonant frequency.

In these experiments, confocal microscopy was used to check the capsule permeability changes under an alternating magnetic field. Before the experiment, the pH value of the capsule suspension was adjusted to about 7.5 to ensure the capsule walls were in a closed, non-permeable state [32, 33, 36]. To check permeability, FITC-labeled dextran (MW 2,000,000 dal, pH 7.5, 1 mg/mL) was added to the capsule suspension by 1:1 volume ratio. Figure 5.9a (see page 78) shows the capsule/FITC-dextran mixture confocal image before applying an alternating magnetic field. The capsules with wall structure of $(\text{PSS/PAH})_4(\text{PSS/Co@Au})_1(\text{PSS/PAH})_6$ were investigated here. The interior of the capsules was dark even after one hour of mixing. From the fluorescence intensity profile shown in the image, one can see no FITC-dextran diffused into the capsules after one hour of incubation; the average fluorescence intensity ratio inside and outside of the capsules was less than 0.2 ($I/I_o < 0.2$). Therefore, the permeability of the capsules before applying alternating magnetic fields was negligible, and FITC-dextran was blocked from diffusion into the capsules. After applying an alternating electromagnetic field (0.1 T, 150 Hz) to the capsule/FITC-dextran mixture for 30 minutes, the capsules became permeable (Figure 5.9b, see page 78). The image shows that the fluorescence intensity

inside the capsules became the same as in bulk solution; the average fluorescence intensity ratio inside and outside of the capsules was about 1.1 ($I/I_o \approx 1.1$), which proved there is a large enhancement of FITC-dextran diffusion into the capsules. The fluorescence intensity in the capsule walls was much higher because the capsule walls were constructed from charged polyelectrolytes, which adsorbed more FITC-dextran than the interior of the capsules. By checking the capsules using CLSM, 99 % of the capsules analyzed were filled with FITC-dextran after applying an alternating magnetic field for 30 minutes. The same permeability experiments were run four separate times with similar results. The experimental results supported the assumption that a low frequency alternating magnetic field changes permeability of magnetic capsules that allow the macromolecules, which are usually excluded from the capsules, to penetrate into the capsules. The permeability control mechanism is given in more detail in the Theoretical Considerations section.

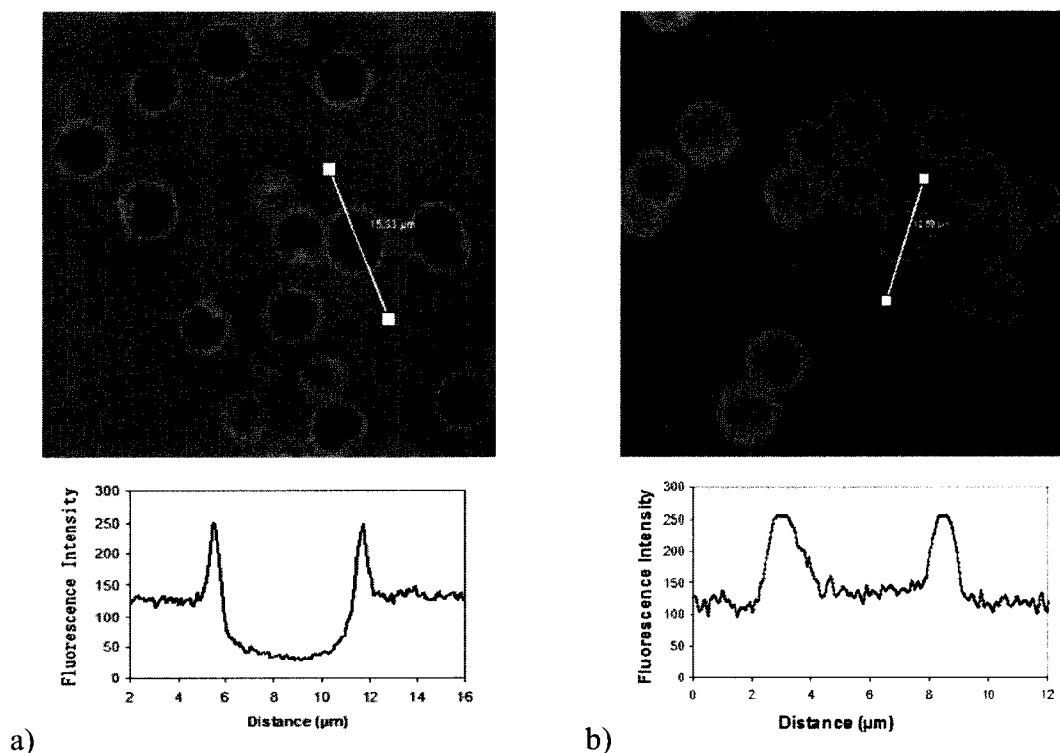


Figure 5.9: Confocal laser scanning microscopy images of magnetic capsules, $(\text{PSS}/\text{PAH})_4(\text{PSS}/\text{Co}@\text{Au})_1(\text{PSS}/\text{PAH})_6$, mixed with FITC-dextran (a) without applying an alternating magnetic field, and (b) after applying an alternating magnetic field for 30 minutes, with corresponding optical density profiles.

Another part of this work had to do with moving and focusing the magnetic microcapsules with a permanent external magnetic field (~ 0.1 T). This was done first by placing a permanent magnet near the $\text{Co}@\text{Au}$ nanoparticles suspended in DI water. After 5 minutes, all the nanoparticles migrated to the magnet, and the bulk solution turned from a murky color to transparent (Figure 5.10, see page 79). Then, similar experiments were done with capsules embedded with $\text{Co}@\text{Au}$ nanoparticles with analogous results. This shows that the microcapsules embedded with $\text{Co}@\text{Au}$ nanoparticles can be concentrated using a permanent magnet. Therefore, any one approach, both "focusing" of the capsules to a specific location followed by "switching" them on to release their contents, are suggested.

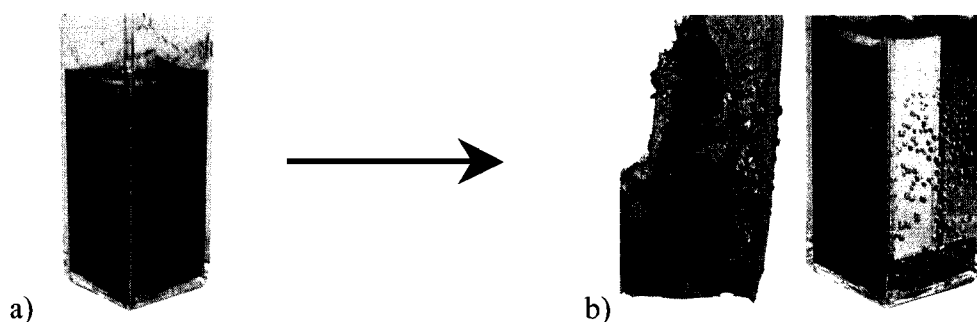


Figure 5.10: (a) Co@Au nanoparticles suspended in DI water. (b) After application of a permanent magnetic field, the magnetic nanoparticles migrate towards the magnet leaving a clear solution of DI water behind.

Temperature and Frequency Effects

During the application of an alternating magnetic field, a ~ 30 °C increase in temperature for the sample was observed, as shown in Figure 5.11a (see page 80). Therefore, the two phenomena possibly contributing to the changing of the polyelectrolyte wall permeability, heating of the sample and disturbing of the capsule walls, must be separated. From the literature [27, 30], it is known that heating provides an opposite effect, decreasing wall permeability. Even so, an experiment was designed to rule out the temperature influence on the capsule permeability. In this experiment, magnetic capsules were mixed with FITC-dextran and heated to 50 °C for 30 minutes (which were typical conditions when applying a magnetic field). The permeability was checked (Figure 5.11b, see page 80), and the capsules were found not to be permeable; the FITC-dextran remained excluded from the capsules even after 30 minutes and longer, the average fluorescence intensity ratio inside and outside of the capsules (I/I_o) was less than 0.2. Thus, one can conclude that the temperature's influence on the permeability of capsules is negligible and even may oppose the magnetic effects, and the influence of magnetic fields is the major factor contributing to the capsule permeability change.

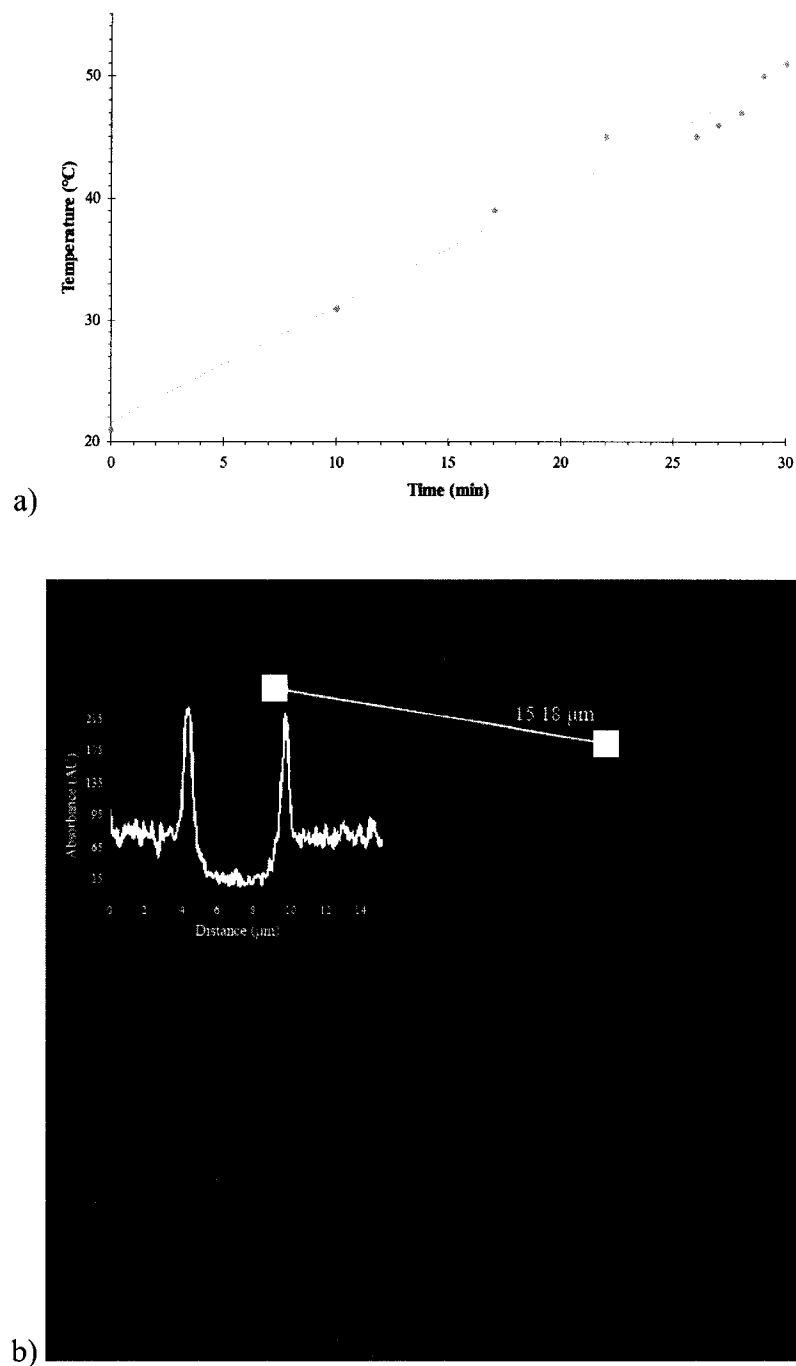


Figure 5.11: (a) Temperature increase tendency of capsule suspensions when applying a magnetic field, and (b) confocal image of magnetic capsules, $(PSS/PAH)_4(PSS/Co@Au)_1(PSS/PAH)_6$, in a 1:1 mixture with FITC-dextran after heating to 50 °C for 30 minutes.

The influence of frequencies of electromagnetic fields on the permeability of capsule walls was also studied. The applied frequencies were ranged from 100 Hz to 1,000 Hz, while the strength of the magnetic field was kept constant at 0.1 T. In frequencies beyond 300 Hz, the diffusion of FITC-dextran into capsules is negligible, even after keeping the mixture for one hour in the magnetic field. For frequencies less than 300 Hz, there is a tendency for faster diffusion of FITC-dextran with lower frequencies. It seems that the increase of frequency reduces agitation effects of the magnetic field on the Co@Au nanoparticles embedded in the capsule walls, which reduces the permeability of the magnetic capsules. This is consistent with the idea that agitating magnetic forces have to correspond with mechanical properties of the magnetic particles and surrounding elasticity.

Optimization of the Capsule Wall Composition

The increase in the number of Co@Au nanoparticle layers significantly reduced the permeability of the capsules. After coating two layers of Co@Au nanoparticles, the capsules were not permeable to FITC-dextran in any case; therefore, the use of more than one layer of Co@Au nanoparticles is unsuitable for the experiments. The influence of the number of PSS and PAH layers on capsule permeability was also investigated. The permeability change of the capsules was evaluated using the fluorescence intensity ratio inside and outside the capsules after adding FITC-dextran into the capsule suspension as the above section described. The blue line with diamond markers in Figure 5.12 (see page 82) shows the permeability change tendency with changes in the number of polyelectrolyte bi-layers for capsules without embedded nanoparticles. The capsules with less than 4 bi-layers are easily permeable to FITC-dextran ($I/I_o > 0.9$). The permeability is

gradually reduced as the number of bi-layers is increased, and totally impermeable to FITC-dextran with more than 8 bi-layers ($I/I_o < 0.1$). The red line with square markers in Figure 5.12 shows the permeability changes of capsules with one layer of embedded Co@Au nanoparticles. The permeability of the magnetic capsules is enhanced when compared to the capsules without nanoparticles, but general curve behavior is the same. It was also found that, in an alternating electromagnetic field, the magnetic capsules will not be open for FITC-dextran if more than 10 polyelectrolyte bi-layers (PSS/PAH) are assembled because of increased electrostatic interactions.

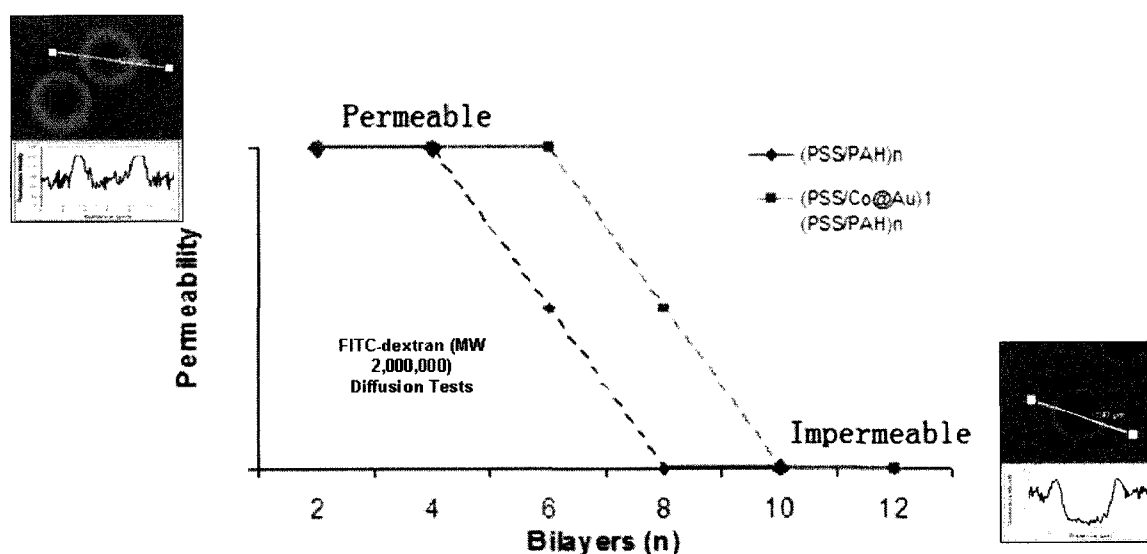


Figure 5.12: Influence of polyelectrolyte bi-layer numbers on the permeability of capsules with and without an embedded layer of Co@Au nanoparticles at pH 7.5.

Theoretical Considerations

It is easy to show that ideal isolated hcp (hexagonal-close packed) Co nanoparticles, with diameter ~ 3 nm, should be superparamagnetic at room temperature with blocking temperature $T_B \sim 4$ K from the equation

$$T_B = \frac{K_u V}{25k_b}, \quad (5.2)$$

where $K_u = 4.1 \times 10^5 \text{ J}\cdot\text{m}^{-3}$ (anisotropy constant), V is the particle volume, and k_B is the Boltzmann constant. Such nanoparticles should have a very low magnetic moment at room temperature in reasonable magnetic fields. In reality, the situation is even worse because it is difficult to expect perfect crystallinity for particles of 3 nm in diameter. Moreover, in our case, partial oxidation of cobalt takes place. A typical shift of the hysteresis loop along the H -axis for nanoparticles brought down to 30 kOe due to unidirectional anisotropy, which is a result of the formation of an oxide layer [120], was observed (Figure 5.13, see page 84). The oxidation should also decrease the magnetic moment of the nanoparticles. However, magnetic data obtained for dried, as-prepared Co@Au nanoparticles show that they have slight ferromagnetic properties due to the small hysteresis. The only possible explanation of this fact is aggregation and coupling of the Co@Au nanoparticles. Due to the magnetostatic interaction between nanoparticles, aggregations became ferromagnetic. Correlation of magnetic moments of chaotically oriented particles leads to a fairly narrow hysteresis loop at room temperature (Figure 5.13, see page 84). Thus, the resulting volume of the aggregates should be at least a hundred times the volume of the individual nanoparticles (i.e. a diameter of the aggregate would be at least 6 times larger than that of the Co@Au nanoparticle).

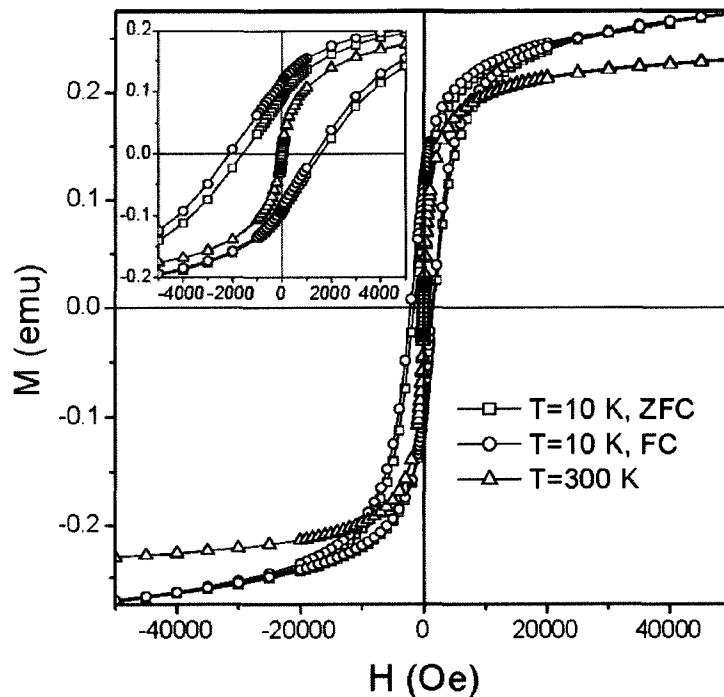


Figure 5.13: Magnetic hysteresis curve for Co@Au nanoparticles. Inset shows zoomed curve. The small hysteresis indicates slight ferromagnetic properties in the material.

Let us consider the action of alternating magnetic fields on polyion capsules with embedded cobalt ferromagnetic nanoparticles. There are several mechanisms, which can lead to formation stresses inside of the shell. One such mechanism is the deformation of the capsule could lead to a decrease of the viscous interaction due to a decreasing cross sectional area. However, we cannot expect considerable gradients of the magnetic field ($\delta H/\delta x$). The magnetic force,

$$F = MV \frac{\delta H}{\delta x}, \quad (5.3)$$

where M is the mean magnetization of the capsule and V is the volume, will be negligible. Another mechanism is that the capsule in the magnetic field tried to stretch itself along the field direction because it leads to a decrease of magnetostatic energy,

$$E_{ms} = \frac{1}{2}(N^{\parallel} - N^{\perp})M^2V, \quad (5.4)$$

where N^{\parallel} and N^{\perp} are demagnetizing factors in the directions parallel and perpendicular to the magnetic field, respectively. Taking into account real physical parameters of the capsules, one can show that the influence of this should also be negligible [77, 121]. Besides, the increase of the thickness of the nanoparticle layer in this case would lead to an increase of the influence of the magnetic field.

Shape and magnetocrystalline anisotropy of individual nanoparticles can affect the permeability of the capsules. The arising forces may be too low for substantial deformation of the capsules walls. This is not the case for aggregations of nanoparticles. Magnetostatic interactions inside the aggregations will lead to an appearance of fairly large demagnetizing fields. In a magnetic field, they will try to align their easy-axis along the direction of the magnetic field. This results in the formation of rather large stresses inside the capsule walls. Such stresses can lead to an increase of pore size in the capsule walls, and in some cases even rupture the walls. It should be noted that all this speculation is true for separated aggregates; otherwise, magnetostatic interactions between the aggregates would suppress the demagnetizing factors of the individual aggregates [121].

As for the frequency behavior of the permeability, the aggregates rotate, or oscillate, under the action of the magnetic field with the elastic deformation of the

capsule walls. At high frequencies, they will not follow the variation of the magnetic field and the deformation will be minimal, which leads to a decrease in permeability. This corresponds to the forced oscillation of a pendulum at frequencies above the resonance frequency. Unfortunately, it is impractical to calculate theoretically elastic forces for such a complex system. Additionally, eigen-frequencies could be determined only by experimentation.

Conclusion

The synthesized 3 nm diameter superparamagnetic Co@Au nanoparticles are positively charged in DI water (~pH 7), and can be successfully absorbed on planar and spherical surfaces in alternation with anionic polyelectrolyte layers. The 5.5 μm diameter microcapsules, with nano-organized polymer walls embedded with Co@Au nanoparticle layers, were successfully fabricated. They form a stable aqueous dispersion. Applying external alternating electromagnetic fields of 100 – 300 Hz and 0.1 T strength disturbed the capsule wall structures and drastically increased their permeability to macromolecules. The embedded nanoparticles can be protected by the surrounding polyelectrolyte layers from oxidation, which will keep them active for a longer time. Capsules with one layer of Co@Au nanoparticles and 10 polyelectrolyte bi-layers are considered optimal for controlling permeability with alternating magnetic fields. This work supports the hypothesis of using magnetic nanoparticles embedded in polyelectrolyte capsules for controlled release of substances, and offers a promising technology for microcapsule “focusing” and “switchable” drug release in the biomedical field by using

an external magnetic field to displace and open the capsules at designated places within the body.

CHAPTER 6

MAGNETICALLY ACTIVATED MICROCAPSULES
FOR THE CONTROLLED RELEASE OF
ENCAPSULATED DEXAMETHASONE

Introduction

The controlled diffusion of dextran macromolecules through polyelectrolyte layers has been established using superparamagnetic nanoparticles embedded in hollow microcapsules [122]. Here, dexamethasone, a hydrophobic drug, is micronized, and biocompatible polyelectrolyte layers are assembled around the core for protection and drug release control. Furthermore, a monolayer of superparamagnetic nanoparticles are assembled between the polyelectrolyte layers in order to “focus” the capsules to specific locations and to “switch on” the release of the encapsulated drug by disturbing the polyelectrolyte film with the use of an external, alternating magnetic field.

Experimental

Materials

Protamine sulfate C (PS, MW 5,120 dal, positive) and gelatin B (GB, MW 20 – 25 kdal, negative) were obtained from Sigma Aldrich. Chondroitin sulfate sodium salt (CS, negative) was purchased from Wako. Dexamethasone (Dexa, MW 392 dal,

negative) was purchased from Spectrum. All of the materials above were used as received. Gold coated cobalt (Co@Au, diameter ~3 nm, positive) was fabricated at the Center for Advanced Microstructures and Devices, Louisiana State University, Baton Rouge, Louisiana, USA [106].

Capsule Preparation

A 40 mg batch of dexamethasone was added to 5 mL phosphate buffered saline (PBS) and sonicated for five minutes in a bath. A 10 mL solution of protamine sulfate C (5 mg/mL) was immediately added to the dexamethasone cores, and further sonication was done for thirty minutes. The cores were then centrifuged at 10,000 RPM for 1 minute, the supernant was removed, and 1 mL fresh BPS buffer was added to the sample. This was done three times to wash the sample. Subsequently, 1 mL chondroitin sulfate sodium salt (5 mg/mL) was added to the samples and allowed to sit for 15 minutes to allow self-assembly to take place. Another washing step took place to again clean the sample. Alternating layers were assembled on the sample with intermediate washings between layers to form the following layer composition: $(\text{PS/CS})_1(\text{PS/GB})_1(\text{Co@Au/GB})_1(\text{PS/GB})_1$.

Drug Release

The sample was separated into four batches. The four samples were analyzed under different conditions: air and alternating magnetic fields of 150 Hz, 200 Hz, and 250 Hz (the samples in the magnetic field were run at a constant 0.1 T at their respective frequencies). A variable voltage, variable frequency power source (Behlman, P1351) connected to a solenoid was used to generate the magnetic fields. A peristaltic pump (913

Mity Flex Peristaltic Pump) was used to flow ice water around the solenoid to keep the sample temperature at 11°C. The samples exposed to a magnetic field were placed in the core of the solenoid, and the sample exposed only to air was kept in a tin can to keep any external magnetic field from affecting the magnetic particles in the sample.

Each sample's release was checked individual by allowing the sample to be exposed to its respective environment for a specific time interval (~7 minutes). Then the sample was centrifuged at 10,000 RPM for 30 seconds, and the supernant was extracted and measured using UV/Vis (Agilent, 8543) at 243 nm to detect the amount of dexamethasone in the supernant. A 1 mL solution of fresh PBS was then added to the sample, and the sample was placed back in its respective environment. This process repeated itself until no more dexamethasone remained in the core of the microcapsules.

Results and Discussion

The ζ -potential (Brookhaven Instruments Corporation Zeta Potential Analyzer) of each layer assembled on dexamethasone cores was monitored to insure proper charge reversal was taking place. The dexamethasone cores had a ζ -potential of -19.79 mV. Upon addition of protamine sulfate C, the surface charge revered to a ζ -potential of +12.00 mV. Again, adding chondroitin sulfate sodium salt reversed the surface charge to give a ζ -potential of -37.75 mV. The surface charge continued to alternate as layers were added (Figure 6.1, see page 91). The addition of the Co@Au layer did not totally reverse the surface charge of the capsules; however, verification of the assembly was done by viewing the capsules under confocal laser scanning microscopy (data not shown).

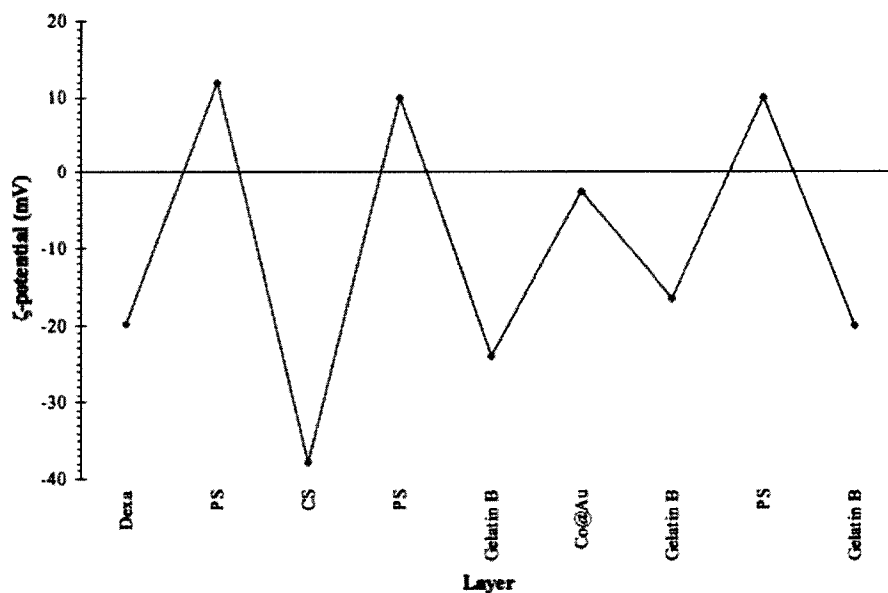


Figure 6.1: Charge reversal of layers as they are assembled on dexamethasone cores with the following composition: $(PS/CS)_1(PS/GB)_1(Co@Au/GB)_1(PS/GB)_1$.

The UV/Vis spectrum of each data point was monitored at 243 nm, which is a characteristic peak of dexamethasone. Each data point is added to the previous data points to give the total amount of dexamethasone released over time. Figure 6.2 (see page 92) shows the release of dexamethasone with (blue diamonds) and without (red squares) an external alternating magnetic field. The magnetic field was applied at 200 Hz, 0.1 T. After 30 minutes, the release of dexamethasone under an applied magnetic field was faster than for the samples without a magnetic field.

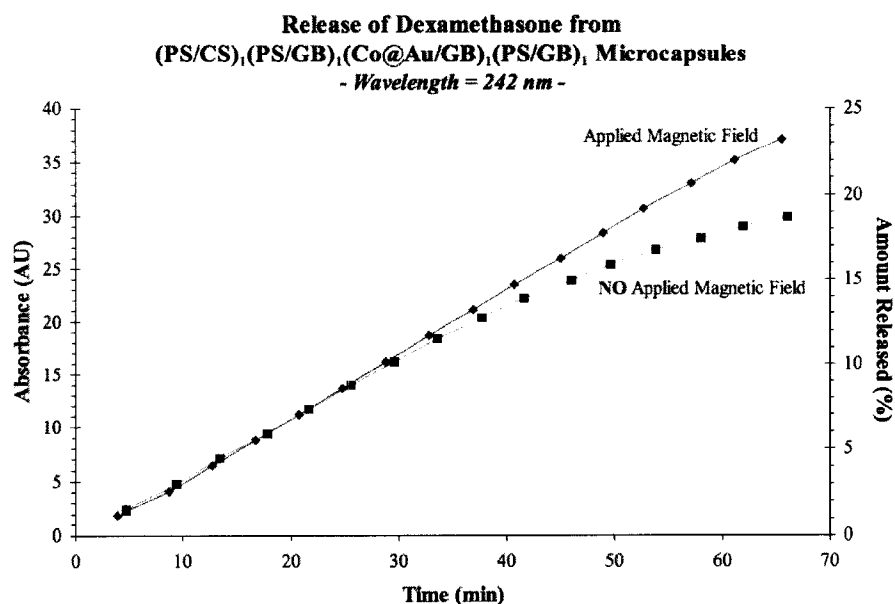


Figure 6.2: Release of dexamethasone with (blue triangles) and without (red squares) an applied alternating magnetic field (200 Hz, 0.1 T). The dexamethasone release was monitored using UV/Vis at 242 nm. The dexamethasone was encapsulated in $(PS/CS)_1(PS/GB)_1(Co@Au/GB)_1(PS/GB)_1$ microcapsules.

Conclusion

Layer-by-layer self-assembly was used to create a protective biocompatible polymer film around the dexamethasone cores. The release of dexamethasone from polyelectrolyte capsules with an embedded layer of superparamagnetic nanoparticles was increased with the application of an external alternating magnetic field. This method offers a promising way of delivering a controlled amount of drugs to specific areas without affecting the entire body.

CHAPTER 7

CONCLUSION

In this dissertation, the use of superparamagnetic nanoparticles was used to enhance the release of macromolecules from polyelectrolyte microcapsules fabricated via layer-by-layer self-assembly; transforming the microcapsules into bio/nano robots activated with external magnetic fields. This dissertation introduces and develops the merger of electrical engineering and pharmaceuticals by incorporating magnetic nanoparticles into drug release applications.

An anticancer polypeptide, Phor21- β CG(ala), was used as one of the layers in the formation of polyelectrolyte shells around a silica core. Release of the peptide was accomplished through varying the pH of the release media. Although this technique was found to be unique, the release mechanisms were still dependent on physiological conditions.

Superparamagnetic nanoparticles were incorporated in the polyelectrolyte shells to create a release mechanism that was not dependent on physiological conditions. Here, permanent and alternating external magnetic fields were used to “focus” and “switch on” the capsules, respectively. It was shown that the polyelectrolyte capsules, embedded with magnetic nanoparticles, inhibited the diffusion of FITC-dextran through the capsule walls when no magnetic field was present; however, upon application of an alternating magnetic field, the capsules became permeable.

The final step was to incorporate a drug with these capsules, to give enhanced release characteristics. Polyelectrolyte multilayers, embedded with superparamagnetic nanoparticles, were assembled around micronized dexamethasone cores. Because of the low molecular weight of the dexamethasone used, dexamethasone was able to continually diffuse through capsules walls; however, upon application of an alternating magnetic field, the release of dexamethasone was increased.

Future Work

There are several things that can be done in future work to further build upon the obtained results. Further studies need to be done to advance this development such as:

- Use of other types of superparamagnetic nanoparticles in the polymer matrix such as $\text{Fe}_2\text{O}_3/\text{Fe}_3\text{O}_4$, which are less toxic than Co-based nanoparticles, $\text{Co}@Cu$, $\text{Fe}@Cu$, and $\text{Fe}@Ag$ should be studied to check the diffusion effects produced by these nanoparticles;
- Use of other encapsulated drugs for release studies such as furosemide, nifedipine, paclitaxel, and tamoxifen in order to check the different diffusion properties through the polyelectrolyte multilayers;
- Modification of the polyelectrolyte layer composition so that there is reduced diffusion of macromolecules with no magnetic field applied, and increased diffusion of macromolecules with an applied magnetic field; and
- Creation of a new setup which allows exposure of magnetic fields to the release chamber during diffusion and sample collection for 100 % exposure.

REFERENCES

1. Ai, H.; Jones, S. A.; Lvov, Y. M., Biomedical Applications of Electrostatic Layer-by-Layer Nano-Assembly of Polymers, Enzymes and Nanoparticles. *Cell Biochemistry and Biophysics* **2003**, 39, (1), 23-43.
2. Maier, S. A.; Kik, P. G.; Atwater, H. A.; Meltzer, S.; Harel, E.; Koel, B. E.; Requicha, A. A. G., Local Detection of Electromagnetic Energy Transport Below the Diffraction Limit in Metal Nanoparticle Plasmon Waveguides. *Nature Materials* **2003**, 2, 229-232.
3. Sershen, S. R.; Westcott, S. L.; Halas, N. J.; West, J. L., Temperature-Sensitive Polymer-Nanoshell Composites for Photothermally Modulated Drug Delivery. *Journal of Biomedical Materials Research* **2000**, 51, (3), 293-298.
4. Mie, G., Beiträge zur Optik Trüber Medien, Speziell Kolloidaler Metallösungen. *Annalen der Physik* **1908**, 330, (3), 377-445.
5. Kreibig, U.; Vollmer, M., *Optical Properties of Metal Clusters*. Springer: 1995; p 552.
6. Oldenburg, S. J.; Averitt, R. D.; Westcott, S. L.; Halas, N. J., *Chemistry Physical Letters* **1995**, 288, 243-247.
7. Prodan, E.; Lee, A.; Nordlander, P., The Effect of a Dielectric Core and Embedding Medium on the Polarizability of Metallic Nanoshells. *Chemical Physics Letters* **2002**, 360, (3-4), 325-332.
8. Hirsch, L. R.; Jackson, J. B.; Lee, A.; Halas, N. J.; West, J. L., A Whole Blood Immunoassay Using Gold Nanoshells. *Analytical Chemistry* **2003**, 75, (10), 2377-2381.
9. Hirsch, L. R.; Stafford, R. J.; Bankson, J. A.; Serchen, S. R.; Rivera, B.; Price, R. E.; Hazle, J. D.; Halas, N. J.; West, J. L. In *Nanoshell-Mediated Near-Infrared Thermal Therapy of Tumors Under Magnetic Resonance Guidance*, Proceedings of the National Association of Science, 11 November 2003; pp 13549-13554.
10. Sun, Y.; Mayers, B.; Xia, Y., Metal Nanostructures with Hollow Interiors. *Advanced Materials* **2003**, 15, (7-8), 641-646.

11. Lvov, Y.; Decher, G.; Möhwald, H., Assembly, Structural Characterization, and Thermal Behavior of Layer-by-Layer Deposited Ultrathin Films of Poly(vinyl sulfate) and Poly(allylamine). *Langmuir* **1993**, 9, (2), 481-486.
12. Decher, G., Fuzzy Nanoassemblies: Toward Layered Polymeric Multicomposites. *Science* **1997**, 277, (5330), 1232-1237.
13. Lvov, Y.; Ariga, K.; Ichinose, I.; Kunitake, T., Assembly of Multicomponent Protein Films by Means of Electrostatic Layer-by-Layer Adsorption. *Journal of the American Chemical Society* **1995**, 117, (22), 6117-6123.
14. Lvov, Y. M.; Caruso, F., Biocolloids with Ordered Urease Multilayer Shells as Enzymatic Reactors. *Analytical Chemistry* **2001**, 73, (17), 4212-4217.
15. Tieke, J. B.; van Ackern, F.; Krasemann, L.; Toutianoush, A., Ultrathin Self-Assembled Polyelectrolyte Multilayer Membranes. *European Physical Journal E* **2001**, 5, (1), 29-39.
16. Iler, R. K., Multilayers of Colloidal Particles. *Journal of Colloidal Science* **1966**, 21, (6), 569-594.
17. Ai, H.; Jones, S. A.; de Villiers, M. M.; Lvov, Y. M., Nano-Encapsulation of Furosemide Microcrystals for Controlled Drug Release. *Journal of Controlled Release* **2003**, 86, (1), 59-68.
18. Sukhorukov, G. B.; Donath, E.; Davis, S.; Lichtenfeld, H.; Caruso, F.; Popov, V. I.; Möhwald, H., Stepwise Polyelectrolyte Assembly on Particle Surfaces: A Novel Approach to Colloid Design. *Polymers for Advanced Technologies* **1998**, 9, (10-11), 759-767.
19. Antipov, A. A.; Sukhorukov, G. B.; Donath, E.; Möhwald, H., Sustained Release Properties of Polyelectrolyte Multilayer Capsules. *Journal of Physical Chemistry B* **2001**, 105, (12), 2281-2284.
20. Suzuki, I.; Ishizaki, T.; Ihoue, H.; Anzai, J.-i., Modification of Polyelectrolyte Layered Assembly Using an Active Ester of Azobenzene Carboxylate. *Macromolecules* **2002**, 35, (16), 6470-6474.
21. Yoo, D.; Shiratori, S. S.; Rubner, M. F., Controlling Bilayer Composition and Surface Wettability of Sequentially Adsorbed Multilayers of Weak Polyelectrolytes. *Macromolecules* **1998**, 31, (13), 4309-4318.
22. Schlenoff, J. B.; Dubas, S. T., Mechanism of Polyelectrolyte Multilayer Growth: Charge Overcompensation and Distribution. *Macromolecules* **2001**, 34, (3), 592-598.

23. Harris, J. J.; Stair, J. L.; Bruening, M. L., Layered Polyelectrolyte Films as Selective, Ultrathin Barriers for Anion Transport. *Chemistry Materials* **2000**, 12, (7), 1941-1946.
24. Lvov, Y. M.; Lu, Z.; Schenkman, J. B.; Zu, X.; Rusling, J. F., Direct Electrochemistry of Myoglobin and Cytochrome P450_{cam} in Alternate Layer-by-Layer Films with DNA and Other Polyions. *Journal of the American Chemical Society* **1998**, 120, (17), 4073-4080.
25. Donath, E.; Sukhorukov, G. B.; Caruso, F.; Davis, S. A.; Möhwald, H., Novel Hollow Polymer Shells by Colloid-Templated Assembly of Polyelectrolytes. *Angewandte Chemie - International Edition* **1998**, 37, (16), 2201-2205.
26. Antipov, A. A.; Sukhorukov, G. B.; Fedutik, Y. A.; Hartmann, J.; Giersig, M.; Möhwald, H., Fabrication of a Novel Type of Metallized Colloids and Hollow Capsules. *Langmuir* **2002**, 18, (17), 6687-6693.
27. Dähne, L.; Loporatti, S.; Donath, E.; Möhwald, H., Fabrication of Micro Reaction Cages with Tailored Properties. *Journal of the American Chemical Society* **2001**, 123, (23), 5431-5436.
28. Ai, H.; Fang, M.; Jones, S. A.; Lvov, Y. M., Electrostatic Layer-by-Layer Microtemplates: Platelets. *Biomacromolecules* **2002**, 3, (3), 560-564.
29. Sukhorukov, G., *Novel Methods to Study Interfacial Layers*. Elsevier Science: 2001; p 536.
30. Ibarz, G.; Dähne, L.; Donath, E.; Möhwald, H., Smart Micro- and Nanocontainers for Storage, Transport, and Release. *Advanced Materials* **2001**, 13, (17), 1324-1327.
31. Mendelsohn, J. D.; Barrett, C. J.; Chan, V. V.; Pal, A. J.; Mayes, A. M.; Rubner, M. F., Fabrication of Microporous Thin Films from Polyelectrolyte Multilayers. *Langmuir* **2000**, 16, (11), 5017-5023.
32. Antipov, A. A.; Sukhorukov, G. B.; Loporatti, S.; Radtchenko, I. L.; Donath, E.; Möhwald, H., Polyelectrolyte Multilayer Capsule Permeability Control. *Colloids and Surfaces A: Physicochemical and Engineering Aspects* **2002**, 198-200, 535-541.
33. Tiourina, O. P.; Antipov, A. A.; Sukhorukov, G. B.; Larionova, N. I.; Lvov, Y.; Möhwald, H., Entrapment of α -Chymotrypsin into Hollow Polyelectrolyte Microcapsules. *Macromolecular Bioscience* **2001**, 1, (5), 209-214.
34. Lvov, Y.; Antipov, A. A.; Mamedov, A.; Möhwald, H.; Sukhorukov, G. B., Urease Encapsulation in Nanoorganized Microshells. *Nano Letters* **2001**, 1, (3), 125-128.

35. Radtchenko, I. L.; Sukhorukov, G. B.; Möhwald, H., A Novel Method for Encapsulation of Poorly Water-Soluble Drugs: Precipitation in Polyelectrolyte Multilayer Shells. *International Journal of Pharmaceutics* **2002**, 242, (1-2), 219-223.
36. Sukhorukov, G. B.; Antipov, A. A.; Voigt, A.; Donath, E.; Möhwald, H., pH-Controlled Macromolecule Encapsulation in and Release from Polyelectrolyte Multilayer Nanocapsules. *Macromolecular Rapid Communications* **2001**, 22, (1), 44-46.
37. Antipov, A. A.; Sukhorukov, G. B.; Möhwald, H., Influence of the Ionic Strength on the Polyelectrolyte Multilayers' Permeability. *Langmuir* **2003**, 19, (6), 2444-2448.
38. Sukhorukov, G. B.; Donath, E.; Moya, E.; Susha, S.; Voigt, A.; Hartmann, A.; Möhwald, H., Microencapsulation by Means of Step-Wise Adsorption of Polyelectrolytes. *Journal of Microencapsulation* **2000**, 17, (2), 177-185.
39. Antipov, A. A.; Sukhorukov, G. B., Polyelectrolyte Multilayer Capsules as Vehicles with Tunable Permeability. *Advances in Colloid and Interface Science* **2004**, 111, (1-2), 49-61.
40. Ghan, R.; Shutava, T.; Patel, A.; John, V. T.; Lvov, Y., Enzyme-Catalyzed Polymerization of Phenols within Polyelectrolyte Microcapsules. *Macromolecules* **2004**, 37, (12), 4519-4524.
41. Shutava, T.; Zheng, Z.; John, V.; Lvov, Y., Microcapsule Modification with Peroxidase-Catalyzed Phenol Polymerization. *Biomacromolecules* **2004**, 5, (3), 914-921.
42. Gao, M.; Lesser, C.; Kirstein, S.; Möhwald, H.; Rogach, A. L.; Weller, H., *Journal of Applied Physics* **2000**, 87, (5), 2297-2302.
43. Stroeve, P.; Vasquez, V.; Coelho, M. A. N.; Rabolt, J. F., Gas Transfer in Supported Films Made by Molecular Self-Assembly of Ionic Polymers. *Thin Solid Films* **1996**, 284-285, 708-712.
44. Shchukin, D. G.; Shutava, T.; Shchukina, E.; Sukhorukov, G. B.; Lvov, Y. M., Modified Polyelectrolyte Microcapsules as Smart Defense Systems. *Chemistry of Materials* **2004**, 16, (18), 3446-3451.
45. Shutava, T.; Prouty, M. D.; Kommireddy, D.; Lvov, Y. M., pH Responsive Decomposable Layer-by-Layer Nanofilms and Capsules on the Basis of Tannic Acid. *Macromolecules* **2005**, 38, (7), 2850-2858.
46. Sano, M.; Lvov, Y. M.; Kunitake, T., Formation of Ultrathin Polymer Layers on Solid Substrates by Means of Polymerization-Induced Epitaxy and Alternate Adsorption. *Annual Review of Materials Science* **1996**, 26, 153-187.

47. Lvov, Y. M.; Ariga, K.; Kunitake, T., Layer-by-Layer Assembly of Alternate Protein/Polyion Ultrathin Films. *Chemistry Letters* **1994**, 23, (12), 2323-2326.
48. Elbert, D. L.; Herbert, C. B.; Hubbell, J. A., Thin Polymer Layers Formed by Polyelectrolyte Multilayer Techniques on Biological Surfaces. *Langmuir* **1999**, 15, (16), 5355-5362.
49. Decher, G.; Lvov, Y. M.; Schmitt, J., Proof of Multilayer Structural Organization in Self-Assembled Polycation-Polyanion Molecular Films. *Thin Solid Films* **1994**, 244, (1-2), 772-777.
50. Tsukruk, V. V.; Rinderspacher, F.; Bliznyuk, V. N., Self-Assembled Multilayer Films from Dendrimers. *Langmuir* **1997**, 13, (8), 2171-2176.
51. Pargaonkar, N.; Lvov, Y. M.; Li, N.; Steenekamp, J. H.; de Villiers, M. M., Controlled Release of Dexamethazone from Microcapsules Produced by Polyelectrolyte Layer-by-Layer Nanoassembly. *Pharmaceutical Research* **2005**, 22, (5), 826-835.
52. Lvov, Y.; Munge, B.; Giraldo, O.; Ichinose, I.; Suib, S. L.; Rusling, J. F., Films of Manganese Oxide Nanoparticles with Polycations or Myoglobin from Alternate-Layer Adsorption. *Langmuir* **2000**, 16, (23), 8850-8857.
53. Lvov, Y. M.; Ariga, K.; Onda, M.; Ichinose, I.; Kunitake, T., A Careful Examination of the Adsorption Step in the Alternate Layer-by-Layer Assembly of Linear Polyanion and Polycation. *Colloids and Surfaces A: Physicochemical and Engineering Aspects* **1999**, 146, (1-3), 337-346.
54. Onda, M.; Lvov, Y. M.; Ariga, K.; Kunitake, T., Sequential Reaction and Product-Separation on Molecular Films of Glucoamylose and Glucose Oxidase Assembled on an Ultrafilter. *Journal of Fermentation and Bioengineering* **1996**, 82, (5), 502-506.
55. Hoogeveen, N. G.; Stuart, M. A. C.; Flier, G. J.; Böhmer, M. R., Formation and Stability of Multilayers of Polyelectrolytes. *Langmuir* **1996**, 12, (15), 3675-3681.
56. Ibarz, G.; Dähne, L.; Donath, E.; Möhwald, H., Controlled Permeability of Polyelectrolyte Capsules via Defined Annealing. *Chemistry Materials* **2002**, 14, (10), 4059-4062.
57. Bäuml, H.; Neu, B.; Voigt, A.; Mitlöhner, R.; Leporatti, S.; Gao, C. Y.; Donath, E.; Kiesewetter, H.; Möhwald, H.; Meiselman, H. J., Biological Cells as Templates for Hollow Microcapsules. *Journal of Microencapsulation* **2001**, 18, (3), 385-395.
58. Moya, S.; Dähne, L.; Voigt, A.; Leporatti, S.; Donath, E.; Möhwald, H., Polyelectrolyte Multilayer Capsules Templated on Biological Cells: Core

- Oxidation Influences Layer Chemistry. *Colloids and Surfaces A: Physicochemical and Engineering Aspects* **2001**, 183-185, 27-40.
59. v. Klitzing, R.; Möhwald, H., A Realistic Diffusion Model for Ultrathin Polyelectrolyte Films. *Macromolecules* **1996**, 29, (21), 6901-6906.
 60. Leporatti, S.; Gao, C.; Voigt, A.; Donath, E.; Möhwald, H., Shrinking of Ultrathin Polyelectrolyte Multilayer Capsules Upon Annealing: A Confocal Laser Scanning Microscopy and Scanning Force Microscopy Study. *European Physical Journal E: Soft Matter* **2001**, 5, (1), 13-20.
 61. Glinel, K.; Sukhorukov, G. B.; Möhwald, H.; Khrenov, V.; Tauer, K., Thermosensitive Hollow Capsules Based on Thermoresponsive Polyelectrolytes. *Macromolecular Chemistry and Physics* **2003**, 204, (14), 1784-1790.
 62. Dai, J.; Jensen, A. W.; Mohanty, D. K.; Emdt, J.; Bruening, M. L., Controlling the Permeability of Multilayered Polyelectrolyte Films through Derivatization, Cross-Linking, and Hydrolysis. *Langmuir* **2001**, 17, (3), 931-937.
 63. Petrov, A. I.; Antipov, A. A.; Sukhorukov, G. B., Base-Acid Equilibria in Polyelectrolyte Systems: From Weak Polyelectrolytes to Interpolyelectrolyte Complexes and Multilayered Polyelectrolyte Shells. *Macromolecules* **2003**, 36, (26), 10079-10086.
 64. Leong, K. W.; Brott, B. C.; Langer, R., Bioerodible Polyanhydrides as Drug-Carrier Matrices. I: Characterization, Degradation, and Release Characteristics. *Journal of Biomedical Materials Research* **1985**, 19, (8), 941-955.
 65. Jeong, B.; Bae, Y. H.; Lee, D. S.; Kim, S. W., Biodegradable Block Copolymers as Injectable Drug-Delivery Systems. *Nature* **1997**, 388, 860-862.
 66. Leslie, C.; Mounkes, L.; Zhong, W.; Cipres-Palacin, G.; Heath, T. D.; Debs, R. J., Proteoglycans Mediate Cationic Liposome-DNA Complex-based Gene Delivery *In Vitro* and *In Vivo*. *Journal of Biological Chemistry* **1998**, 273, (40), 26164-26170.
 67. Junyaprasert, V. B.; Mitrevej, A.; Sinchaipanid, N.; Boonme, P.; Wurster, D. E., Effect of Process Variables on the Microencapsulation of Vitamin A Palmitate by Gelatin-Acacia Coacervation. *Drug Development and Industrial Pharmacy* **2001**, 27, (6), 561-566.
 68. Keller, S. W.; Kim, H.-N.; Mallouk, T. E., Layer-by-Layer Assembly of Intercalation Compounds and Heterostructures on Surfaces: Toward Molecular "Beaker" Epitaxy. *Journal of the American Chemical Society* **1994**, 116, (19), 8817-8821.
 69. Schlenoff, J. B.; Laurent, D.; Ly, H.; Stepp, J., Redox-Active Polyelectrolyte Multilayers. *Advanced Materials* **1998**, 10, (4), 347-351.

70. Qiu, X.; Leporatti, S.; Donath, E.; Möhwald, H., Studies on the Drug Release Properties of Polysaccharide Multilayers Encapsulated Ibuprofen Microparticles. *Langmuir* **2001**, 17, (17), 5375-5380.
71. Beyers, H.; Malan, S. F.; van der Watt, J. G.; de Villiers, M. M., Structure-Solubility Relationship and Thermal Decomposition of Furosemide. *Drug Development and Industrial Pharmacy* **2000**, 26, (10), 1077-1083.
72. Ye, S.; Wang, C.; Liu, X.; Tong, Z., Deposition Temperature Effect on Release Rate of Indomethacin Microcrystals from Microcapsules of Layer-by-Layer Assembled Chitosan and Alginate Multilayer Films. *Journal of Controlled Release* **2005**, 106, (3), 319-328.
73. Sukhorukov, G. B.; Möhwald, H.; Decher, G.; Lvov, Y. M., Assembly of Polyelectrolyte Multilayer Films by Consecutively Alternating Adsorption of Polynucleotides and Polycations. *Thin Solid Films* **1996**, 284-285, 220-223.
74. Caruso, F.; Niikura, K.; Furlong, D. N.; Okahata, Y., 2. Assembly of Alternating Polyelectrolyte and Protein Multilayer Films for Immunosensing. *Langmuir* **1997**, 13, (13), 3427-3433.
75. Kong, J.; Lu, Z.; Lvov, Y. M.; Desamero, R. Z. B.; Frank, H. A.; Rusling, J. F., *Journal of the American Chemical Society* **1999**, 120, 7371-7372.
76. Rashba-Step, J.; Darvari, R.; Lin, Q.; Kelly, J.; Shutava, T.; Lvov, Y. M.; Scott, T. In *Surface Modification of PROMAXX Microparticles*, 33rd Annual Controlled Release Society Meeting, Vienna, Austria, 26 July 2006; pp 126-129.
77. Fang, M.; Grant, P. S.; McShane, M. J.; Sukhorukov, G. B.; Golub, V. O.; Lvov, Y. M., Magnetic Bio/Nanoreactor with Multilayer Shells of Glucose Oxidase and Inorganic Nanoparticles. *Langmuir* **2002**, 18, (16), 6338-6344.
78. Hergt, R.; Andrä, W.; d'Ambly, C. G.; Hilger, I.; Kaiser, W. A.; Richter, U.; Schmidt, H.-G., Physical Limits of Hyperthermia Using Magnetite Fine Particles. *IEEE Transactions on Magnetics* **1998**, 34, (5), 3745-3754.
79. Groß, C.; Büscher, K.; Romanus, E.; Helm, C. A.; Weitschies, W., Characterization of a Ferrofluid by Atomic Force Microscopy and Photon Correlation Spectroscopy After Magnetic Fractionation. *European Cells and Materials* **2002**, 3, (2), 163-166.
80. Rosensweig, R. E., Heating Magnetic Fluid with Alternating Magnetic Field. *Journal of Magnetism and Magnetic Materials* **2002**, 252, (1-3 Spec Iss), 370-374.
81. O'Handley, R. C., *Modern Magnetic Materials: Principles and Applications*. John Wiley & Sons, Inc.: New York, 2000; p 740.

82. Buschow, K. H. J., *Handbook of Magnetic Materials*. Elsevier Science B. V.: Amsterdam, 1999; Vol. 12, p 569.
83. Ariga, K.; Onda, M.; Lvov, Y.; Kunitake, T., Alternate Layer-by-Layer Assembly of Organic Dye and Proteins is Facilitated by Premixing with Polyions. *Chemistry Letters* **1997**, 26, (1), 25.
84. Burke, S. E.; Barrett, C. J., pH-Dependent Loading and Release Behavior of Small Hydrophilic Molecules in Weak Polyelectrolyte Multilayer Films. *Macromolecules* **2004**, 37, (14), 5375-5384.
85. Chung, A. J.; Rubner, M. F., Methods of Loading and Releasing Low Molecular Weight Cationic Molecules in Weak Polyelectrolyte Multilayer Films. *Langmuir* **2002**, 18, (4), 1176-1183.
86. Kharlampieva, E.; Sukhishvili, S. A., Release of a Dye from Hydrogen-Bonded and Electrostatically Assembled Polymer Films Triggered by Adsorption of a Polyelectrolyte. *Langmuir* **2004**, 20, (22), 9677-9685.
87. Zhang, J.; Chua, L. S.; Lynn, D. M., Multilayered Thin Films that Sustain the Release of Functional DNA Under Physiological Conditions. *Langmuir* **2004**, 20, (19), 8015-8021.
88. Tan, W.; Wang, K.; He, X.; Zhao, X. J.; Drake, T.; Wang, L.; Bagwe, R. P., Bionanotechnology Based on Silica Nanoparticles. *Medicinal Research Reviews* **2004**, 24, (5), 621-638.
89. Panyam, J.; Labhasetwar, V., Biodegradable Nanoparticles for Drug and Gene Delivery to Cells and Tissue. *Advanced Drug Delivery Reviews* **2003**, 55, (3), 329-347.
90. Leuschner, C.; Hansel, W., Membrane Disrupting Lytic Peptides for Cancer Treatments. *Current Pharmaceutical Design* **2004**, 10, (19), 2311-2334.
91. McShane, M. J.; Lvov, Y. M., Layer-by-Layer Electrostatic Self-Assembly. In *Dekker Encyclopedia of Nanoscience and Nanotechnology*, Schwartz, J.; Contescu, C.; Dekker, M., Eds. Marcel Dekker, Inc.: Ney York, 2004; pp 1-20.
92. Marx, K. A., Quartz Crystal Microbalance: A Useful Tool for Studying Thin Polymer Films and Complex Biomolecular Systems at the Solution - Surface Interface. *Biomacromolecules* **2003**, 4, (5), 1099-1120.
93. Peppas, N. A., Analysis of Fickian and Non-Fickian Drug Release From Polymers. *Pharmaceutica Acta Helveticae* **1985**, 60, 110-111.
94. Okubo, T.; Suda, M., Alternate Sign Reversal in the ζ Potential and Synchronous Expansion and Contraction in the Absorbed Multi-Layers of Poly(4-vinyl-*N-n*-

- butylpyridinium bromide) Cations and Poly(styrene sulfonate) Anions on Colloidal Silica Spheres. *Colloid Polymer Science* **1999**, 277, (9), 813-817.
95. Khopade, A. J.; Arulsudar, N.; Khopade, S. A.; Hartmann, J., Ultrathin Antibiotic Walled Microcapsules. *Biomacromolecules* **2005**, 6, (1), 229-234.
 96. Hiller, S.; Leporatti, S.; Schnäkel, A.; Typlt, E.; Donath, E., Protamine Assembled in Multilayers on Colloidal Particles can be Exchanged and Released. *Biomacromolecules* **2004**, 5, (4), 1580-1587.
 97. Schüer, C.; Caruso, F., Decomposable Hollow Biopolymer-Based Capsules. *Biomacromolecules* **2001**, 2, (3), 921-926.
 98. Babincova, M.; Cicmanec, P.; Altanerova, V.; Altaner, C.; Babinec, P., AC-Magnetic Field Controlled Drug Release from Magnetoliposomes: Design of a Method for Site-Specific Chemotherapy. *Bioelectrochemistry* **2002**, 55, (1-2), 17-19.
 99. Saslawski, O.; Weingarten, C.; Benoit, J. P.; Couvreur, P., Magnetically Responsive Microspheres for the Pulsed Delivery of Insulin. *Life Sciences* **1988**, 42, (16), 1521-1528.
 100. Ruuge, E. K.; Rusetski, A. N., Magnetic Fluids as Drug Carriers: Targeted Transport of Drugs by a Magnetic Field. *Journal of Magnetism and Magnetic Materials* **1993**, 122, (1-3), 335-339.
 101. Wilhelm, C.; Billotey, C.; Roger, J.; Pons, J. N.; Bacri, J. C.; Gazeau, F., Intracellular Uptake of Anionic Superparamagnetic Nanoparticles as a Function of Their Surface Coating. *Biomaterials* **2003**, 24, (6), 1001-1011.
 102. Kost, J.; Wolfrum, J.; Langer, R., Magnetically Enhanced Insulin Release in Diabetic Rats. *Journal of Biomedical Materials Research* **1987**, 21, (12), 1367-1373.
 103. Kumar, C. S. S. R.; Leuschner, C.; Doomes, E. E.; Henry, L.; Juban, M.; Hormes, J., Efficacy of Lytic Peptide-Bound Magnetite Nanoparticles in Destroying Breast Cancer Cells. *Journal of Nanoscience and Nanotechnology* **2004**, 4, (3), 245-249.
 104. Kumar, C. S. S. R.; Leuschner, C.; William, H.; Hormes, J. Magnetic Nanoparticles for Therapy and Diagnosis. 10/816,732, 2004, 2004.
 105. Guo, Z.; Kumar, C. S. S. R.; Henry, L. L.; Hormes, J.; Podlaha, E. J. In *Electroless Method to Fabricate Core-Shell Nanoparticles*, 205th Meeting of the Electrochemical Society, San Antonio, TX, United States, 2004; p 23.
 106. Guo, Z.; Kumar, C. S. S. R.; Henry, L. L.; Doomes, E. E.; Hormes, J.; Podlaha, E. J., Displacement Synthesis of Cu Shells Surrounding Co Nanoparticles. *Journal of the Electrochemical Society* **2005**, 152, (1), D1-D5.

107. Shon, Y.-S.; Dawson, G. B.; Porter, M.; Murray, R. W., Monolayer-Protected Bimetal Cluster Synthesis by Core Metal Galvanic Exchange Reaction. *Langmuir* **2002**, 18, (10), 3880-3885.
108. Huang, T.; Murray, R. W., Luminescence of Tiopronin Monolayer-Protected Silver Clusters Changes to That of Gold Clusters Upon Galvanic Core Metal Exchange. *Journal of Physical Chemistry B* **2003**, 107, (30), 7434-7440.
109. Bönnemann, H.; Brijoux, W.; Jousen, T., The Preparation of Finely Divided Metal and Alloy Powders. *Angewandte Chemie - International Edition* **1990**, 29, (3), 273-274.
110. Antipov, A. A.; Shchukin, D.; Fedutik, Y.; Petrov, A. I.; Sukhorukov, G. B.; Möhwald, H., Carbonate Microparticles for Hollow Polyelectrolyte Capsules Fabrication. *Colloids and Surfaces A: Physicochemical and Engineering Aspects* **2003**, 224, (1-3), 175-183.
111. Petit, C.; Pileni, M. P., Nanosize Cobalt Boride Particles: Control of the Size and Properties. *Journal of Magnetism and Magnetic Materials* **1997**, 166, (1-2), 82-90.
112. Clifffel, D. E.; Zamborini, F. P.; Gross, S. M.; Murray, R. W., Mercaptoammonium-Monolayer-Protected, Water-Soluble Gold, Silver, and Palladium Clusters. *Langmuir* **2000**, 16, (25), 9699-9702.
113. Salazar-Alvarez, G.; Mikhailova, M.; Toprak, M.; Zhang, Y.; Muhammed, M. In *Fabrication and Properties of Self-Assembled Nanosized Magnetic Particles*, Materials Research Society Symposium Proceedings, 2002; pp 263-268.
114. Sun, Y.; Mayers, B. T.; Xia, Y., Template-Engaged Replacement Reaction: A One-Step Approach to the Large-Scale Synthesis of Metal Nanostructures with Hollow Interiors. *Nano Letters* **2002**, 2, (5), 481-485.
115. Sun, Y.; Xia, Y., Alloying and Dealloying Processes Involved in the Preparation of Metal Nanoshells Through a Galvanic Replacement Reaction. *Nano Letters* **2003**, 3, (11), 1569-1572.
116. Fang, J.; He, J.; Shin, E. Y.; Grimm, D.; O'Connor, C. J.; Jun, M.-J. In *Colloidal Preparation of $\gamma\text{-Fe}_2\text{O}_3\text{@Au}$ [core@shell] Nanoparticles*, Materials Research Society Symposium Proceedings, 2003; pp 149-154.
117. Lal, S.; Westcott, S. L.; Taylor, R. N.; Jackson, J. B.; Nordlander, P.; Halas, N. J., Light Interaction Between Gold Nanoshells Plasmon Resonance and Planar Optical Waveguides. *Journal of Physical Chemistry B* **2002**, 106, (22), 5609-5612.
118. Jackson, J. B.; Halas, N. J., Silver Nanoshells: Variations in Morphologies and Optical Properties. *Journal of Physical Chemistry B* **2001**, 105, (14), 2743-2746.

119. Mizukoshi, Y.; Fujimoto, T.; Nagata, Y.; Oshima, R.; Maeda, Y., Characterization and Catalytic Activity of Core-Shell Structured Gold/Palladium Bimetallic Nanoparticles Synthesized by the Sonochemical Method. *Journal of Physical Chemistry B* **2000**, 104, (25), 6028-6032.
120. Teng, X.; Yang, H., Synthesis of Face-Centered Tetragonal FePt Nanoparticles and Granular Films from Pt@Fe₂O₃ Core-Shell Nanoparticles. *Journal of the American Chemical Society* **2003**, 125, (47), 14559-14563.
121. Golub, V. O.; Kakazei, G. N.; Kravets, A. F.; Lesnik, N. A.; Pogorelov, Y. G.; Sousa, J. B.; Vovk, A. Y. In *FMR Linewidth and Magnetic Structures in CoFe-Al₂O₃ Granular Thin Films*, Materials Science Forum, Kyiv, 2001; pp 197-200.
122. Lu, Z.; Prouty, M. D.; Guo, Z.; Golub, V. O.; Kumar, C. S. S. R.; Lvov, Y. M., Magnetic Switch of Permeability for Polyelectrolyte Microcapsules Embedded with Co@Au Nanoparticles. *Langmuir* **2005**, 21, (5), 2042-2050.

VITA

Malcolm D. Prouty received his Bachelors of Science degree in electrical engineering from Louisiana Tech University in 2003. During that time, Mr. Prouty worked as an undergraduate research assistant under Dr. Tianhong Cui at the Institute for Micromanufacturing. His undergraduate research work focused on the design, fabrication, and characterization of polymer-based microelectronic devices such as diodes and capacitors.

After graduating with his Bachelors degree, Mr. Prouty continued his studies at Louisiana Tech University as a Ph.D. candidate in engineering under Dr. Yuri Lvov. His graduate research work was focused on merging electrical engineering with pharmaceutics by incorporating superparamagnetic nanoparticles in polyelectrolyte microcapsules for the enhanced control of diffusion of macromolecules through the polymer membrane.

With all of his accomplishments, Mr. Prouty was given an instructor position for a digital electronics design course for undergraduate students in the College of Engineering and Science, as well as serve on the university's honor council. He has also been chosen to represent Louisiana Tech University at several conferences and social events. Malcolm Prouty, along with his colleagues, successfully transformed one of his research topics, layer-by-layer self-assembly on pulp fibers, into a small company, Better Paper Technologies, LLC. This company placed second in a university sponsored business plan competition, and was able to take one of their products, **reFib**, and receive first runner-up

in an international idea-to-product competition at the Nano Nexus conference in 2007 held at Oak Ridge National Laboratory.

Mr. Prouty has had many publications and attended many conferences throughout his graduate studies. He has also been invited to three talks through the American Chemical Society Tour Speaker Association. His publications and other works are listed here.

Peer Reviewed Journals

- Malcolm Prouty, Zonghuan Lu, Carola Leuschner, Yuri Lvov, "Layer-by-Layer Engineered Nanoparticles for Sustained Release of Phor21- β CG(ala) Anticancer Peptide," *Journal of Biomedical Nanotechnology*, 3(2), Jun. **2007**, 184-189.
- Tatsiana G. Shutava, Malcolm D. Prouty, Vladimir E. Agabekov, Yuri M. Lvov, "Antioxidant Properties of Layer-by-Layer Films on the Basis of Tannic Acid," *Chemistry Letters*, 35(10), Oct. **2006**, 1144-1145.
- Tatsiana Shutava, Malcolm Prouty, Dinesh Kommireddy, Yuri Lvov, "pH Responsible Decomposable Layer-by-Layer Films and Capsules on the Basis of Tannic Acid," *Macromolecules*, 38(7), Mar. **2005**, 2850-2858.
- Zonghuan Lu, Malcolm D. Prouty, Zhanhu Guo, Challa S. S. R. Kumar, Yuri M. Lvov, "Magnetic Switch of Permeability for Polyelectrolyte Microcapsules Embedded with Co@Au Nanoparticles," *Langmuir*, 21(5), Jan. **2005**, 2042-2050.

Conference Proceedings

- Zonghuan Lu, Malcolm D. Prouty, Zhanhu Guo, Challa S. S. R. Kumar, and Yuri M. Lvov, "Layer-by-Layer Nanoengineered Magnetic Encapsulation System for Drug Delivery," *Polymeric Materials: Science & Engineering*, 93, Sept. **2005**, 656-657.
- Tatsiana Shutava, Malcolm D. Prouty, Dinesh S. Kommireddy, Gopal Krishna, and Yuri M. Lvov, "Multilayered Polyelectrolyte/Natural Polyphenol Nanofilms and Microcapsules for Protein Encapsulation and Protection Against Free Radical Oxidation," *Polymeric Materials: Science & Engineering*, 93, Sept. **2005**, 643-644.

Invited Talks

- Malcolm D. Prouty, “Layer-by-Layer Nanoengineered Magnetic Encapsulation System for Drug Delivery,” *ACS Speaker Services – 2007 Crisholm Circuit*, Oklahoma State University, Stillwater, OK; Conoco Phillips Co., Ponca City, OK; 23-24 Apr. **2007**.
- Malcolm D. Prouty, “Layer-by-Layer Nanoengineered Magnetic Encapsulation System for Drug Delivery,” *ACS Speaker Services – 2007 Mid-South Circuit*; Midwestern State University, Wichita Falls, TX; Texarkana College, Texarkana, TX; University of Arkansas at Little Rock, Little Rock, AR; 16-18 Apr. **2007**.
- Malcolm D. Prouty, “Layer-by-Layer Nanoengineered Magnetic Encapsulation System for Drug Delivery,” *ACS Speaker Services – 2007 Hoosier Circuit*; University of Southern Indiana, Evansville, IN; Rose-Hulman Institute of Technology, Terre Haute, IN; Indianapolis, IN; University of Saint Francis, Fort Wayne, IN; 5-8 Mar. **2007**.

Conference Talks

- Malcolm D. Prouty, Zonghuan Lu, Zhanhu Guo, Challa S. S. R. Kumar, Yuri M. Lvov, “Permeability Changes in Co@Au Embedded Polyelectrolyte Microcapsules Using an Alternating Magnetic Field,” *The Annual Southeastern Meeting of the American Chemical Society*, Durham, NC, Nov. **2004**.

Conference Posters

- Yuri M. Lvov, Nalinkanth G. Veerabadrán, Malcolm D. Prouty, Shantanu Balkundi, “Biomimetic Nanoassembly for Protein and Drug Encapsulation”, *ACS Conference: Macromolecules for a Safe, Sustainable and Healthy World*, New York, NY, 10-13 Jun. **2007**.
- Malcolm Prouty, Zonghuan Lu, Carola Leuschner, Yuri Lvov, “Inter-Layer Peptide Release from Layer-by-Layer Engineered Nanoparticles,” *The 7th Louisiana Materials and Emerging Technologies Conference*, Baton Rouge, LA, 23-24 Oct. **2006**.
- Malcolm Prouty, Zonghuan Lu, Carola Leuschner, Yuri Lvov, “Anti-Cancer Peptide Drug Release from Layer-by-Layer Silica-Peptide Nanoshells,” *62nd ACS Southwest Regional Meeting*, Houston, TX, 19-22 Oct. **2006**.
- M. Prouty, Z. Lu, G. Krishna, S. Balkundi, A. Yaroslavov, C. Kumar, C. Leuschner, Y. Lvov, “Drug Polyelectrolyte Nanocapsules for Sustained Release,” *Fostering Collaborations with a Bio Research Day*, Shreveport, LA, 1 May **2006**.

- C. Leuschner, Z. Lu, M. Prouty, Y. Lvov, “Nanoshells for Sustained Release of Phor21- β CG(ala) Anticancer Peptide,” *Annual AACR (American Association for Cancer Research) Conference*, Washington, D. C., 6-9 Apr. **2006**.
- M. Prouty, Z. Lu, N. Veerabadran, G. Krishna, A. Yaroslavov, C. Kumar, C. Leuschner, Y. Lvov, “Drug Nanoencapsulation and Controlled Release,” *Louisiana Materials and Emerging Technologies Conference*, Ruston, LA, 12-13 Dec. **2005**.
- Zonghuan Lu, Malcolm D. Prouty, Zhanhu Guo, Challa S. S. R. Kumar, Yuri M. Lvov, “Layer-by-Layer Nanoengineered Magnetic Encapsulation System for Drug Delivery,” *The 230th ACS National Meeting*, Washington, D. C., Aug. **2005**.
- Malcolm D. Prouty, Tatsiana Shutava, Dinesh Kommireddy, Gopal Krishna, Yuri Lvov, “Multilayered Polyelectrolyte/Natural Polyphenol Nanofilms and Microcapsules for Protein Encapsulation and Protection Against Free Radical Oxidation,” *The 230th ACS National Meeting*, Washington, D. C., Aug. **2005**.
- T. Shutava, M. Prouty, D. Kommireddy, A. Shutova, Y. Lvov, “Layer-by-Layer Nanoengineered Thin Films and Microcapsules with Antioxidant Properties Based on Polyelectrolytes and Natural Polyphenols,” *Society for Biomaterials 30th Annual Meeting*, Memphis, TN, 27-30 Apr. **2005**.
- Jingshi Shi, Xiaodong Yan, Malcolm Prouty, Frank Ji, Yuri Lvov, “Nanocomposite Cantilever Array Sensors,” *National DoE Conference on Nanotechnology for Nonproliferation*, Ruston, LA, 26-27 Jul. **2004**.
- Yuri Lvov, Tatsiana Shutava, Malcolm Prouty, Zonghuan Lu, Nikhil Pargaonkar, “Nanoshells for Enzyme and Drug Encapsulation,” *Louisiana Nanotechnology Day Conference*, Baton Rouge, LA, Jun. **2004**.